# MAREES TERRESTRES

# BULLETIN D'INFORMATIONS

**INTERNATIONAL CENTER FOR EARTH TIDES**
**CENTRE INTERNATIONAL DES MAREES TERRESTRES**

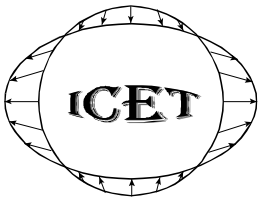


**International Association of Geodesy - International Gravity Field Service**
**(IAG – IGFS)**

**Publié par l'Université de la Polynésie française**

## BIM n° 149

## ISSN n°0542-6766

## 13 FÉVRIER 2015

*Editeur: Prof. Jean-Pierre BARRIOT*
*Observatoire Géodésique de Tahiti*
*Université de Polynésie française*
*BP6570 – 98702 Faaa*
*Tahiti-Polynésie française*

BLANK PAGE

The precious help of Prof. Bernard Ducarme is gracefully acknowledged for his guidance and help in completing this issue of the BIM.

BLANK PAGE

BIM 149

13 février 2015

**17th International Symposium on Earth Tides**
**"Understand the Earth"**
**15-19 April, 2013**
**Warsaw, Poland**



## SCIENTIFIC PAPERS



## 60th anniversary of gravimetry (1954-2014) in Strasbourg

BLANK PAGE

# Artificial neural network model as a potential alternative for barometric correction of extensometric data

Gyula Mentes

Geodetic and Geophysical Institute, Research Centre for Astronomy and Earth Sciences, Hungarian Academy of Sciences, Csatkai Endre u. 6-8, H-9400 Sopron, Hungary.
Email: mentes@ggki.hu

**Abstract**
The solid Earth crust is deformed by atmospheric pressure variations due to periodic and aperiodic loading. When barometric admittance is determined the local, regional or global loading effect can be calculated depending on the available pressure data. The effect of horizontally moving weather systems across the extensometric station can be taken into account with a good approximation when locally measured air pressure data before and after each individual strain data are involved into the correction. For this purpose neural networks with delayed input lines seem to be suitable. Three different neural networks were developed. All of them have delayed inputs taking six or twelve air pressure data before and after each momentary extensometric data into account to correct for remote atmospheric pressure variations on the basis of local pressure measurements. The effectiveness of the barometric pressure correction carried out by the three neural networks were investigated by tidal, Fast Fourier and coherence analyses and the results were compared with each other and with the results of simple regression methods. Tests of the neural network models show that they can be useful tools to correct extensometric data for barometric pressure and in contrast with the simple linear regression models the regional and global atmospheric effects can also be taken into account. Correction by neural networks yielded an improvement in the tidal factors relative to the correction by simple regression methods 2–5% and 30–40% in the semidiurnal and diurnal bands, respectively.

**Keywords:** Atmospheric pressure; Extensometer; Barometric correction; Neural network; Tidal factors

## 1. Introduction

Atmospheric pressure variations associated with atmospheric tides and weather changes deform the Earth in a wide frequency range (Farrell, 1972). Although the magnitude of atmospheric tides is smaller than that of ocean tide loading, the incoherent atmospheric pressure variations are the major cause of random fluctuations in local gravity and Earth deformations (Warburton and Goodkind, 1977; Spratt, 1982; Merriam, 1992; van Dam, et al., 1994, 1997, 2010; Wunsch and Stammer, 1997; Boy et al., 2006, 2009). A lot of publications deal with the correction of gravity measurements for atmospheric pressure (e.g. Niebauer 1988; Crossley et al., 1995, 2002; Neumeyer et al., 2004; Klügel and Wziontek, 2009) and with the deformation of the Earth's surface due to atmospheric variations (e.g. Rabbel and Zschau, 1985; van Dam and Wahr, 1987; van Dam et al., 1997, 2010; Latynina et al., 2003; Steffen et al., 2006; Gebauer et al., 2009, 2010). Kroner and Jentzsch (1999) summarized and compared the methods which are widely used for pressure correction. At present four methods and sometimes their combinations are used for the pressure reduction: local regression coefficient (effective admittance) applied also in the ETERNA 3.40 Earth tide data processing

program package (Wenczel, 1996); frequency-dependent admittance function (e.g. Crossley et al., 2002; Neumeyer et al., 2004); atmospheric Green's function based on local air pressure data (e.g. Niebauer, 1988); atmospheric Green's function calculated from local and regional pressure data (e.g. Spratt, 1982; van Dam and Wahr, 1987).

Correction of gravity measurement for atmospheric pressure using global (<1000 km) and regional (<50 km) pressure data yields improvement in the synoptic (days to seasonal) band, while using local pressure data improves the correction in the intertidal frequency bands down to periods of some hours, because the atmospheric pressure variations in the regional and global zones will be averaged out to some degree (Merriam, 1992; Boy et al., 1998). Front passages above the station have effects on gravity data in the semidiurnal and diurnal tidal bands (Müller and Zürn, 1983). Rabbel and Zschau (1985) showed that the shape of the horizontal strain curve is similar to the corresponding continuous pressure distribution curve, however it has opposite sign. The effect of the slowly changing global and regional pressure distributions is approximately $(-1.5)–(-2.0)\cdot10^{-10}$ strain per hPa below the centre of the pressure anomaly while it can be disregarded in the diurnal and semidiurnal tidal bands. A discontinuous (stepwise) pressure distribution causes a nearly constant horizontal strain change with an extent of about ±50 km from the centre of the abrupt pressure change. This is the case when the front is moving above the station. The strain leads and lags relative to pressure variation during the passage of the front. This relationship can be applied for the improvement of the correction of extensometric data for atmospheric pressure loading by local pressure data.

Gebauer et al. (2010) modelled the behaviour of the Sopronbánfalva Geodynamic Observatory (SGO) during passage of high pressure front and they found that the observatory is very sensitive to pressure fronts due its topography, namely that the steep western rock face of the observatory is perpendicular to the extensometer and the prevailing wind direction (WE) and consequently the rock deformation caused by the absorbed wind energy is parallel with the instrument. The strain shows significant changes even when the pressure front is far away from the observatory.

Tidal analysis of uncorrected strain data measured at the SGO show that the tidal amplitude factors are 10% and 40% lower than one in the diurnal and semidiurnal band, respectively. The tidal factors of strain data corrected by ETERNA are in the semidiurnal band 2–3% and in the diurnal band 10% bigger than in the uncorrected ones (Mentes, 2010; Eper-Pápai et al., 2014). These results and the investigations of Gebauer et al. (2010) suggested that better tidal factors could be obtained when regional and global air pressure data were applied for correction. To avoid the time-consuming and tiring correction by regional and global air pressure data, neural networks with delayed inputs are suggested to correct strain data by locally measured pressure data. This kind of neural networks, in contrast with the correction by a simple linear regression method, can take more air pressure data before and after the momentary strain data into account to correct strain data. The applicability of neural networks to correct strain data on the basis of local pressure measurements is investigated in this paper.

## 2. Neural network

The Artificial Neural Network (ANN) is a computing tool consisting of many simple elements called neurons (Fig. 1), each having the capability of recognizing underlying relationship between input and output signals. Neurons have one or more scalar inputs ($x_1$, $x_2$, ... $x_n$) which are multiplied by a scalar ($w_1$, $w_2$, ... $w_n$) and transferred to a summer to add up the weighted inputs ($x_1\cdot w_1+x_2\cdot w_2$, ... $x_n\cdot w_n$). This sum is the argument of the transfer function which

produces the output (F(*x*)). Usually, ANN consists of more neurons arranged in layers. The efficiency of an ANN depends on the number of layers and neurons.

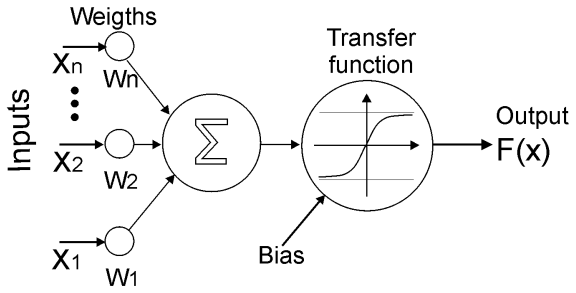


**Fig. 1.** A typical artificial neuron

Three different feed-forward neural networks with different complexity were developed for air pressure correction of extensometric data using the Neural Network Toolbox of Matlab (Demuth and Beale, 2001). Fig. 2 shows the simplest neural network NNW1. It consists of three layers (*l*=3, two input and an output layer) each containing four neurons (*n*=4) with seven inputs (*i*=7). In Layer#1 six inputs are for the delayed pressure data (*d*=6) and one input for the extensometric data and in Layer#2 six inputs are for the delayed extensometric data (*d*=6) and one input for the pressure data. In Layer#1 six hourly delayed pressure data are combined with each momentary extensometric data while in Layer#2 it is inverse: six hourly delayed extensometric data are combined with each pressure data. It means that twelve locally measured pressure data can be taken into account for the pressure correction of each extensometric data. The transfer functions of the neurons in the input layers of the NNW1 are "tansig" and the transfer function in the output layer is "purelin" (see the transfer functions in Fig. 2). Each neuron in the network has a bias input (*b*) to add a constant to the weighted inputs in order to shift the transfer function to the left by an amount of *b*.

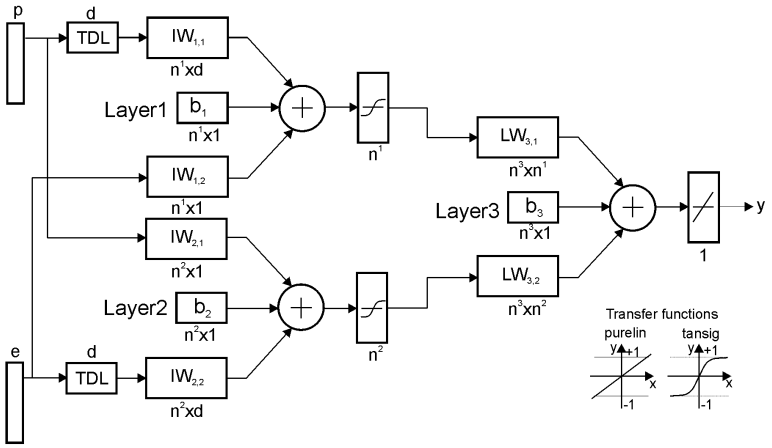


**Fig. 2.** Block diagram of the neural network NNW1 designed for air pressure correction of extensometric data. *e* and *p* denote extensometric and air pressure data series, respectively; *d* is the number of delays (hours); *l* is the number of layers; $n^l$ is the number of neurons in layer *l*; $IW_{l,i}$ is the weight from input *i* to layer *l*; $LW_{l,k}$ is the weight from layer *k* to layer *l*, ($k \leq l$); y is the output.

The other two neural networks (NNW2 and NNW3) are similar to NNW1. They contain a hidden layer between the output and the input layers (*l*=4) with 13 neurons (*n*=13) in the input

and hidden layers. In Layer#1 one input is for the extensometric and twelve inputs are for the delayed ($d$=12) pressure data and in Layer#2 one input is for the pressure data and twelve inputs for the delayed extensometric data. In this case the number of the delayed inputs is twelve thus twenty four locally measured pressure data can be taken into account for the pressure correction of each extensometric data. The output layer has one neuron with 13 inputs. In NNW2 all transfer functions are "purelin", while in NNW3 the transfer functions are "tansig" in the first three layers and "purelin" in the output layer. The output layer of each NNW has a target input (not denoted in Fig. 2). The $y$ output signal of the NNW is compared to the target signal to get the best approach of the target during learning process of the neural network.

The neural networks were initialized by the Nguyen-Widrow layer initialization function (initnw). Widrow-Hoff weights/bias learning rule (learnwh) was used for updating the biases and weights during learning. The Levenberg-Marquardt backpropagation function (trainlm) served for training the networks, while the theoretical tide, calculated by the ETERNA for the actual year, was applied as a target function and the measured extensometric and pressure data were the input functions. During training the weights and biases of the network are iteratively adjusted to minimize the network performance function, which is the averaged squared error (mse) between the network output and the target. Error level of $10^{-3}$ was given as performance goal. After training the network the air pressure correction was carried out by the "sim" function, which takes the network inputs (extensometric ($e$) and pressure ($p$) data), the network parameters (weights and biases obtained during training) and returns the $y$ output (Fig. 2).

## 3. Methods

Eleven years (2000–2010) extensometric data were yearly corrected for air pressure by different methods and analysed by the ETERNA 3.40 Earth tide data processing program (Wenzel, 1996) using the Wahr–Dehant Earth model (Dehant, 1987), the HW95 tidal potential catalogue (Hartmann and Wenzel, 1995) and the built-in high-pass filter with a cut-off frequency of 0.8 cpd. To compare the effectiveness of the air pressure correction by neural networks with other methods the following extensometric raw data were subjected to tidal analysis: uncorrected, corrected by linear regression model (local admittance), corrected by the ETERNA during the analysis, and data corrected by neural networks (NNW1, NNW2, NNW3). The efficiency of the air pressure correction by neural networks compared to other methods was investigated through tidal parameters from ETERNA and Fast Fourier Transformation, regression and coherence analyses of the tidal adjustment residuals.

## 4. Results and discussion

### 4.1. Results of the corrections

The training of the networks continued till the average mean square error reached a minimum value. The results can be seen in Table 1. In every case, the errors are about one order of magnitude higher than the given performance goal ($10^{-3}$). The training process of NNW3 produces the smallest errors and the simplest neural network NNW1 has slightly higher errors than NNW3. The smaller errors of NNW3 compared to NNW2 can probably be attributed to the non-linear transfer functions in the first three layers of NNW3 (see Demuth and Beale, 2001).

**Table 1.** Average mean square errors of the training

| Year | NNW1 | NNW2 | NNW3 |
|---|---|---|---|
| 2000 | 0.047 | 0.057 | 0.016 |
| 2001 | 0.041 | 0.066 | 0.026 |
| 2002 | 0.032 | 0.058 | 0.020 |
| 2003 | 0.024 | 0.043 | 0.016 |
| 2004 | 0.018 | 0.031 | 0.012 |
| 2005 | 0.029 | 0.022 | 0.010 |
| 2006 | 0.038 | 0.023 | 0.010 |
| 2007 | 0.027 | 0.048 | 0.021 |
| 2008 | 0.061 | 0.031 | 0.013 |
| 2009 | 0.048 | 0.102 | 0.039 |
| 2010 | 0.042 | 0.075 | 0.023 |

Fig. 3 shows the results of tidal analysis of extensometric data corrected for air pressure by different methods, as an example, for the year 2005. Analysis results for other years are similar. All the three neural networks provide better amplitude factors (with the exception of the OO1 and M3M6 wave groups) than those calculated from the extensometric data corrected by simple regression methods. The small difference between the amplitude factors means that a good correction can be achieved. In Fig. 4 the amplitude factors of the main lunar diurnal O1 and main semidiurnal M2 tidal constituents are shown for the whole investigated period (2000–2010). The amplitude factors of O1 from the NNW3 model are nearer to the value of one than those from other methods. Correction by NNW1 produces also similar good amplitude factors as NNW3. The amplitude factors obtained by the correction with NNW3 are in every year about 0.9, while in the case of NNW1 there are nearer to one but the dispersion of the factors is high. While the amplitude factors of M2 from analysis of the corrected data by neural networks are slightly smaller than one those from the correction with simple regression methods are generally much higher than one. The situation is similar in the whole diurnal and semi diurnal band (see also Fig. 3). On the basis of tidal analysis it can be inferred that the NNW3 is more suitable for air pressure correction of extensometric data than the other two neural networks.

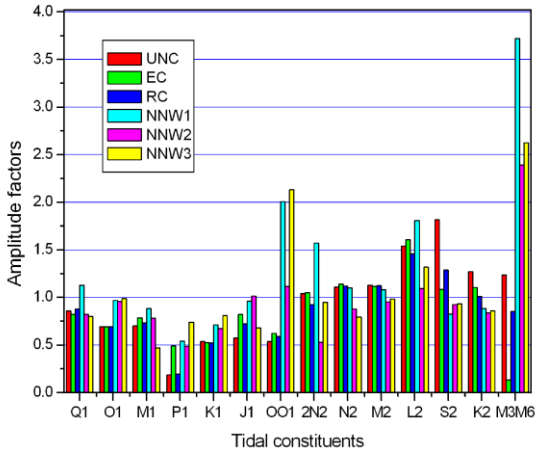


**Fig. 3.** Amplitude factors obtained for year 2005 from tidal analysis of extensometric data corrected by different methods. UNC is uncorrected data; EC is data corrected by ETERNA; RC is data corrected by linear regression method; NNW1, NNW2, NNW3 are data corrected by neural networks.

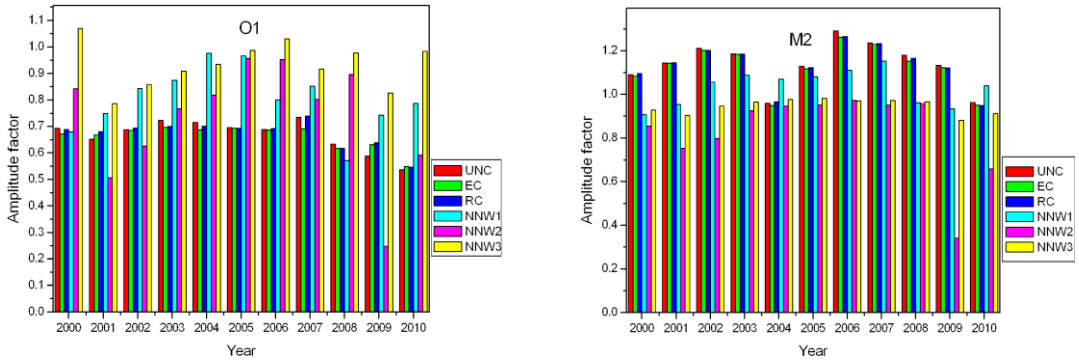


**Fig. 4.** Amplitude factors of the O1and M2 tidal constituents obtained for years 2000–2010 from tidal analysis of extensometric data corrected by different methods. UNC is uncorrected data; EC is data corrected by ETERNA; RC is data corrected by linear regression method; NNW1, NNW2, NNW3 are data corrected by neural networks.

### 4.2. Investigation of the effectiveness of the correction

Looking at the tidal results the question arises: are the good amplitude factors due to the air pressure correction or the neural network adjusts its output data to the theoretical tide? To answer this question the residual curves from tidal analysis (the adjusted tidal components are subtracted from the measured data) were investigated.

The residual data and the local air pressure were subjected to linear regression analysis to investigate the remaining pressure data in the residuals. Since the NNW3 yielded the best amplitude factors, the regression coefficients between air pressure and the residuals from analysis of uncorrected data, corrected by ETERNA and by NNW3 were calculated. The results are summarized in Table 2.

**Table 2.** Regression coefficients between tidal residuals and air pressure in the case of different correction of extensometric data for air pressure

| Year | Uncorrected [nstr/hPa] | Corrected by ETERNA [nstr/hPa] | Corrected by NNW3 [nstr/hPa] |
|---|---|---|---|
| 2000 | 1.9689 | 0.009 | 0.229 |
| 2001 | 1.935 | 0.112 | 0.153 |
| 2002 | –3.881 | 0.046 | –0.053 |
| 2003 | –3.280 | 0.027 | 0.112 |
| 2004 | –4.114 | 0.053 | 0.026 |
| 2005 | –3.546 | 0.078 | 0.037 |
| 2006 | –3.838 | –0.001 | 0.203 |
| 2007 | –4.269 | 0.001 | 0.187 |
| 2008 | –3.823 | 0.184 | 0.199 |
| 2009 | –3.202 | 0.165 | 0.182 |
| 2010 | –3.380 | –0.014 | 0.049 |

Regression coefficients are slightly larger in the case of NNW3 than in the case of the ETERNA correction. This may be explained by the fact that the neural network takes twelve

air pressure data before and after the actual extensometric data while the ETERNA takes only each individual extensometric and pressure data into account during the correction and similarly the related pressure and residual data are used for calculation of the regression coefficients. To investigate this assumption the amplitude spectrum of the residuals and the air pressure were calculated (Fig. 5). It can be seen that the spectral amplitudes from the NNW3 correction in the diurnal and semidiurnal frequency ranges are about the half of the amplitudes obtained by the tidal analysis of uncorrected extensometric data (UNC) and data corrected by ETERNA (EC).

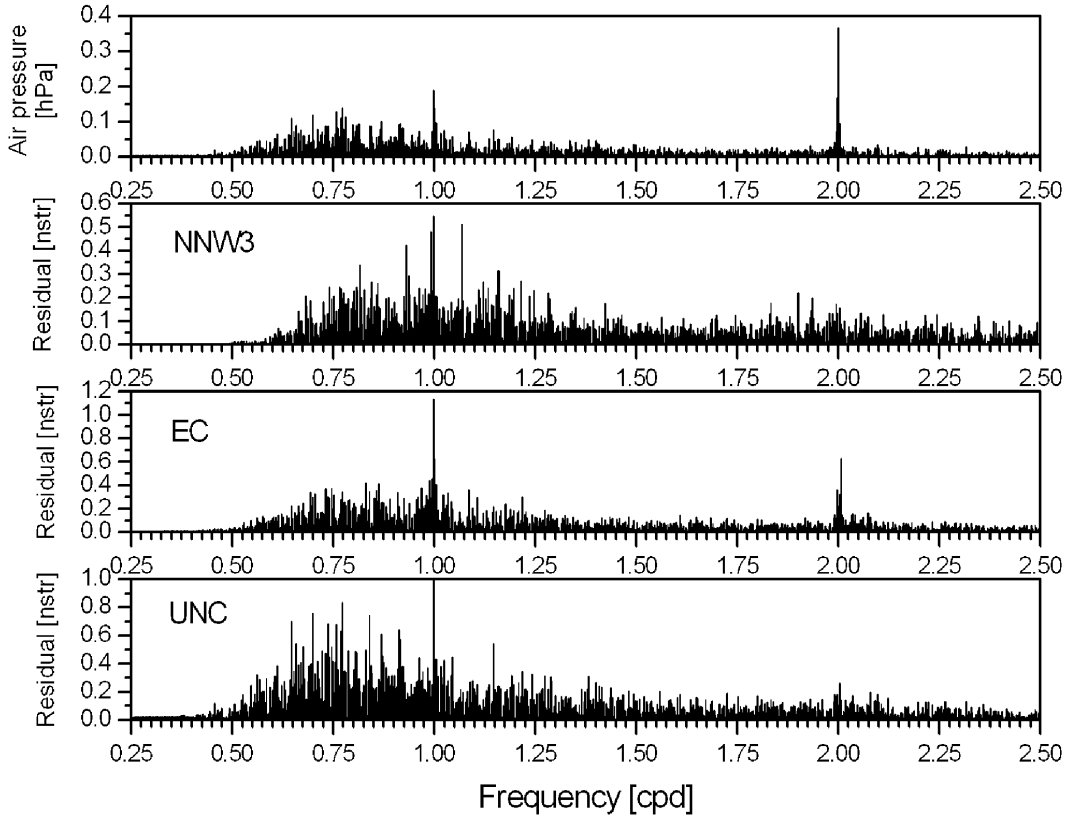


**Fig. 5.** Amplitude spectrum of the air pressure data, the residuals of tidal analysis of the uncorrected extensometric data (UNC), data corrected by ETERNA (EC), and data corrected by neural network (NNW3).

The coherence analysis between pressure and residual data (Fig. 6) also shows that the neural network eliminates the air pressure effect in the whole frequency range while the correction by the ETERNA decreases it only in the diurnal and semidiurnal frequency domains. Fig. 7 shows the coherence between the theoretical tide and the uncorrected extensometric data as well as extensometric data corrected by different methods (EC, NNW2 and NNW3). While correction by ETERNA improves the coherence, the neural networks decrease it. It is somewhat inconsistent with the former findings. The coherence between two signals is low when the signals are nonlinear, either there is a phase shift between the signals or the signals have high noise (Formenti, 1999). The transfer functions of NNW2 are linear ("purelin"). The coherence functions of NNW2 and NNW3 are similar which means that the non-linear transfer functions in the first three layers of NNW3 do not cause signal non-linearity during the correction. The noises are in the same order in the case of all corrections, so we can assume that the noise cannot cause the coherence results of Fig. 7. The phase shifts

of the O1 and M2 tidal waves from the uncorrected data are –5 and –13 degrees, respectively. Both neural networks change these phases into –70 degrees. Phases of other waves are practically unchanged. It can be inferred that this phase shift causes the lower coherence in the diurnal and semi diurnal band in the case of the neural networks. In contrast with this, the correction by ETERNA changes the phases of P1 and K2 significantly (by about 130 degree) and lefts the phases of O1 and M2 unchanged compared to the uncorrected data. The coherence here is better than the coherence between the theoretical tide and uncorrected extensometric data (Fig. 7). This result queries the assumption that the phase shifts decrease the coherence but this question needs further investigations. The lower coherence in the case of the extensometric data corrected by neural networks hints to the characteristic of the neural network that it does not tend to fit the measured data to the target function (theoretical tide) during the correction procedure.

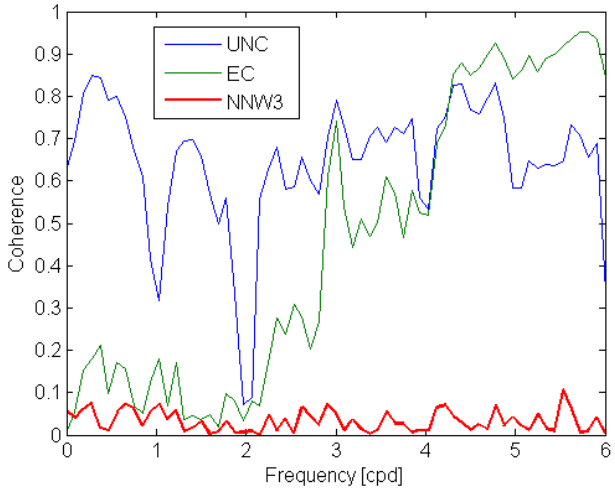


**Fig. 6.** Coherence between air pressure and tidal residuals obtained by the analysis of uncorrected extensometric data (UNC), data corrected by ETERNA (EC) and data corrected by neural network (NNW3).

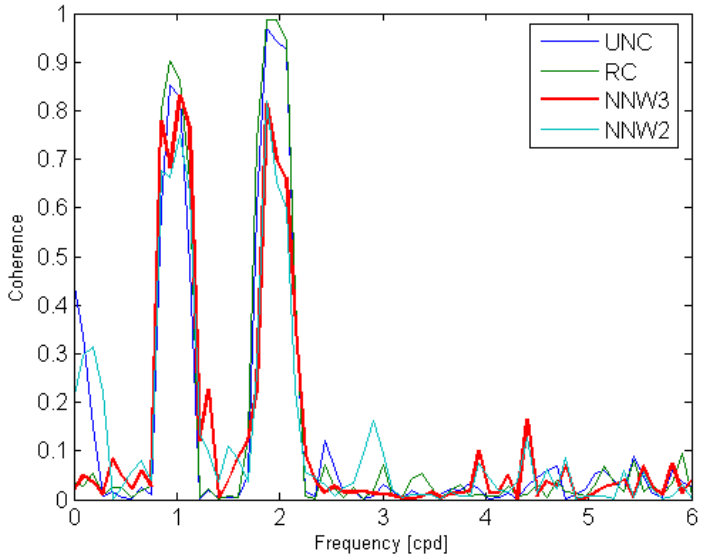


**Fig. 7.** Coherence between theoretical tide and uncorrected extensometric data (UNC), extensometric data corrected by ETERNA (EC) and neural networks (NNW2 and NNW3).

## 5. Conclusions

The purpose of this study is to investigate the applicability of neural networks to correct extensometric data for barometric pressure on the basis of local pressure measurements. Three neural networks with different complexity were designed and tested. The first neural network (NNW1) has 3 layers with 4 neurons and non-linear transfer function in the first two layers and a linear transfer function in the last layer. The NNW1 combines 6 hourly pressure data before and after each individual extensometric data to correct extensometric data for barometric pressure. The other two neural networks (NNW2 and NNW3) have 4 layers with 13 neurons in each layer. The NNW2 has linear transfer function in each layer while the NNW3 has non-linear transfer function in the first three layers and a linear transfer function in the output layer. Both neural networks combine 12 hourly pressure data before and after each individual extensometric data.

The results from the effectiveness investigations show that the correction can be made by all of the investigated neural networks. Increasing the complexity of the model the effectiveness of the correction increases only slightly. The best correction was obtained from the NNW3 model.

NNW3 decreased the pressure induced strain amplitudes in the tidal residual by 50% compared to the residual of the simple regression method. While the NNW3 removed the pressure in the whole investigated frequency range the regression method of ETERNA corrected the strain data only in the diurnal and semidiurnal frequency bands.

Correction by neural networks yielded an improvement in the tidal factors relative to the simple regression methods by 2–5% and 30–40% in the semidiurnal and diurnal bands, respectively.

Coherence analysis between theoretical tide and corrected extensometric data resulted in better coherence when strain data was corrected by the ETERNA than when the data were uncorrected, while the coherence was lower in the case of NNW3 correction. The reason for this must be investigated. Probably a further improvement of the NNW3 is necessary.

Investigations show that neural networks can be a useful tool to correct extensometric data for barometric pressure, whereas, in contrast with the simple linear regression models, they can include more air pressure data before and after each individual strain data into the correction than simple regression methods and thus the regional atmospheric effects can be taken into account to some extent on the basis of local atmospheric data.

## Acknowledgements

This work was funded by the Hungarian National Research Fund (OTKA) under projects No. K 71952 and K 109060. Special thanks to Ildikó Eperné-Pápai for her help in data preprocessing and Tibor Molnár for his careful maintenance of the instruments.

## References

Boy, J.-P., Hinderer, J., Gegout, P., 1998. Global atmospheric pressure loading and gravity. Phys. Earth Planet. Inter. 109, 161–177.

Boy, J.-P., Longuevergne, F., Boudin, F., Jacob, T., Lyard, F., Llubes, M., Florsch, N., Esnoult, M.-F., 2009. Modelling atmospheric and induced non-tidal oceanic loading contributions to surface gravity and tilt measurements. J. Geodyn. 48 (3–5), 182–188, doi:10.1016/j.jog.2009.09.22.

Boy, J.-P., Ray, R., Hinderer, J., 2006. Diurnal atmospheric tide and induced gravity variations. J. Geodyn. 41 (1–3), 253–258, doi:10.1016/j.jog.2005.10.010.
Crossley, D.J., Jensen, O.G., Hinderer, J., 1995. Effective barometric admittance and gravity residuals, Phys. Earth Planet Inter. 90, 221–241.
Crossley, D.J., Hinderer, J., Rosat, S., 2002. Using Atmosphere-Gravity Correlation to Derive a Time-Dependent Admittance. Bull. d'Inf. Marées Terr. 136, 10809–10820
Dehant, V., 1987. Tidal parameters for an unelastic Earth. Phys. Earth Planet. Inter. 49, 97–116.
Demuth, H., Beale, M., 2001. Neural Network Toolbox for Use with MATLAB, User's Guide, Version 4. The Math Works, Inc.
Eper-Pápai, I., Mentes, G., Kis, M., Koppán A., 2014. Comparison of two extensometric stations in Hungary. J. Geodyn, 80, 3–11, dx.doi.org/10.1016/j.jog.2014.02.007.
Farrell, W.E., 1972. Deformation of the Earth by surface loads. Rev. Geophys. Space Phys. 10, 761−797.
Formenti, D., 1999. What is the coherence function and how can it be used to find measurement and test setup problems. Sound and Vibration, Questions and Answers, Sage Technologies, Morgan and Hill, California, 2–3.
Gebauer, A., Kroner, C., Jahr, T., 2009. The influence of topographic and lithologic features on horizontal deformations. Geophys. J. Int. 177, 586–602, doi:10.1111/j.1365-246X.2009.04072.x.
Gebauer, A., Steffen, H., Kroner, C., Jahr, T., 2010. Finite element modelling of atmosphere loading effects on strain, tilt and displacement at multi-sensor stations. Geophys. J. Int. 181, 1593–1612, doi: 10.1111/j.1365-246X.2010.04549.x.
Hartmann, T., Wenzel, H.G., 1995. The HW95 tidal potential catalogue. Geophys. Res. Lett. 22, 3553–3556.
Klügel, T., Wziontek, H., 2009. Correcting gravimeters and tiltmeters for atmospheric mass attraction using operational weather models. J. Geodyn. 48 (3–5), 204–210, doi:10.1016/j.jog.2009.09.01.
Kroner, C., Jentzsch, G., 1999. Comparison of different barometric pressure reductions for gravity data and resulting consequences. Phys. Earth Planet. Inter. 115, 205–218.
Latynina, L.A., Vasil'ev, I.M., 2003. The Earth surface deformations caused by air pressure variations. J. Geodyn. 35, 541–551, doi:10.1016/S0264-3707(03)00013-9.
Mentes, Gy., 2010. Quartz tube extensometer for observation of Earth tides and local tectonic deformations at the Sopronbánfalva Geodynamic Observatory, Hungary. Rev. Sci. Instrum. 81, 074501, doi:10.1063/1.3470100.
Merriam, J.B., 1992. Atmospheric pressure and gravity. Geophys. J. Int., 109, 488−500.
Müller, T., Zürn, W., 1983. Observations of Gravity Changes During the Passage of Cold Fronts. J. Geophys. 53, 155−162.
Niebauer, T.M., 1988. Correcting gravity measurements for the effects of local air pressure. J. Geophys. Res. 93 (B7), 7989–7991.
Neumeyer, J., Hagedoorn, J., Leitloff, J., Schmidt, T., 2004. Gravity reduction with three-dimensional atmospheric pressure data for precise ground gravity measurements. J. Geodyn. 38, 437–450.
Rabbel, W., Zschau, J., 1985. Static deformations on gravity changes at the earth's surface due to atmospheric loading. J. Geophys. 56, 81−99.
Spratt, R.S., 1982. Modelling the effect of atmospheric pressure variations on gravity. Geophys. J. R. Astr. Soc. 71, 173–186.
Steffen, H., Kuhlmann, S., Jahr, T., Kroner, C., 2006. Numerical modelling of the barometric pressure-induced noise in horizontal components for the observatories Moxa and Schiltach. J. Geodyn. 41 (1–3), 242–252, doi:10.1016/j.jog.2005.08.011.

van Dam, T.M., Altamimi, Z., Collilieux, X., Ray, J., 2010. Topographically induced height errors in predicted atmospheric loading effects. J. Geophys. Res. 115, B07415, doi:10.1029/2009JB006810.

van Dam, T.M., Blewitt, G., Heflin, M.B.,1994. Atmospheric pressure loading effects on Global Positionig System coordinate determinations. J. Geophys. Res. 99 (B12), 23,939−23,950.

van Dam, T.M., Wahr, J., 1987. Displacements of the Earth's Surface Due to Atmospheric Loading: Effects on Gravity and Baseline Measurements. J. Geophys. Res. 92 (B2), 1281−1286.

van Dam, T.M., Wahr, J., Chao, Y., Leuliette, E., 1997. Predictions of crustal deformation and of geoid and sea-level variability caused by oceanic and atmospheric loading. Geophys J. Int. 129, 507–517.

Warburton, R.J., Goodkind, J.M., 1977. The influence of barometric pressure variations on gravity. Geophys. J. R. Astr. Soc. 48, 281–292.

Wenzel, H.G., 1996. The nanogal software: Earth tide data processing package ETERNA 3.30. Bull. d'Inf. Marées Terr. 124, 9425–9439.

Wunsch, C., Stammer, D., 1997. Atmospheric loading and the oceanic "inverted barometer" effect. Rev. Geophys. 35 (1), 79–107.

BLANK PAGE

# Analysis of 4-year observations of the gPhone#59 in Tahiti

O. Francis[1], J.-P. Barriot[2] and D. Reymond[3]

[1] University of Luxembourg, FSTC, Luxembourg, olivier.francis@uni.lu
[2] Geodesy Observatory of Tahiti (OGT), University of French Polynesia (UPF), Tahiti, jean-pierre.barriot@upf.pf
[3] Laboratory of Geophysics (LDG), French Atomic Energy Agency (CEA), Tahiti, reymond.d@labogeo.pf

**Abstract.** Since 2009, the relative spring gravimeter gPhone#059 is operating almost continuously in Pamatai, Tahiti. Although Tahiti is an island, the tidal oceanic gravitational attraction and elastic loading effects are relatively moderate. However, the data are affected by a huge microseismic signal. We present the results of the earth tides analysis and compare them with the latest theoretical WDD Earth tides model combined with modeled oceanic loading and attraction effects. The atmospheric pressure regime is unique with a strong semi-diurnal component.

## 1. Introduction

Tahiti Island (17° 34 S, 149° 36 W) is part of French Polynesia, a swarm of 120 islands located in the middle of the South Pacific Ocean. It comprises three volcanic edifices: Moorea, Tahiti-Nui and Tahiti-Iti, spread over 100 km (Figure 1). The formation is dated 0.5-1.4 Million years, with an end of the volcanism activities 250,000 years ago (Hildenbrand et al., 2008).

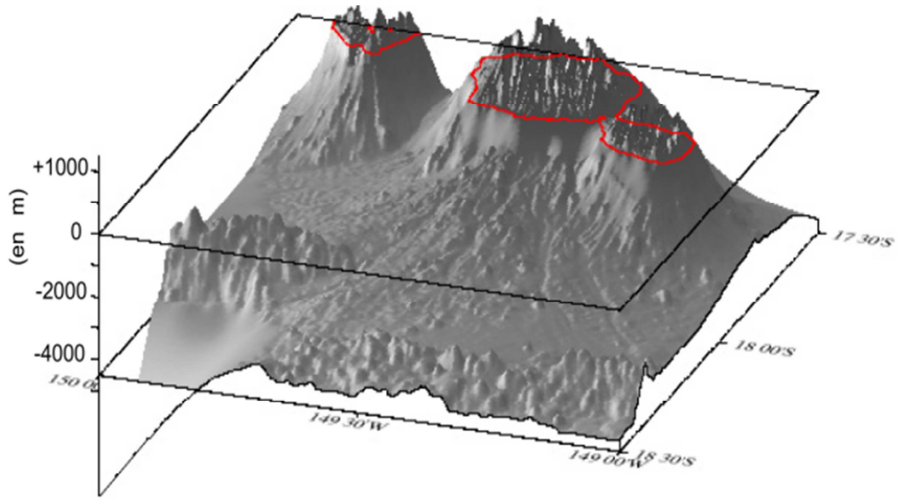


**Figure 1.** Tahiti islands complex (from left to right: Moorea, Tahiti-Nui and Tahiti-Iti volcanic edifices). Clouard and Bonneville (2003), with permission.

In 2009, the University of French Polynesia acquired the gPhone#59 relative spring gravimeter manufactured by MicrogLaCoste Inc. It was installed in a remote vault with difficult access, next to the GEOSCOPE instruments in Tahiti-Pamatai (Figures 2). Since then, the gravity variations are measured almost continuously. Despite all the care, there are some gaps due to electric power shortages.

**Figures 2.** Instrument vault in Tahiti-Pamatai (left) and the gPhone#59 with Geoscope broadband seismometers (right) in Tahiti (GPS coordinates: latitude: -17.5896 ; longitude: -149.5625 and altitude: 705 m).

The station is at an altitude of 705 m above the mean sea level at a distance of 5 km from the sea. Despite the proximity to the sea and the high altitude, the tidal oceanic attraction and elastic loading effects are quite reasonable: 1.4 microgal for $M_2$ and 0.5 microgal for $K_1$, respectively. The altitude enhances the magnitude of the gravitational attraction effects of the tidal water around Tahiti (if the altitude was at the same level as the mean sea level, the direct attraction effects would be zero). It means that the quality and the resolution of the ocean tides around Tahiti will play a crucial role to accurately model the oceanic loading and attraction effects.

In this paper, we begin with a short presentation of the gPhone along the results of an assessment of its performance carried out in the Walferdange Underground Laboratory for Geodynamics in Luxembourg. We then describe the observations and the data processing of the gravity observations. The Earth tides analysis results are then presented and discussed. We conclude with some perspectives for future work.

## 2. The gPhone: a portable Earth tidal spring gravimeter

The gPhone is the last born relative spring gravimeter based on the LaCoste-Romberg meter patented in 1952. The first generation meter had a single oven heating system for thermal stability and a zero length spring. In 2004, MicrogLaCoste Inc. started to redesign and improve the hardware and software components. This includes: a low drift metal zero length spring, a CPI (Capacitance Position Indicator) feedback system, a coarse screw to adjust the spring tension (world-wide gravity range), a linear electronic feedback with a range between 20 to 40 mGal (insuring 2 years operation without adjusting the spring), a double-oven container (very accurate and stable temperature control at 1 mK), an inner oven filled with dry Nitrogen (stable humidity environment), 3 sealed chambers to protect from outside ambient humidity and pressure variation, inner and outer oven chambers thick walled aluminum O-ring sealed and leak tested, outer grey box O-ring sealed for water tightness. Additional and interesting features were added like: a rubidium clock for keeping the time steered by GPS, 1-second data sampling including the long and cross levels, the ambient pressure and temperature, the sensor temperature, the meter inside pressure and the beam position. The gPhone is not designed to be moved around to measure a network of stations as a Scintrex, for example. It is devoted to semi-permanent stations to estimate the tidal parameters and to measure continuously temporal gravity change at a fixed station.

In order to illustrate the performance of the gPhone, the noise power spectral density of four different sensors operating at the same time in the Walferdange Underground Laboratory for Geodynamics is presented in Figure 3. The gPhone has a performance lying between the superconducting gravimeter and the relative spring gravimeter Scintrex CG-5. At short period less than 10 seconds, the signal of the superconducting gravimeter is attenuated by the analog low-passed filter of its electronics. At periods less than 20 seconds, the gPhone and the Streckeisen STS-2 broadband seismometer (for more information about the STS-2 go to the web site https://www.passcal.nmt.edu/content/instrumentation/sensors/broadband-sensors/sts-2-bb-sensor) noises are similar. Obviously, the STS-2 can sample the data at much higher frequency than the gPhone. However, the gPhone could be used to calibrate the STS-2. This cannot be done with the superconducting gravimeter because of its low-pass analog filter.

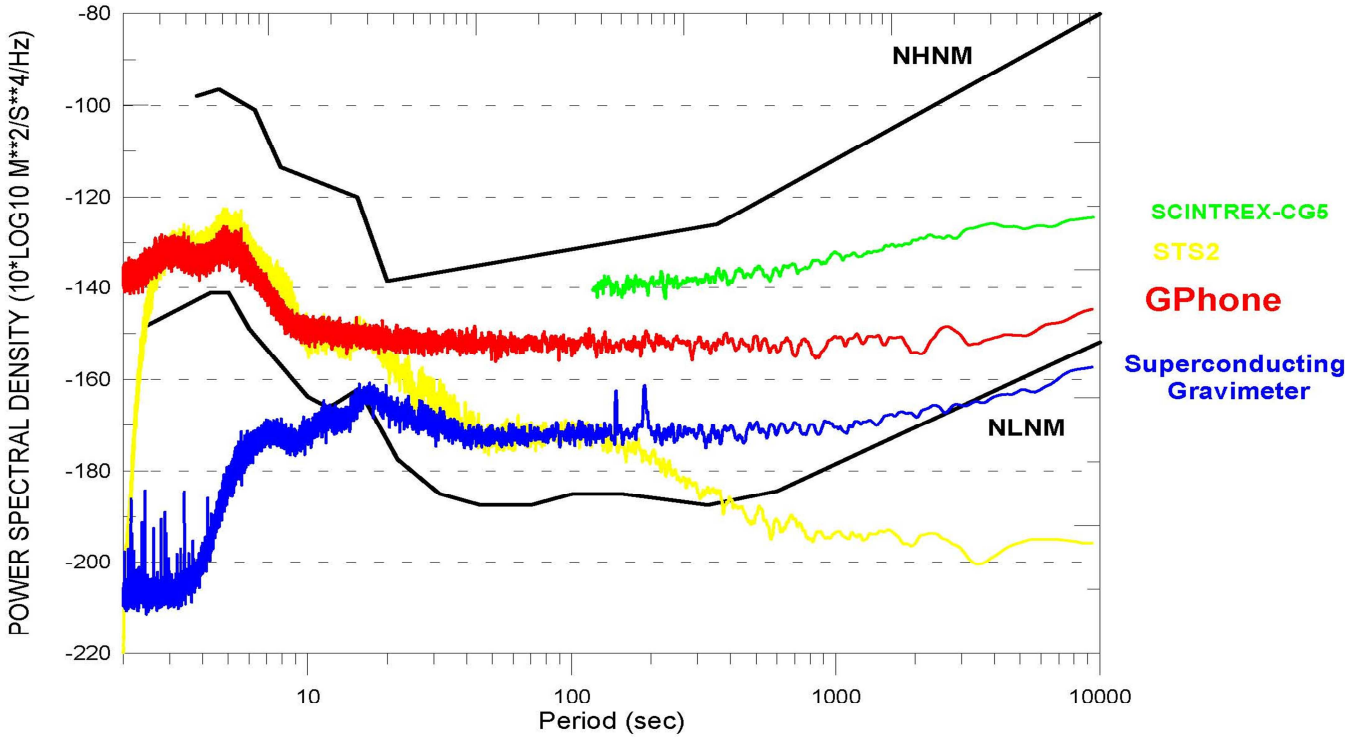


**Figure 3.** Noise power spectral density (in decibel) of the superconducting gravimeter CT-040, gPhone#32, Scintrex CG5 #010 and a STS-2 broadband seismometer, measured in 2005 in the Walferdange Underground Laboratory for Geodynamics (Luxembourg). It shows the variation of the noises as function of the period as compared to the USGS (Peterson, 1993) low noise model (NLNM) and USGS high noise model (NHNM) with respect to vertical ground acceleration.

## 3. Observations

We used 940 days of gPhone#59 data from 04-18-2009 to 12-01-2012. The raw gravity and atmospheric pressure data are displayed in Figures 4. There are 33 gaps in the time series due to power outages, very common in Tahiti.

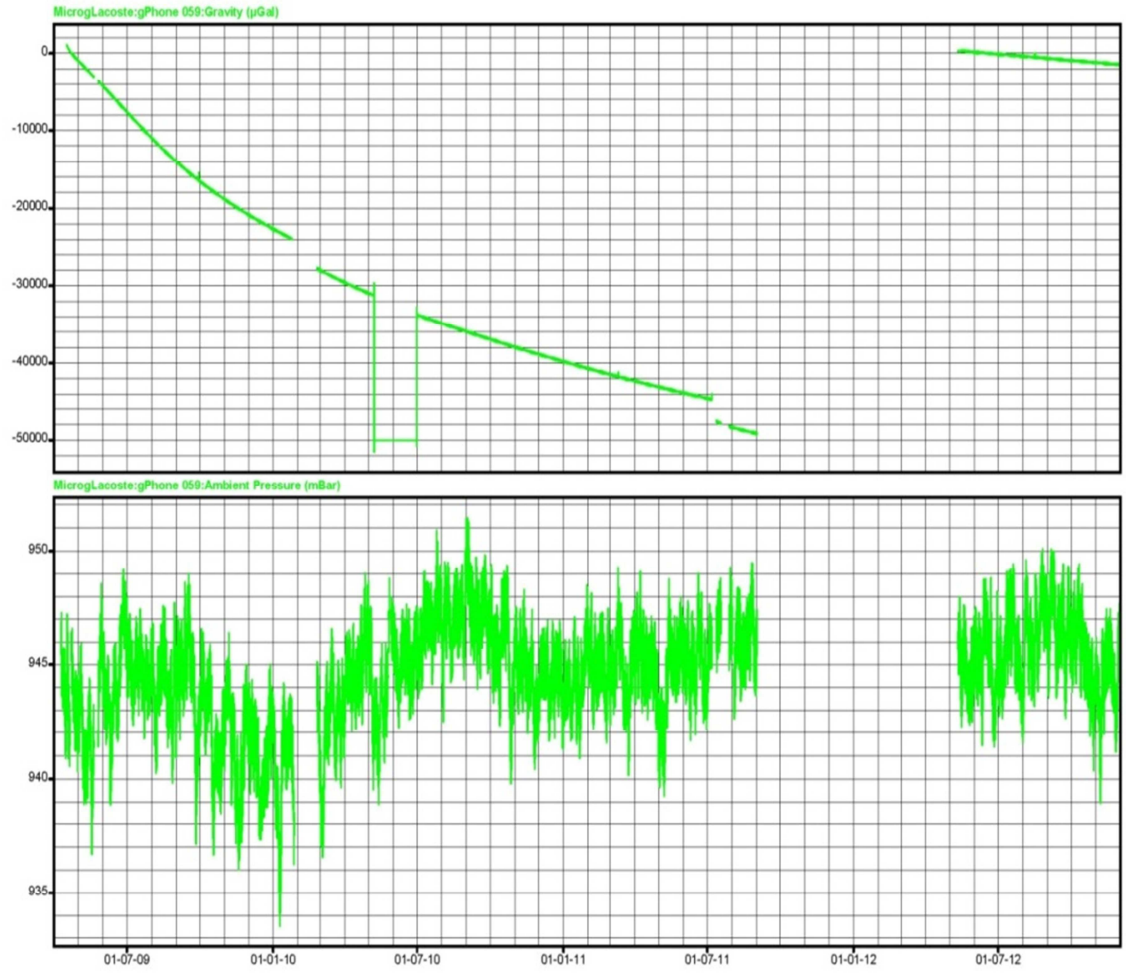


**Figures 4**. Raw gravity data (top) of the gPhone#059 spring gravimeter and atmospheric pressure observations (bottom), from 04-18-2009 to 12-01-2012, at the vault of Figure 2.

A zoom on the 1-second data (Figure 5) reveals two interesting characteristics of the gravity measurements on an island in the middle of the South Pacific. First, we observe the presence of a huge micro-seismic noise due to the sea swell. It mainly originates from Antarctica with period between 5 s to 25 second with a peak at 10 seconds. In the same figure, we compare with data collected at the same time in a station near Montpellier (South of France) with the gPhone#32 from the University of Luxembourg. The magnitude of the micro-seismic noise in Tahiti is astounding: one cannot even see any tidal signal… Using a low-pass filter, the micro-seismic noise can be eliminated from the raw observations (straight lines in the figure).

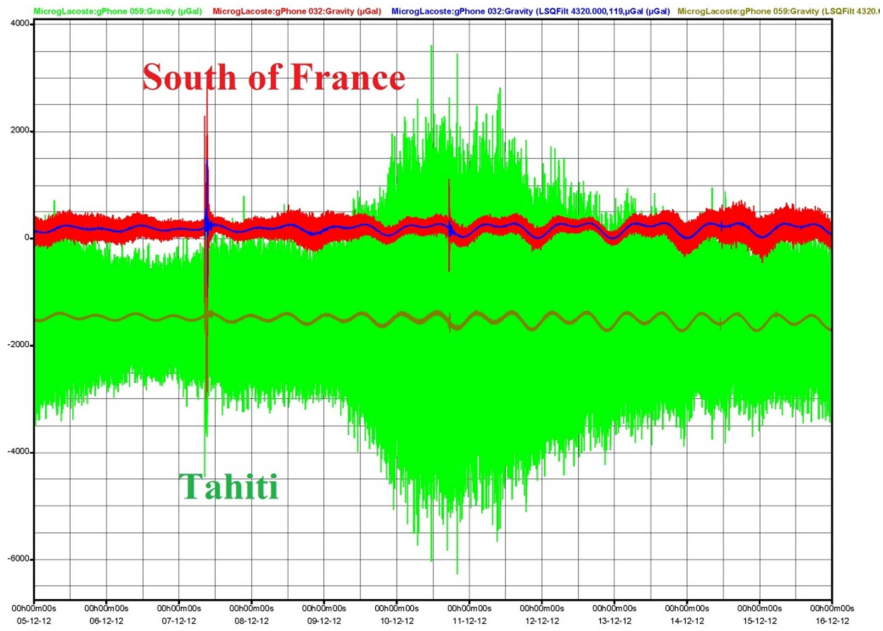


**Figure 5.** Comparison between the gravity observations in Tahiti (gPhone#59) and in a station near Montpellier in the South of France (gPhone#32). The "green buldge" in the middle of the figure is due to high sea swell around Tahiti during that period.

In Figures 6, we compare the atmospheric pressure data from the two same stations. The strong semi-diurnal signal in the barometric pressure in Tahiti is also striking.

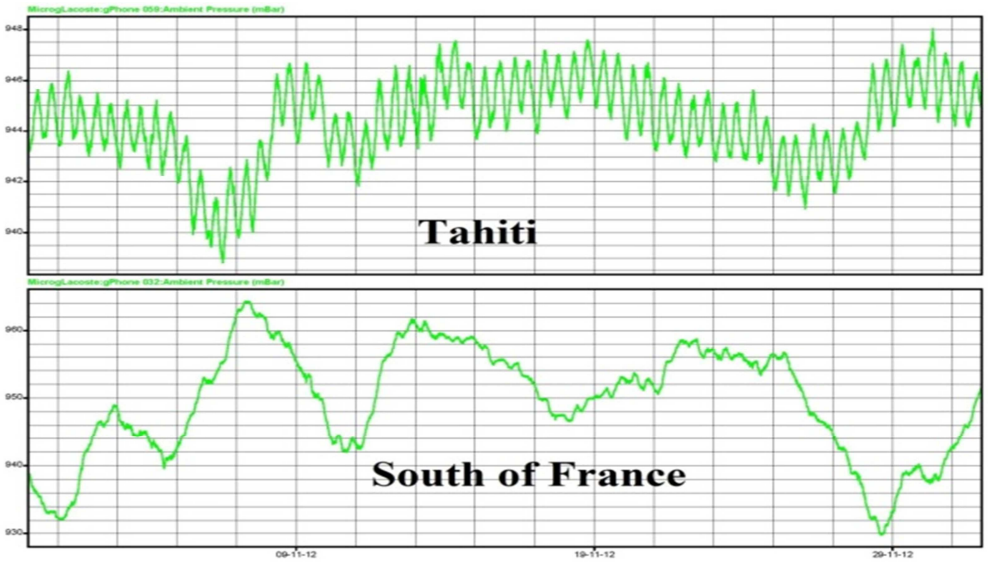


**Figures 6.** Comparison between the atmospheric pressure recordings in Tahiti and in a station near Montpellier in the South of France.

**Table 1.** Tidal Parameters at Tahiti-Pamatai estimated using 940-days of observations taken with the gPhone#59 (from 04-18-2009 to 12-01-2012).

| Wave | Start frequency /cpd | End frequency /cpd | Amplitude /nm/s$^2$ | Amplitude Factor | Standard Deviation | Phase Lead /degree | Standard deviation /degree |
|---|---|---|---|---|---|---|---|
| $SGQ_1$ | 0.721499 | 0.833113 | 1.636 | 1.2393 | 0.0722 | 0.94 | 4.14 |
| $2Q_1$ | 0.851182 | 0.859691 | 5.287 | 1.1676 | 0.0222 | 2.37 | 1.27 |
| $SGM_1$ | 0.860896 | 0.870023 | 6.434 | 1.1775 | 0.0185 | 0.89 | 1.06 |
| $Q_1$ | 0.887325 | 0.896130 | 40.026 | 1.1697 | 0.0029 | 1.47 | 0.16 |
| $RO_1$ | 0.897806 | 0.906315 | 7.616 | 1.1717 | 0.0151 | 0.98 | 0.87 |
| $O_1$ | 0.921941 | 0.930449 | 208.725 | 1.1679 | 0.0005 | 0.83 | 0.03 |
| $TAU_1$ | 0.931964 | 0.940488 | 2.762 | 1.1848 | 0.0412 | -4.99 | 2.36 |
| $NO_1$ | 0.958085 | 0.966756 | 16.241 | 1.1554 | 0.0058 | -0.74 | 0.33 |
| $CHI_1$ | 0.968565 | 0.974189 | 3.151 | 1.1723 | 0.0349 | -0.40 | 2.00 |
| $PI_1$ | 0.989048 | 0.995144 | 5.505 | 1.1322 | 0.0207 | 0.87 | 1.18 |
| $P_1$ | 0.996967 | 0.998028 | 95.2 | 1.1448 | 0.0012 | -0.21 | 0.07 |
| $S_1$ | 0.999852 | 1.000148 | 2.218 | 1.1283 | 0.0752 | -3.86 | 4.92 |
| $K_1$ | 1.001824 | 1.003651 | 285.279 | 1.1350 | 0.0004 | -0.21 | 0.02 |
| $PSI_1$ | 1.005328 | 1.005623 | 2.16 | 1.0986 | 0.0509 | 5.28 | 2.93 |
| $PHI_1$ | 1.007594 | 1.013689 | 4.221 | 1.1796 | 0.0280 | -3.41 | 1.60 |
| $TET_1$ | 1.028549 | 1.034467 | 2.98 | 1.1088 | 0.0353 | 0.48 | 2.02 |
| $J_1$ | 1.036291 | 1.0448 | 15.855 | 1.1280 | 0.0067 | -0.47 | 0.39 |
| $SO_1$ | 1.064841 | 1.071083 | 2.415 | 1.0356 | 0.0422 | 6.90 | 2.41 |
| $OO_1$ | 1.072583 | 1.080945 | 8.626 | 1.1217 | 0.0112 | -0.96 | 0.64 |
| $NU_1$ | 1.099161 | 1.216397 | 1.677 | 1.1391 | 0.0571 | 2.36 | 3.27 |
| $EPS_2$ | 1.71938 | 1.83797 | 5.953 | 1.1819 | 0.0376 | 0.27 | 2.15 |
| $2N_2$ | 1.85392 | 1.862429 | 20.099 | 1.1636 | 0.0118 | -0.06 | 0.68 |
| $MU_2$ | 1.863634 | 1.872142 | 24.465 | 1.1736 | 0.0098 | 0.59 | 0.56 |
| $N_2$ | 1.888387 | 1.896748 | 149.738 | 1.1471 | 0.0015 | 1.03 | 0.09 |
| $NU_2$ | 1.897954 | 1.906462 | 28.372 | 1.1443 | 0.0080 | 1.12 | 0.46 |
| $M_2$ | 1.923765 | 1.942754 | 783.127 | 1.1486 | 0.0003 | 1.36 | 0.02 |
| $LAM_2$ | 1.958232 | 1.963709 | 5.838 | 1.1613 | 0.0390 | 2.02 | 2.23 |
| $L_2$ | 1.965827 | 1.976926 | 21.948 | 1.1389 | 0.0100 | 0.69 | 0.57 |
| $T_2$ | 1.991786 | 1.998288 | 21.015 | 1.1335 | 0.0108 | 0.23 | 0.62 |
| $S_2$ | 1.999705 | 2.000766 | 354.057 | 1.1162 | 0.0008 | 1.07 | 0.10 |
| $K_2$ | 2.00259 | 2.013689 | 96.062 | 1.1142 | 0.0022 | 1.21 | 0.13 |
| $ETA_2$ | 2.031287 | 2.04739 | 5.353 | 1.1105 | 0.0379 | 4.16 | 2.17 |
| $2K_2$ | 2.067579 | 2.182844 | 1.411 | 1.1179 | 0.1066 | 3.60 | 6.11 |
| $MN_3$ | 2.753243 | 2.869714 | 3.867 | 1.1033 | 0.0156 | 0.56 | 0.89 |
| $M_3$ | 2.89264 | 3.081254 | 14.249 | 1.1156 | 0.0043 | -0.15 | 0.24 |

## 4. Tidal analysis

The raw 1-second data (Figures 4) were edited for spikes and other non-tidal disturbances mostly due to earthquakes using Tsoft (van Camp and Vauterin, 2005). The corrected data were then decimated to hourly data by applying a low-pass filter with a cutoff period of 2 hours. An Earth tidal analysis was performed using the ETERNA software (Wenzel, 1996) in which the tidal parameters, the amplitude factor (delta factor) and phase (alpha), were estimated simultaneously with the barometric admittance factor.

The results of the tidal analysis are presented in Table 1. Due to the length of the time series, it was possible to recover 37 tidal waves in the diurnal and semi-diurnal bands. The barometric admittance is -2.51 +/-0.15 $nm/s^2/mbar$.

## 5. Discussion

The estimated delta factors for the diurnal and semi-diurnal tides are displayed in Figures 7 and 8. We also corrected the observed tidal parameters for the ocean loading and attraction effects using three different global ocean tides models (Table 2): Schwiderski, FES2004 (Lyard et al., 2006) and CSR3.0 (Eanes and Bettadpur, 1995). Overall, the agreement between the experimental and theoretical tidal factors, hereafter called WDD theoretical model (Dehant et al., 1999), improves with the oceanic loading and attraction effects correction whatever ocean tide models are used. In average, the CSR3.0 model performs the best. The corrected tidal factors are very close to the theoretical values for $Q_1$, $N_2$ and $M_2$. The discrepancies for $S_2$ and $K_2$ could be due to the strong amplitude of the semi-diurnal signal in the atmospheric pressure or errors in the ocean tides models. A frequency dependent barometric admittance factors may be required for a better correction.

The results in the diurnal band have no apparent sign of any error on the gravimeter calibration factor. The discrepancies in both diurnal and semi-diurnal bands are most likely due to the imperfections in the oceanic loading and attraction calculation. Those affect less the results in the diurnal band as the oceanic loading and attraction is 3 times smaller than in the semi-diurnal band. It is worth to improve the ocean tides maps and methods to compute the direct gravitational attraction of the nearby tidal water masses. One way would be to include local and regional ocean tides maps. As already mentioned, the barometric admittance factor may also play a role in the semi-diurnal band especially for $S_2$ and $K_2$.

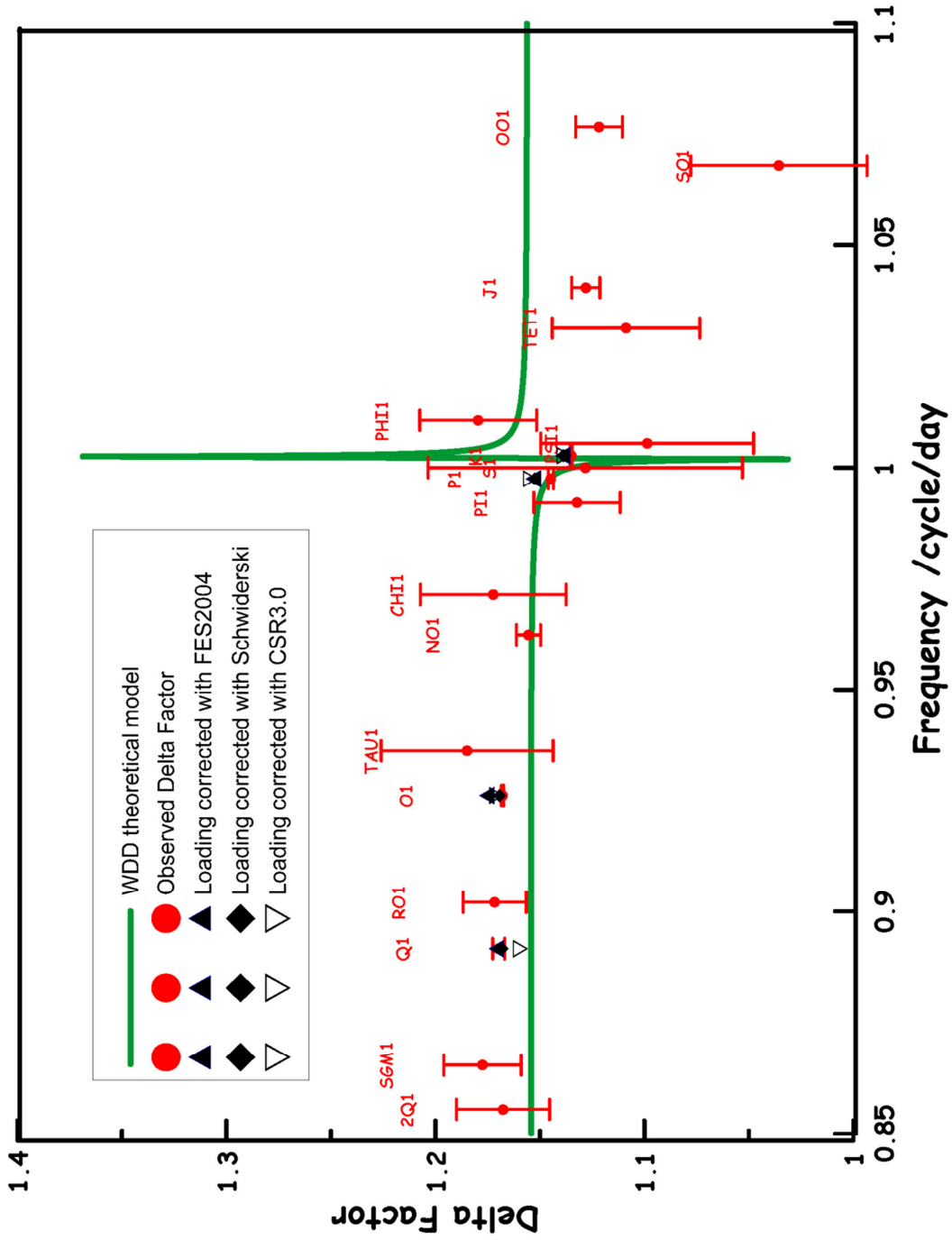


**Figure 7.** Observed diurnal tidal parameters (red dots). When a tides model is available the observed delta factors are corrected for oceanic loading and attraction (see legend in the figure). The continuous green line represents the WDD Earth tide model.

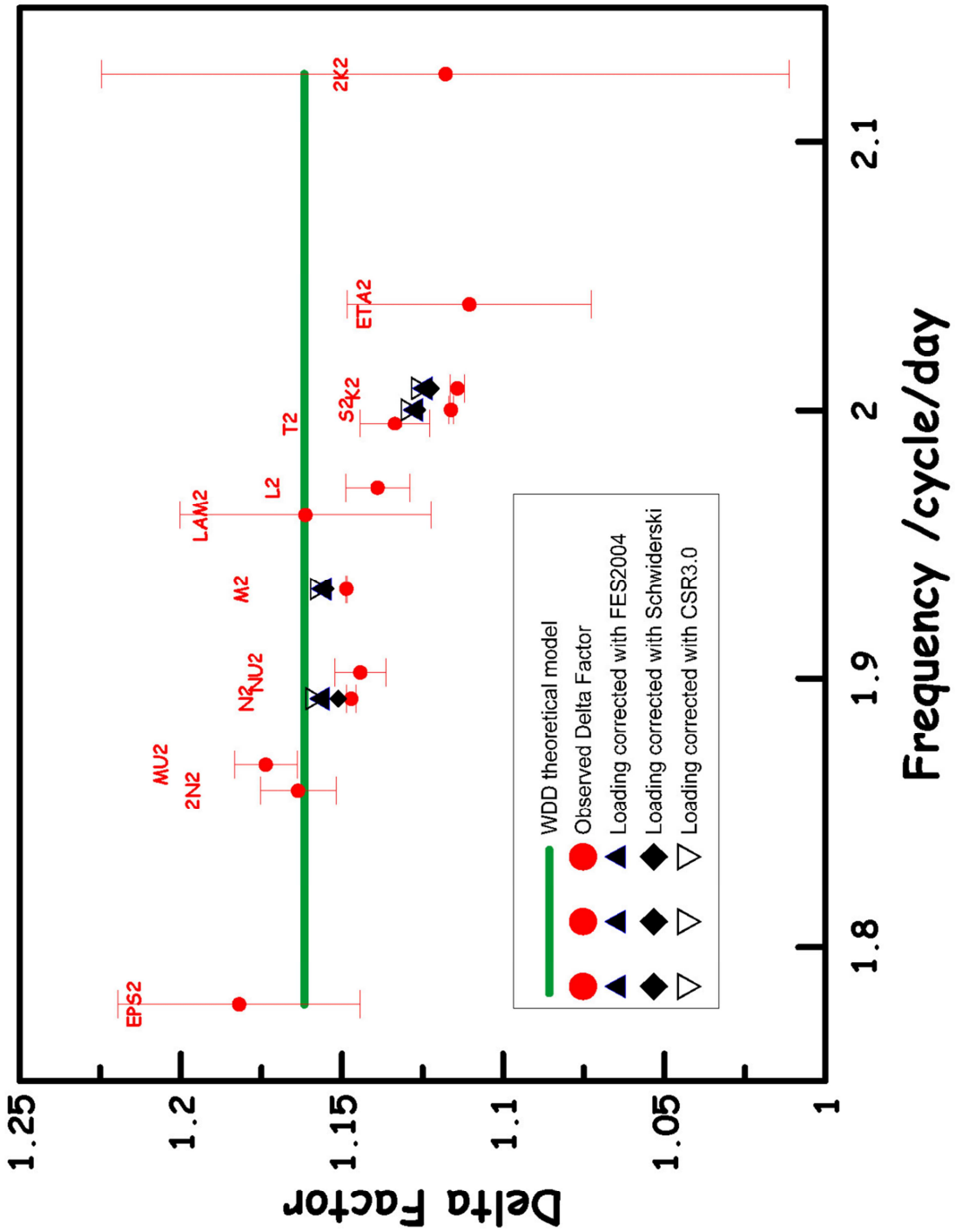


**Figure 8.** Observed semi-diurnal tidal parameters (red dots). When a tides model is available the observed delta factors are corrected for oceanic loading and attraction (see legend in the figure). The continuous green line represents the WDD Earth tide model.

**Table 2.** WDD body Earth tides model compared to the observed tidal parameters corrected for the oceanic loading and attraction effects from 3 different global ocean tides models.

| Wave | WDD model | Observed tidal parameters corrected for the oceanic loading and attraction effects | | | | | |
|---|---|---|---|---|---|---|---|
| | | Schwiderski | | CSR3.0 | | FES2004 | |
| $Q_1$ | 1.1541 | 1.1681 | 1.62 | 1.1593 | 1.37 | 1.1695 | 1.39 |
| $O_1$ | 1.1541 | 1.1692 | 0.59 | 1.1708 | 0.73 | 1.1741 | 0.74 |
| $P_1$ | 1.1493 | 1.1524 | -0.18 | 1.1546 | -0.25 | 1.1519 | -0.19 |
| $K_1$ | 1.1357 | 1.1387 | -0.08 | 1.1384 | -0.31 | 1.1378 | -0.20 |
| $N_2$ | 1.1617 | 1.1512 | 0.94 | 1.1582 | 0.84 | 1.1559 | 0.63 |
| $M_2$ | 1.1617 | 1.1551 | 0.79 | 1.1569 | 1.10 | 1.1554 | 0.93 |
| $S_2$ | 1.1617 | 1.1266 | 1.01 | 1.1287 | 1.24 | 1.1269 | 1.11 |
| $K_2$ | 1.1617 | 1.1224 | 1.24 | 1.1254 | 1.23 | 1.1240 | 1.05 |

In the ICET data bank (Melchior, 1994), we found the results of the tidal analysis of a previous registration of 163.5 days near the Tahiti-Pamatai site with the LaCoste-Romberg#402 by Ducarme in 1997. In figure 9, the results of 1997 are compared with the results of the gPhone#59 in the diurnal band after corrections for the oceanic tidal loading and attraction effects. The precision of the tidal factors is drastically improved. It also appears that the results of the gPhone#59 are in better agreement with the WDD model. There may be a few explanations: the better calibration of the gPhone#59 by the manufacturer MicrogLaCoste Inc., the duration of our records which is four to five times longer than the previous one in 1997, and the improvement in the hardware and software of the gravimeter.

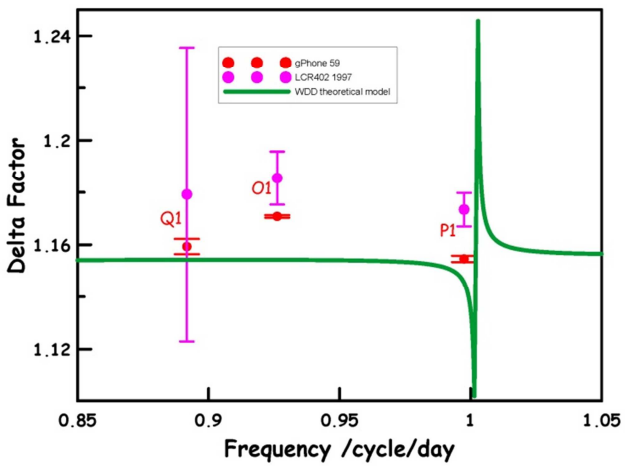


**Figure 9.** Comparison of the tidal parameters in Tahiti obtained from the LaCoste-Romberg#402 in 1997 and from the gPhone#59, corrected for the ocean tidal loading and attraction effects. The continuous green line represents the WDD Earth tide model.

## 6. Conclusions

We presented the tidal analysis results of 940 days of gravity measurements with the gPhone#059 in Tahiti. The observations are unique in terms of the presence of an impressive micro-seismic noise and a strong semi-diurnal atmospheric pressure signal. The new observed tidal parameters shows a better fit to the WDD model. However, a comparison with the WDD Earth tides model reveals that the ocean tides loading and attraction effect calculations are very effective for some waves but could still be improved for a few others. Future works will also focus on comparing the measurements of the gPhone with those of the Geoscope seismometers as well as on investigating the observations in terms of loading and hydrology.

## Acknowledgments

The gPhone#59 of the Geodesy Observatory of Tahiti was bought in 2008 thanks to funds from the French Space Agency (CNES) and the University of French Polynesia (UPF). It is operated in an isolated vault provided by the French Atomic Energy Agency (CEA) in the high Pamatai valley of Tahiti. This paper was presented during the 17th International Symposium on Earth Tides, “Understand the Earth”, 15-19 April, 2013, Warsaw, Poland.

## References

Clouard V., and Bonneville A., Submarine landslides in Society and Austral Islands, French Polynesia: evolution with the age of edifices in submarine mass movements and their consequences, edited by Locat J., and Mienert J., pp. 335-341, Kluwer Academic Publishers, 2003.

Dehant V., Defraigne P., and Wahr J.M., Tides for a convective Earth, J. Geophys. Res., 104, B1, 1035-1058, 1999.

Eanes R.J., and Bettadpur S., The CSR 3.0 global ocean tide model, Technical Memorandum CSR-TM-95-06, Center for Space Research, University of Texas, Austin, Texas, 1995.

Hildenbrand A., Gillot P.-Y., and Marlin, C., Geomorphological study of long-term erosion on a tropical volcanic ocean island: Tahiti-Nui (French Polynesia), Geomorphology, 93,460-481, 2008.

Lyard F., Lefevre F., Letellier T., and Francis O., Modelling the global ocean tides: modern insights from FES2004, Ocean Dynamics, DOI 10.1007/s10236-006-0086-x, 2006.

Melchior P., A new data bank for tidal gravity measurements (DB92), Phys. Earth Planet Int., 82, 125-155, 1994.

Peterson J., Observations and modeling of seismic background noise, U.S. Geological Survey, Open-File, report 93-322, 95 pp., 1993.

Van Camp M., and Vauterin P., Tsoft: graphical and interactive software for the analysis of time series and Earth tides, Computers in Geosciences, 31(5) 631-640, 2005.

Wenzel H-G., The nanogal software: Earth tide data processing package: ETERNA 3.3, Bulletin d'Information des Marées Terrestres, 124, 9425-9439, 1996.

# Theoretical Basis for Earth Tide Analysis with the New ETERNA34-ANA-V4.0 Program

**Klaus Schueller**

397/75 Moo 13,Baan Bunhiranyarak, T.Nokmueang, A.Mueang Surin Province 32000, Thailand,
klaus.e.schueller@t-online.de

## Abstract

The theoretical basis for the new version of the ETERNA34 program for Earth tide analysis is presented. The functional model for the least squares analysis is derived including the tidal signal and additional processes. A hypothesis-free model of higher potential degree constituents in the basic tidal wave groups is introduced. For physical regression processes transfer functions of arbitrary length can be modelled leading to frequency dependent regression coefficients and phase shifts. The least squares parameter estimation is discussed especially with respect to the impacts of window functions, leading to maximum resolution and minimum leakage least squares estimators. The condition number $\kappa$ , derived from the eigenvalues of the normal equation matrix , proved to be the overall quality criterion. The stochastical model, as implemented in the new version, is explained, now being fully in accordance with least squares theory. It is emphasized that spectrum estimation of the residuals should be based on its autocovariance function. Furthermore, it is shown, how the processing of the residuals is performed by a new tool, the "High Resolution Spectral Analyser". Finally, the problem of time-variant parameters is examined and proposals are given for detection and interpretation.

**Keywords**: tidal analysis, ETERNA, window functions, least squares, parameter estimation, error propagation, autocovariance function, residual spectrum.

## Introduction

The objective of this initiative is to acknowledge and preserve the extraordinary intellectual and technical work of my colleague and friend Prof. Dr.-Ing. habil. Hans-Georg (Schorsch) Wenzel who passed away a long time ago. Therefore, the intention is to maintain and enhance a comprehensive and sustainable platform for Earth tide analysis which will meet the requirements of the user community all over the world.

Over the past years a considerable amount of tasks has piled up which has to be tackled and solved now. As a result of recent efforts the **new version ETERNA34-ANA-V4.0** is ready to be released to interested scientists totally free of charge.

The most important features of the new **version** are:

- Enhancement of the functional model
  - Hypothesis free modelling of the higher orders of the tidal force development.
  - Modelling of additional harmonics of tidal and non-tidal origin.
  - Modelling of transfer functions of physical regression processes leading to frequency dependent regression coefficients and phase shifts
  - Comprehensive uniform polynomial model with identical coefficients for each block.
  - Deployment of window function in combination with the least squares technology for improving analysis design and interpretation.
- Redesign of the stochastical model now fully based on statistical theory
  - Frequency dependent RMS $m_0$ of arbitrary spectral ranges over the whole Nyquist interval, derived from the spectrum of the autocovariance function of the residuals.
  - Derivation of 95% confidence intervals for the frequency dependent RMS $m_0$ and all estimated parameters, now in full agreement with least squares and statistical theory.
- Information enhancements
  - Introducing the "High Resolution Spectral Analyser (HRSA)" for thoroughly analysing the residuals and estimating and presenting residual amplitudes together with their signal to noise ratios.
  - Correction of the main tidal constituent parameters for ocean influence.
  - Comparing the corrected parameters with those of different Earth models.
  - Consequent parameterization for gaining the utmost flexibility for the users of Earth tide analysis.
- Computer platforms
  - Providing an executable of the new **ETERNA34-ANA-V4.0 version** on MS Windows 7 and 8.1.
  - Support of 32- and 64-bit MS-Windows computers.
- Further maintenance and enhancement
  - Fixing detected software problems.
  - Survey and realizing of common user requirements.
  - Realizing already planned enhancements like
    - Estimating the frequency transfer functions of physical channels as performed in the HYCON method (SCHUELLER, K. 1986).
    - Built-in time-variant analysis as performed in the HYCON method

In this presentation some important concepts of statistical inference are revisited in order to provide the basis for the latest modifications and enhancements of the ETERNA program. We will refer to the modified ETERNA program as "**the new version**" throughout this presentation. Generally, no derivations or proofs of formulas will be given, when they can easily be reviewed in literature. Also, program descriptions and implementation aspects will be dealt with in a different paper, the "**ETERNA34-ANA-V4.0 USER's GUIDE**" (SCHÜLLER, K. 2014).

# 1. The Earth tide observation process

## 1.1 The sampling process in time domain

We think of a tidal observation record as the realization of the ubiquitous tidal force as input to specific instruments ( gravimeter, pendulums, strain meters etc.). This tidal force signal can then be thought of being the output y(t) of a system, ideally with infinite past and future. We assume this system to be linear and comprising all features of measurement, calibration, etc.. In the following the notations for the tidal vertical component and gravimeter observations are used although the derivatives and conclusions are analogously valid for the other components.
The sampling process, i.e. the analogue-digital converter itself and the confinement of y(t) to a specific observation interval T can be abstracted by the following model:

Let the Dirac $\delta$ –function be

$$\delta(x) = \begin{cases} +\infty, & x = 0 \\ 0, & x \neq 0 \end{cases}$$

with

$$\int_{-\infty}^{\infty} \delta(x)\, dx = 1 \qquad (1.1)$$

From (1.1) the so-called Dirac comb is generated as pulse train of N unity values:

$$\mathrm{i}(t_m) = \sum_{m=-\infty}^{\infty} \delta(t - m\Delta) \qquad \{m = 0,1,2, \ldots . N \qquad (1.2)$$

with Δ as the **sampling interval** between two consecutive values.

Let

$$w(t) = \begin{cases} 1 & -T/2 \leq t \leq T/2 \\ 0 & elsewhere \end{cases} \qquad (1.3)$$

be a continuous rectangular function representing the time interval T of an observation record, then

$$\mathrm{w}(t_m) = \mathrm{w}(t) \cdot \mathrm{i}(t_m) \qquad (1.4)$$

is a discrete rectangular function at discrete time points $t_m$ in the interval T = NΔ.

The discrete observations at time $t_m$ =mΔ within the observation period T will now be derived by (Fig.1.1) :

$$y(t_m) = \mathrm{y}(t) \cdot \mathrm{w}(t_m) \qquad (1.5)$$

The function w ($t_m$) is known as discrete time **window function** which often is not explicitly represented in subsequent formulas. Its importance, however, will be explained in next sections.

**Fig. 1: From continuous to sampled observations.**

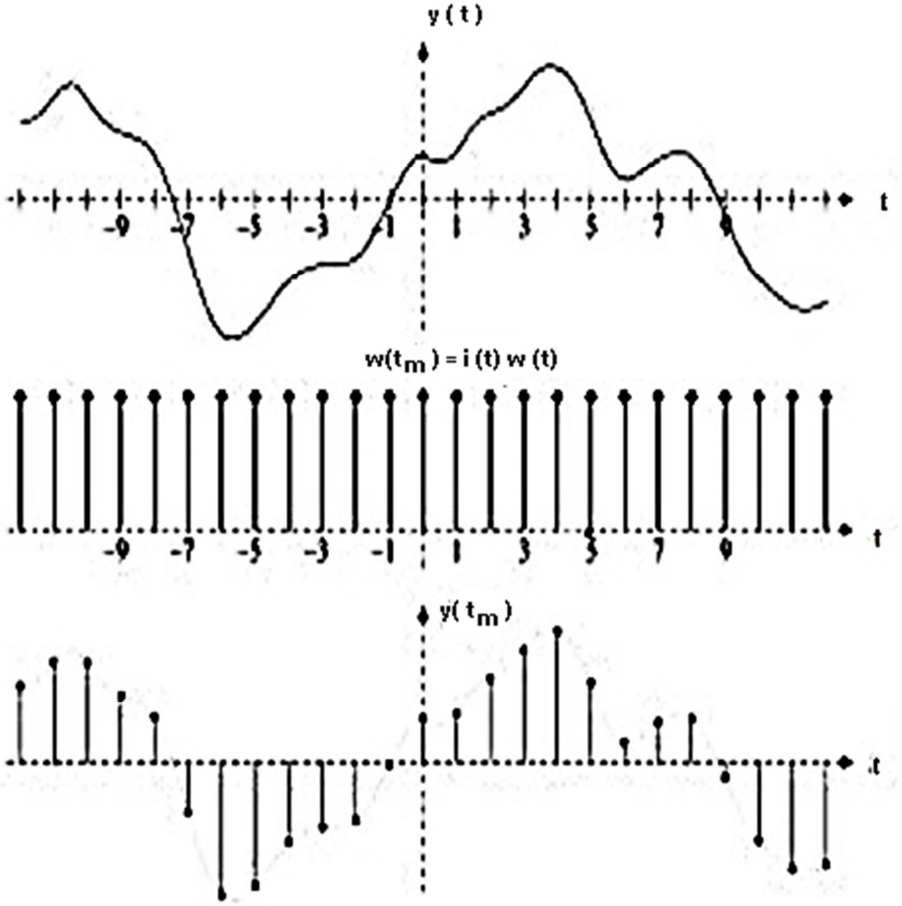


## 1.2 Frequency domain representation of sampled time series

Associated with the time domain, there exists a frequency domain representation for y(t), the so called "true" spectrum Y($\omega$). $Y(\omega)$ is continuous in frequency with an infinite frequency range. Both representations are linked by Fourier transformation:

$$y(t) = \frac{1}{2\pi}\int_{-\infty}^{\infty} Y(\omega)e^{i\omega t}d\omega \qquad (1.6a)$$

and

$$Y(\omega) = \int_{-\infty}^{\infty} y(t)e^{-i\omega t}dt \qquad (1.6b)$$

Likewise, the discrete time window function $w(t_m)$ of (1.4) as sampling function possesses a frequency domain representation W($\omega$), the so-called spectral window function. Because $w(t_m)$ is a rectangular function, W($\omega$) can analytically be written as discrete sinc-function :

$$W_R(\omega) = \frac{\Delta}{N}\frac{\sin(\frac{\omega N\Delta}{2})}{sin(\frac{\omega\Delta}{2})} \qquad (1.7)$$

**Fig. 2 : sinc-function,** $\Delta = 1$

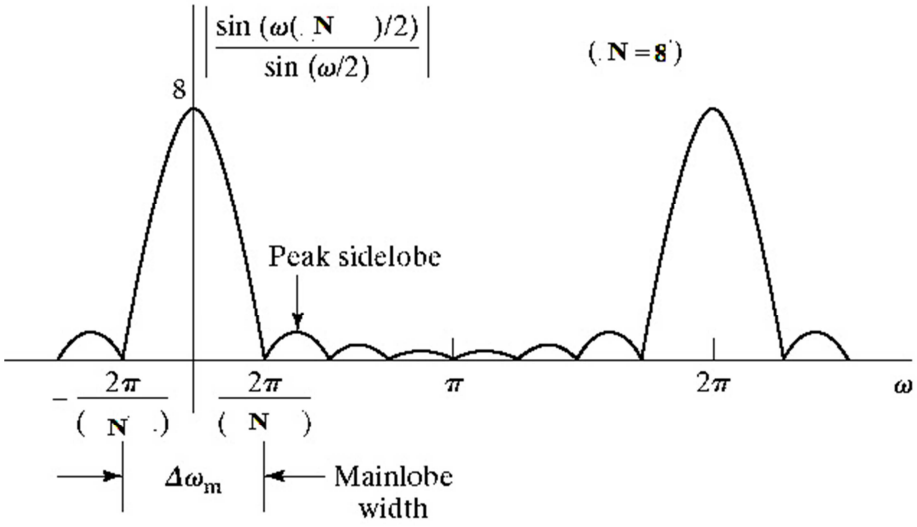


Since multiplication of any two time series in the time domain means convolution of their two spectra in the frequency domain, we obtain the spectral representation $Y^{OBS}(\omega)$ of an observed time series y(t) as the **convolution** of the theoretical "true" spectrum $Y(\omega)$ with the spectral window $W(\omega)$ :

$$Y^{OBS}(\omega) = \int_{-\infty}^{\infty} y(t)w(t)e^{-i\omega t}dt$$

$$= \int_{-\infty}^{\infty} Y(\lambda)W(\omega - \lambda)d\lambda \qquad (1.8)$$

Fig. 2 and (1.8) exhibit that the spectral window $W(\omega)$ acts as a "slit" function through which we see the true spectrum $Y(\omega)$ within an uncertainty. The width of that slit is governed according to (1.7) by $T = N\Delta$ , the length of the observation record. Also, we can imagine the convolution process (1.8) as bringing W(0) (the origin of $W(\omega)$) in coincidence with a specific peak of the true spectrum $Y(\omega)$ and then taking a weighted sum of $Y(\omega)$ over the whole frequency range with $W(\omega)$ as the weight function.

**Conclusion:**
The time window function $w(t_m)$ is fundamentally associated with the observation record because it contains all information about its frequency domain properties. The spectral window function $W(\omega)$ not only has a main lobe but is stretching over frequency with considerable side lobe peaks (see Fig. 2). Consequently, the result of the convolution at a certain frequency will be more or less a mix or smear of the "true" $Y(\omega)$ over the whole frequency domain.

## 1.3 General properties of window functions

It follows from (1.7) and Fig.2 that there are 2 properties which are of utmost importance when dealing with window functions, i.e.

- 1. Resolution
- 2. Side lobe convergence

Resolution is directly linked to the width of the main lobe, and is characterized by the frequency distance from the centre of the main lobe to the 1st zero position (Fig. 2). A considerable amount of window functions are offered in literature (some of them are represented in Fig. 3), but no window functions which optimally incorporate both properties.

For the rectangular window this distance is identical to the fundamental (Fourier) frequency $\omega_0$ (1.7) which is defined as

$$\omega_0 = \frac{2\pi}{T} \quad = \frac{2\pi}{N\Delta} \tag{1.9}$$

The rectangular window stands for a window function class with optimal resolution but rather poor side lobe convergence (Fig.4,6).

The Hanning window stands for a second class of window functions with optimal side lobe convergence (Fig. 5, 6) but double frequency distance from the centre of the main lobe to the 1st zero position, i.e. $2\,\omega_0$ . That means that its resolution is 2 times less the rectangular window. Its representation in the time domain is

$$w_H\,(t) = \frac{1}{2}\left(1 - \cos\left(\frac{2\pi}{N-1}t\right)\right) \qquad \text{(t= 0,.....N-1 )} \tag{1.10}$$

while it's spectral window $W_H(\omega)$ can be written as a smoothed function of the rectangular window $W_R(\omega)$ (1.7) as :

$$W_H(\omega) = \frac{1}{2}W_R(\omega) + \frac{1}{4}\left(W_R\left(\omega - \frac{\omega_0}{2}\right) + W_R\left(\omega + \frac{\omega_0}{2}\right)\right) \tag{1.11}$$

**Fig. 3 : Examples of window functions in the time domain**

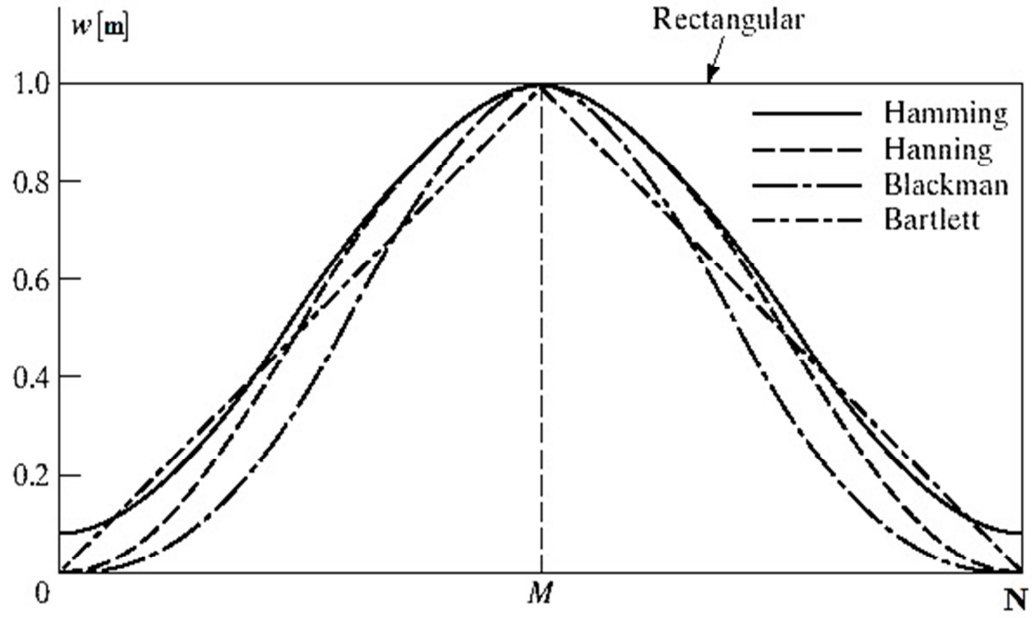

**Fig. 4 : Spectral rectangular window function**

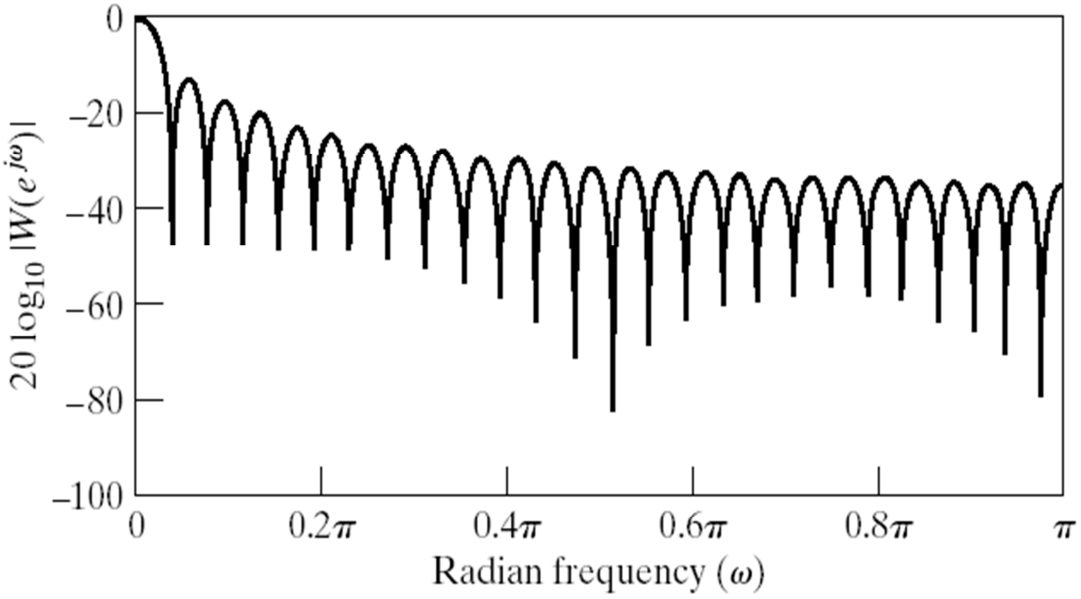


**Fig. 5 : Spectral Hanning window function**

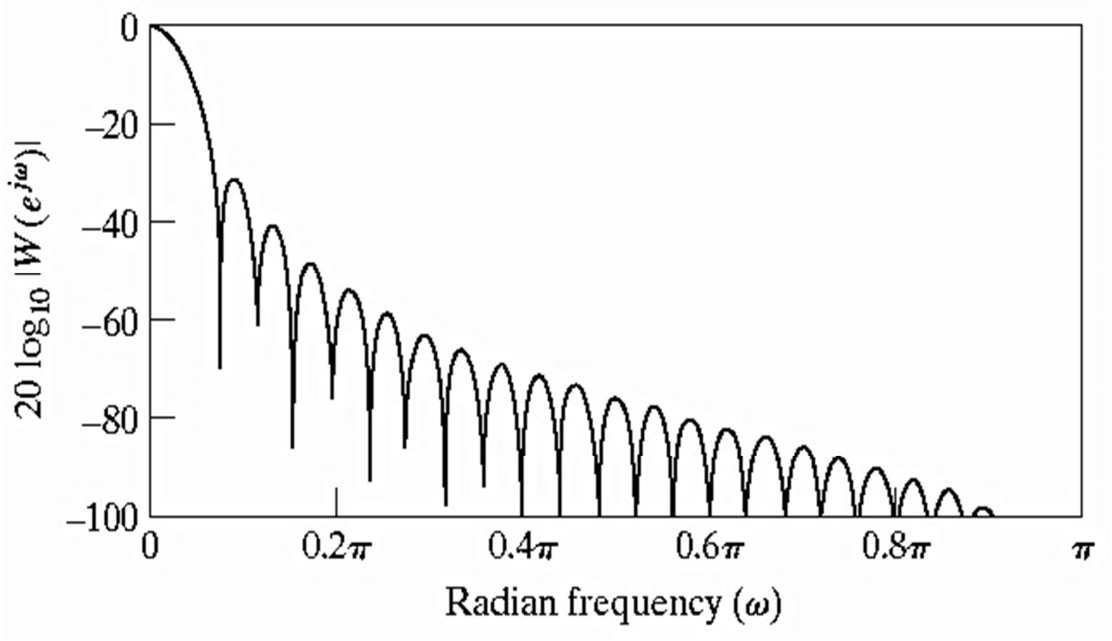


From what is presented so far, it becomes quite obvious that the application of the often cited Rayleigh-criterion is nothing else than exploiting the spectral rectangular window function: for all frequencies in the observation record to be resolved, it demands a frequency distance from the centre of the main lobe to the 1st zero position of the spectral window (Fig. 2).

It will be shown later on that is criterion is by far too pessimistic, when applied in the least squares procedure.

**Fig. 6: Presentation of the rectangular and Hanning spectral window function**

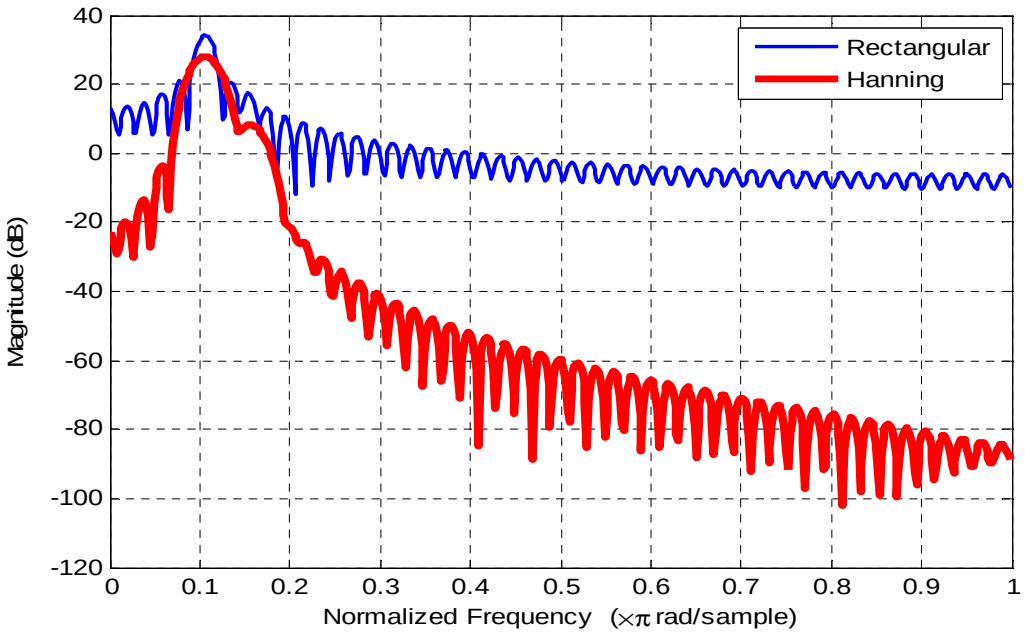


# 2. The functional model for tidal observations

## 2.1 Tidal signal

It is well known from (Chojnicki, T. 1973), (SCHÜLLER, K. 1976), (WENZEL, H.-G. 1996) that the tidal signal $y_{ET}\ (t)$ can be modelled as

$$y_{ET}\ (t) = \sum_{i=1}^{n_{wg}} \delta_i \sum_{j=1}^{l_i} A_{ij}\, cos\left(\omega_{ij} t + \varphi_{ij} + \kappa_i\right) =$$

$$\sum_{i=1}^{n_{wg}} \delta_i\, cos(\kappa_i) \sum_{j=1}^{l_i} A_{ij}\, cos\left(\omega_{ij} t + \varphi_{ij}\right) - \sum_{i=1}^{n_{wg}} \delta_i sin\,(\kappa_i) \sum_{j=1}^{l_i} A_{ij}\, sin\left(\omega_{ij} t + \varphi_{ij}\right) =$$

$$\sum_{i=1}^{n_{wg}} \delta_i\, cos(\kappa_i) e_i(t) - \sum_{i=1}^{n_{wg}} \delta_i sin\,(\kappa_i) f_i(t) \qquad (2.1)$$

where

- $n_{wg}$ - number of wave groups i, i=1,..... $n_{wg}$
- $\delta_i$ , $\kappa_i$ - tidal parameters (amplitude quotient, phase lead)
- $l_i$ - number of tidal constituents j of wave group i, j=1,... $l_i$
- $A_{ij}, \omega_{ij}, \varphi_{ij}$ - theoretical amplitudes, angular velocities and phases of the i-th tidal frequency band and the j-th constituent for a rigid model Earth
- $e_i(t), f_i(t)$ - model time signals with theoretical amplitudes, angular velocities and phases of the i-th tidal frequency band introduced for abbreviation purposes

In (2.1) the underlying assumption is that the tidal parameters are constant within the $n_{wg}$ wave groups.
However, this is principally not true, because the tidal potential is composed of different degrees l and orders m, where the orders are associated with long periodic, diurnal, semidiurnal,…etc. frequencies. The most precise development implemented in Standard ETERNA is published by (Hartmann T., Wenzel, HG. 1994) up to degree l = 6. From Earth modelling we know that the tidal amplitude factors are different for degrees 2, 3, 4, and 5 and for V2 within the different orders. Moreover, in all Earth models the phase shift $\kappa$ is supposed to be 0.

The following table shows the overlapping frequency scheme of the different potential degrees:

| | | |
|---|---|---|
| $V_{20}\ V_{30}\ V_{40}\ V_{50}\ V_{60}$ … …. | – | long periodic |
| $V_{21}\ V_{31}\ V_{41}\ V_{51}\ V_{61}$ … …. | – | 1/1-diurnal |
| $V_{22}\ V_{32}\ V_{42}\ V_{52}\ V_{62}$ … …. | – | 1/2- diurnal |
| $V_{33}\ V_{43}\ V_{53}\ V_{63}$ … …. | – | 1/3-diurnal |
| $V_{44}\ V_{54}\ V_{64}$ … …. | – | 1/4-diurnal |
| $V_{55}\ V_{65}$ … …. | – | 1/5-diurnal |
| $V_{66}$ … …. | – | 1/6-diurnal |

……..

To overcome this modelling problem in (2.1), the amplitude factors of an Earth model are introduced to harmonize the heterogeneous situation within the tidal frequency bands by

$$y_{ET}\ (t) = \sum_{i=1}^{n_{wg}} \delta_i^* \sum_{j=1}^{l_i} A_{ij}^{EM}\ co\ s\left(\omega_{ij}t + \varphi_{ij} + \kappa_i\right) =$$

$$\sum_{i=1}^{n_{wg}} \delta_i^*\ co\ s(\kappa_i) \sum_{j=1}^{l_i} \delta_{ij}^{EM} A_{ij}\ cos\left(\omega_{ij}t + \varphi_{ij}\right) - \sum_{i=1}^{n_{wg}} \delta_i^* sin(\kappa_i) \sum_{j=1}^{l_i} \delta_{ij}^{EM} A_{ij}\ sin\left(\omega_{ij}t + \varphi_{ij}\right)$$

$$= \sum_{i=1}^{n_{wg}} x_{c_i} \sum_{j=1}^{l_i} \delta_{ij}^{EM} A_{ij}\ cos\left(\omega_{ij}t + \varphi_{ij}\right) - \sum_{i=1}^{n_{wg}} x_{s_i} \sum_{j=1}^{l_i} \delta_{ij}^{EM} A_{ij}\ sin\left(\omega_{ij}t + \varphi_{ij}\right) \qquad (2.2)$$

with

$\delta_{ij}^{EM}$ = the amplitude factors of an Earth model for each potential degree and order
$A_{ij}^{EM}$ = Earth model amplitudes
$\delta_i^*$ = Amplitude factors between observed and model tide which is $\delta_i^*$= 1 in case of agreement between Earth model and observations.
$\delta_i^* co\ s(\kappa_i)$ , $\delta_i^* \sin(\kappa_i)$ -> $x_{c_i}$, $x_{s_i}$ – auxiliary tidal parameters

The approach of (2.2) is equivalent to normalizing the higher potential degree amplitudes of a wave group relative to the lowest degree by the ratio higher potential degree amplitude factor to the lower one, for example: $\delta_{V3}^{EM} / \delta_{V2}^{EM}$.

(2.2) is implemented in STANDARD ETERNA, based on the Dehant-Wahr-Zschau (DWZ) model (Zschau, J. et al 1981) of a non-hydrostatic, inelastic Earth. Since wave grouping in ETERNA assumes

consecutive frequencies for the different wave groups, no other modelling could be achieved, because the constituents belonging to a certain potential degree and order l,m do not exhibit consecutive frequencies but can be distributed all over the whole wave group.

In **the new version**, however, appropriate wave grouping can be automatically done by the program. The procedure comprises the following steps, each step meaning a more accurate model than the precursor step:

Step 0 : standard procedure by means of the DWZ Earth model = standard wave grouping.

Step 1: Grouping all constituents of a certain higher potential degree in a separate wave group, i.e. V3, V4, V5, V6 while the standard wave grouping refers to V20-V66.

Step2 : Grouping all constituents of a certain higher potential degree and order in a separate wave group, i.e. V30,V31,V32,V40,V41,V42,V43,V50,V51,V52,V53,V54,V60,V61,V62,V63,V64,V65, while the standard wave grouping refers to V20-V66.

Step3 : Grouping all constituents of a certain higher potential degree of a standard wave group as subgroup; for example: O1 will refer to V2, O1-3 to all V3 –constituents within the O1 group, O1-4 to all V4 –constituents within the O1-group etc..

Which step or combination of steps is adequate depends on the record length and model signal strength. It is important to emphasize that all steps can be arbitrarily combined. Hence, for each standard wave group one has to define which step should be used. This information has to be provided in the project.ini file by adding a 4-digit code for each wave group defined. This code is composed of 4 consecutive digits, one for each degree, beginning with V3, followed by V4, V5, and V6. The digits can take the values 0 to 3, meaning: 0 = step0, 1=step1, 2=step2, 3=step3.

By this procedure **the new version** is principally able to model the higher potential degrees and orders without relying on Earth model assumptions. In this context we will consider to implement the potential development of Kudryavtsev, S.M. 2004 of some 27000 constituents in **the new version.**

However, especially for weak model signals, shorter series, etc., it may be indicated to select the DWZ-Earth model information (step0) and combine it moderately with step1 (i.e. only moderate resolution requirements). Also, there will be relatively high mathematical correlations between these groups due to being fairly close together in frequency. Model calculations, however, proved that the numerical stability is guaranteed as long as the normal equation matrix is solvable.

## 2.2 Model enhancement by non-linear and additional harmonics

Often, the residuals of a least squares tidal analysis exhibit energy concentrations at tidal plus non-tidal frequencies. The cause of these concentrations may have various reasons, e.g.

- Oceanographic effects
  - Loading
  - Attraction of water masses
  - ……

- Meteorological influences
    - Air pressure
    - Rainfall

      ……
- Unknown influences
    - …….

The **first group** is characterised by the fact that the influencing processes are progressing with the same frequency as the Earth tides. In this case, analytical separation is not possible . Corrections can only be applied aposteri by means of load vectors from model calculations. To meet this requirement in **the new version** , loading information of different ocean models can be processed. Furthermore, in addition to the DWZ, different Earth models can be defined which will be compared to the corrected tidal parameters. Also, Melchior's amplitude ratios $\frac{\delta_{M2}}{\delta_{O1}}$ and $\frac{\delta_{O1}}{\delta_{K1}}$ are calculated and compared to the Earth models results. From all these results, conclusion can be drawn to what degree the ocean corrected parameters will fit to a specified Earth model.
In case of **non-linear loading by shallow water tides** (MERRIAM ,J.B 1995), (SCHÜLLER,K. et al 1979), loading effects in the Earth tide record can be observed at frequencies where the body tide is close to or zero at all. Since spectral estimates are comparably imprecise and usually without any error information, we want to estimate the amplitudes and phases of these non-linear **(NL)** harmonics, and also derive statistical estimates about their reliability and significance. Therefore, we calculate the frequencies of the non-linear tides according to the assumed non-linear model (usually quadratic), and introduce them together with the tidal signal as harmonics into a least squares adjustment.

The **second group** can be dealt with by monitoring these processes at the observation station with the same sampling rate as the tidal signal, and introducing this information as a regression process (section 2.4). However, if such monitoring is not available, their influence in the tidal observations cannot be identified. It may produce peaks in the residual spectrum and will be treated like the third group.

The **third group** comprises significant signals of unknown origin. The frequencies $\omega_m$ of these additional constituents **(ADCONS**) are taken from the residual spectrum or any other source of information and are fed back into the least squares adjustment.

The functional model for this enhancement can then be derived by generalizing (2.2) to

$$y_{ET}\ (t) = \sum_{i=1}^{n_{wg}} \delta_i \sum_{j=1}^{l_i} \delta_{ij}^{EM} A_{ij}\ cos\left(\omega_{ij} t + \varphi_{ij} + \kappa_{ij}\right) + \sum_{m=1}^{n_{add}} A_m\ cos(\omega_m t + \varphi_m). \quad (2.3)$$

where $\omega_m$ is given and $A_m and\ \varphi_m$ are unknown, and $n_{add}$ the number of additional constituents. Similar to the tidal potential development, the $n_{add}$ constituents are to be initially defined in a **new definition file** named **NL+ADCONST.dat**. This file serves as a memory for these constituents, and is placed in the COMMDAT directory like the tidal potential definition files. To perform a specific analysis, a selected subset of the constituents of **NL+ADCONST.dat** has to be specified in the "project".ini file, similar to the body tide wave groups.

In a subsequent least squares analysis, amplitudes and phases with respect to the 1st observation time point of the record are obtained together with their RMS-errors and confidence intervals for further treatment and interpretation. This process may be performed in several iteration cycles.

## 2.3 Enhancement of the drift model

### 2.3.1 Filters

The advantage of trend removal by filters is that their properties can mathematically be evaluated by their transfer functions which are the Fourier transforms of the filter weights.
STANDARD ETERNA provides several filters in the COMMDAT directory, which can be initialized for the analysis in project.ini definition file.
Low pass filters like Pertsev 51 or HYCON-MC-49 are provided by STANDARD ETERNA. Although Pertsev's filter is working fairly well at the low frequencies, there are significant deviations from gain values = 1 at higher frequencies. Therefore, an alternative filter also with 51 coefficients is provided in **the new version** , based on the Hanning window. This filter converges at the higher frequencies to the ideal high pass filter shape ( gain values = 1). It also lets pass a significant percentage of the long periodic tides so that an analysis is possible despite of filtering the drift.(Note that the published filter *5.nlf from HYCON is in error due to a typing mistake: the 1st coefficient must carry a minus sign.)
When dealing with minute observation data, care has to be taken due to aliasing. To avoid aliasing, a band pass filter has been designed based on the Blackman-Tuckey-Window to allow proceeding with hourly values after filtering. This filter can be found in the COMMDAT directory of **the new version** as BMLPA60M.nlf.
Since filtering is done by time domain convolution of the observations with the filter weights, this operation means multiplication of their spectra in the frequency domain. Beyond the stop band of the filter, where parameter estimation is occurring there can be significant deviations from the ideal properties, i.e. gain values = 1 as described for the Pertsev filter. Consequently, the effect of filtering has to be corrected for by applying the filter gain to the estimated amplitudes provided the filter gain is not too close to 0.
STANDARD ETERNA correctly applies the gain in parameter and error estimation. However, all spectral amplitudes and related quantities of the residuals are not accounted for filtering. **In the new version** a gain correction due to filtering will be applied to all residual amplitudes provided the gain is above a predefined level ,i.e. not too close to zero. Note that such corrections can reverse filtering only to a certain degree, because they are applied to the convolved spectrum $Y^{OBS}(\omega)$ (1.8), while the filter acts on the original $Y(\omega)$ .
STANDARD ETERNA does not allow for modelling long periodic (LP) -tides when using filters. However, there are situations when this is desirable. Therefore, in the **new version** we do allow modelling of LP tides although a numerical high pass filter has been applied. This can be useful, when the filter eliminates only the very low frequencies and letting the LP-tides pass with sufficient signal strength.
For meteorological channels, consistency with respect to the filter is gained when these channels are processes with the same filter before being introduced into an analysis.

### 2.3.2 Chebychev polynomials

Chebychev polynomials are defined as

$\cos(n\varphi) = T_n(\cos(n\varphi)) = T_n(x), \qquad x = \cos(\varphi),\ x \in [-1,1],\ n \in N$

with

$$T_0(x) = 1$$
$$T_1(x) = x$$
$$T_2(x) = 2x^2 - 1$$
$$T_3(x) = 4x^3 - 3x$$
$$T_4(x) = 8x^4 - 8x^2 + 1$$
$$\ldots\ldots\ldots\ldots\ldots\ldots\ldots\ldots\ldots\ldots$$

where

$$|T_n(x)| \leq 1 \; for \; x \in [-1,1] \quad and \; n \in N \tag{2.4}$$

The first 10 polynomials are shown in Fig. 7:

**Fig 7: Chebychev polynomials $T_0$ - $T_9$**

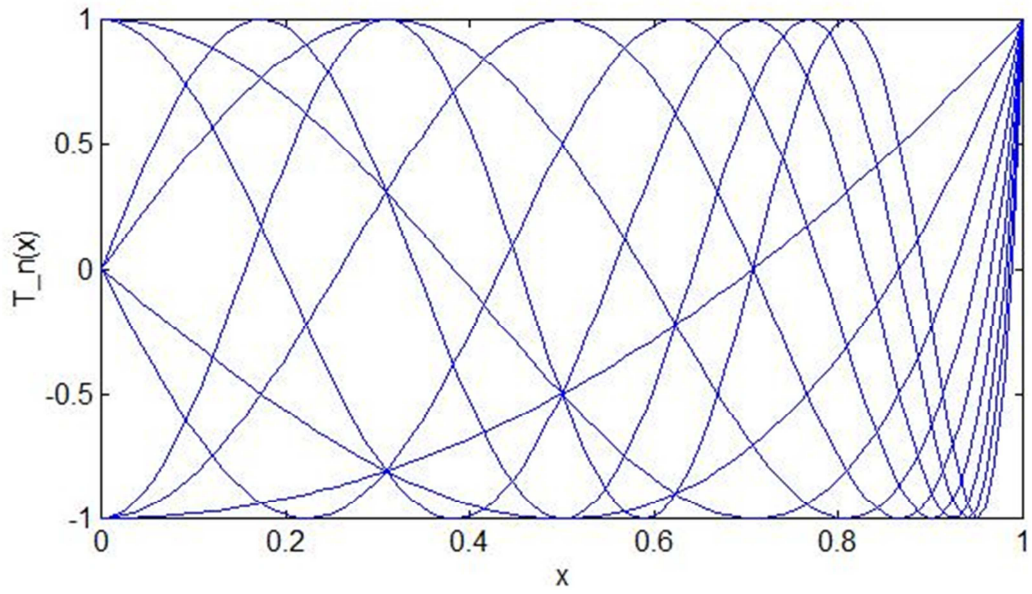


The following facts about Chebychev polynomials have to be emphasized:

- the observation interval is normalized to $\pm 1$
- the Chebychev polynomials $T_i$ are orthogonal to each other as long as there are no gaps in the record
- other as in the case of filters, where the filter gain represents the degree of effectiveness, there is no such quantity for the Chebychev polynomials.
- a reasonable measure of the effectiveness is the minimum RMS $m_0$ criterion for approximations of different order combined with a statistical t- and F-Test, testing the

effectiveness of additional model parameters with a given probability.

A heuristic rule for the order u of the Chebychev polynomials to be modelled can be adopted as

$$u < \frac{N\Delta}{P_T}$$

where $N\Delta$ is the observation interval and $P_T$ is the longest tidal period in absolute time. Otherwise, due the oscillating nature of the Chebychev polynomials (Fig.7), extremely high mathematical correlations of the polynomials with tidal (long periodic) constituents or regression processes could occur.

### *1.3.2.1 Block wise polynomial modelling*

In case of observations with gaps STANDARD ETERNA models the polynomials for each block by a different set of polynomials coefficients. This procedure has the following disadvantages:

- the Chebychev polynomials are set up for every single block without joining conditions for the parameters over the block boundaries, so they might introduce artificial, unwanted steps into the residuals.
- each block is generally different in length so there will be different number of coefficients for each block.
- the number of polynomial coefficients will be inflated when there are many gaps in the record.

### *1.3.2.2 Uniform polynomial model*

Since we have to assume that the observation record is homogeneous in such a sense that discontinuities are eliminated by data pre-processing**, the new version** optionally offers the definition of a polynomial over the block boundaries with one uniform parameter set. Hence, in case of applying polynomials as drift model ,the functional model (2.3) is extended as

$$y(t) = \sum_{i=1}^{n_{wg}} \delta_i \sum_{j=1}^{l_i} \delta_{ij}^{EM} A_{ij}\, cos\left(\omega_{ij} t + \varphi_{ij} + \kappa_{ij}\right) + \sum_{m=1}^{n_{add}} A_m\, cos(\omega_m t + \varphi_m) + \sum_{k=0}^{n_p} a_k T_k(x). \quad (2.5)$$

where

$a_k$ - k =1,… $n_p$ - polynomial coefficients also denoted as bias parameters

$T_k(x)$ - Chebychev polynomials

Moreover, in **the new version** ,the table of the bias parameters is extended by the student value

$$t_i = \frac{a_i}{m_{a_i}} \quad (2.6)$$

which is an analogue to the signal-to-noise-ratio for the spectrum in order to test the significance of the polynomial coefficients (see section 5.4).

## 2.4 Meteorological and other regression processes

Meteorological input channels like air pressure, ground water, temperature etc. as well as channels like the pole tide are modelled in STANDARD ETERNA by a single regression coefficient which is constant over frequency. The **new version** generalizes this model by introducing for each channel l of $n_r$ channels a transfer function $h_l(t)$ of arbitrary length $\tau_l$ (Box, G.E.P. et al. 1994) . The total functional model of tidal observations can now be written as

$$y(t) = \sum_{i=1}^{n_{wg}} \delta_i \sum_{j=1}^{l_i} \delta_{ij}^{EM} A_{ij} \cos\left(\omega_{ij} t + \varphi_{ij} + \kappa_{ij}\right) + \sum_{m=1}^{n_{add}} A_m \cos\left(\omega_m t + \varphi_m\right) + \sum_{k=0}^{n_p} a_k T_k(x) + \sum_{l=1}^{n_r} \sum_{j=0}^{\tau_l} h_l(j)\, p_l(t-j) \quad (2.7)$$

where

$r_l$ - l =1,… $n_r$ - regression coefficients
$p_l(t)$ - physical channels ( air pressure, groundwater… etc.)
$h_l(j), j = 0,..\tau_l$ - unknown transfer function weights of physical channels ( air pressure, groundwater… etc.)

Fourier transforms $H_l(\omega)$ of $h_l(j)$ lead to frequency dependent regression coefficients $R_l(\omega)$ and associated phase shifts $\phi(\omega)$.

## 2.5 Stochastic and residual processes

Since tidal observations are obtained by measurements a stochastic component has to be taken into account which change (2.7) to

$$y(t) = \sum_{i=1}^{n_{wg}} \delta_i \sum_{j=1}^{l_i} \delta_{ij}^{EM} A_{ij} \cos\left(\omega_{ij} t + \varphi_{ij} + \kappa_{ij}\right) + \sum_{m=1}^{n_{add}} A_m \cos\left(\omega_m t + \varphi_m\right) + \sum_{k=0}^{n_p} a_k T_k(x) + \sum_{l=1}^{n_r} \sum_{j=0}^{\tau_l} h_l(j)\, p_l(t-j) + \varepsilon(t) \quad (2.8)$$

The assumption here is that the *process* $\varepsilon(t)$ is (at least an asymptotically) an ergodic and stationary process in time, i.e. the stochastic properties of $\varepsilon(t)$ are the same for the ensemble and sample space and are not dependent of absolute time. Furthermore, it is supposed to be normally distributed with mean $\mu$ and variance $\sigma^2$ as

$$E[\varepsilon(t)] = \mu = 0,$$

and

$$E[\varepsilon(t)\, \varepsilon(t)] = \sigma_{\varepsilon\varepsilon}^2$$

A process with these properties will also be referred to as “white noise”.

Even if the normal assumption is not fulfilled, we can adopt the results from the normally distributed case as approximation with respect to the Central Limit Theorem (Jenkins ,G.M. et al 1968) .
In most practical cases $\varepsilon(t)$ will not only contain stochastic parts but various kinds of residual processes , e.g. measurement errors, model errors due to inappropriately modelled signal components as well as non-modelled signals. Further examples of such contents could be :

- remaining parts of the instrumental drift,
- other additional signals due to physical reasons (e.g. ocean loading, additional unmodeled physical signals like rainfall temperature etc.),
- part time or seasonal signals like storm surge loading etc.,
- white and coloured noise .

These processes lead to $\varepsilon(t)$ not being initially random . In this case an iterative analysis procedure is suited to eliminate these contents to the highest possible degree.

## 2.6 Sampling intervals of tidal observations

### 2.6.1 Nyquist frequency

The Nyquist frequency is defined as

$$\omega_{\upsilon} = \frac{360}{2\Delta} \tag{2.9}$$

It represents the highest frequency that can uniquely be resolved for a given sampling interval Δ.
For hourly data the Nyquist frequency will be

$\omega_{\upsilon 1h} = \frac{360}{2}$ =180°/h or 12 cpd.

For minute data the Nyquist frequency will increase to

$\omega_{\upsilon 1m} = \frac{360}{2\frac{1}{60}}$ =10800°/h =720 cpd.

### 2.6.2 Hourly data

There is no strong argument for introducing shorter sampling intervals than 1 hour to the observation record, because STANDARD ETERNA is mainly designed for hourly data and only processes tidal frequencies in the least squares adjustment. Filtering is only possible at this sampling interval. Furthermore, the spectral analysis of the residuals is restricted to 65°/h or 4.3 cpd.
Nowadays, the trend goes to shorter sampling intervals without taking advantage of the larger Nyquist frequency interval.
In the **new version,** any frequency of the Nyquist interval can be processed in least squares as well as spectral analysis..

Despite of the fact that enormous computer power is nowadays available, there is no need for dealing with a 60 times higher amount of data, if there is no gaining of additional information from the observations.
As pointed out in section 2.3.1,if minute data are sampled and transformed to one hour sampling interval, an aliasing filtering has to be done in advance.

### 2.6.3 Minute data

**In the new version**, two filters dealing with minute samples are added and placed into the COMMDAT directory:

- interpolated Pertsev 51 filter (PERLP60M.nlf ,length =3001 min)
- filter based on the Hanning window (SCHLP60M.nlf, length = 3001min)

These filters can be applied for removing the long periodic signals from minute data.
It is planned for the new version to provide an option to perform Earth tide analysis with hourly data even if the input data set is composed of minute data. Also, for estimating the autocovariance function the minute sampling interval will be changed to an hourly one.

These two objectives, however, demand that there no significant energies at frequencies higher than 180°/h or 12 cpd in the observation record. If this assumption cannot be assured in advance, an aliasing filtering with stop band higher than 180°/h has to be processed first in order to avoid aliasing effects.
**The new version** provides such a filter also in the COMMDAT directory denoted by

- BMLPA60M.nlf, based on the Blackman-Tuckey window.

Its 1st part is a filter of length = 3001 min filtering out the very low frequency energies. This part is combined with a 2nd part of filter removing energies higher than 180°/h or 12 cpd by smoothing the minute observations over 361 min. All in all the filter is of length 3361 min and it is removing the long period signals with cut-off at 120°/h= 8 cpd. Applying this filter solves the problem of aliasing to a sufficient degree.

# 3. Parameter estimation in the least squares model

Let us define conventions first:
In statistic references there are presentations where “estimators” and “estimates” always exhibit different notations.
In this presentation when dealing with least squares analysis, “estimators” (=estimation rules) are given whenever possible in matrix notations while the “estimates” (=results of a specific analysis) will be the elements of the associated vectors or matrices. Also, the context will make clear when we are dealing with estimators or estimates.

## 3.1 Least squares target functions

In matrix-notation (in the following written in bold) the complete model of (2.8) can be written as (Wolf ,H. 1968):

$$\boldsymbol{v} + \boldsymbol{y} = \boldsymbol{A}\boldsymbol{x}$$

or

$$\boldsymbol{v} = \boldsymbol{A}\boldsymbol{x} - \boldsymbol{y} \tag{3.1}$$

where according to least squares convention v(t) = - $\varepsilon(t)$ and **v** being the estimator of $\boldsymbol{\varepsilon}$.

Applying the least squares principle to (3.1) means to minimize the (scalar) target function

$$\Omega = \boldsymbol{v}^{\boldsymbol{T}}\boldsymbol{v} = min \tag{3.2}$$

with respect to the unknown parameters **x.** (3.2) then leads then to the well-known set of normal equations :

$$\boldsymbol{A}^{\boldsymbol{T}}\boldsymbol{A}\ \boldsymbol{x} = \boldsymbol{N}\ \boldsymbol{x} = \boldsymbol{A}^{\boldsymbol{T}}\boldsymbol{y}$$

or

$$\begin{bmatrix} \sum e_1(t)\, e_1(t) & \cdots & \sum e_1(t) f_u(t) \\ \vdots & \ddots & \vdots \\ \cdots & \cdots & \sum f_u(t)\, f_u(t) \end{bmatrix} \mathbf{x} = \begin{bmatrix} e_1(t) & \cdots & e_1(t) \\ \vdots & \ddots & \vdots \\ f_u(t) & \cdots & f_u(t) \end{bmatrix} \mathbf{y} =$$

$$\begin{bmatrix} \sum e_1(t)\, y(t) \\ \cdots \\ \sum f_u(t)\, y(t) \end{bmatrix}$$

with the estimator

$$\mathbf{x} = (\boldsymbol{A}^{\boldsymbol{T}}\boldsymbol{A})^{-1}\boldsymbol{A}^{\boldsymbol{T}}\boldsymbol{y} \tag{3.3}$$

In (3.3) $e_i(t), g_i(t)$ are meant to comprise all model signals (2.1)-(2.7) of the function model.

The coefficients of the normal equation matrix **N** will be recognized as the auto and cross energies of the model signals, while the absolute term $\boldsymbol{A}^{\boldsymbol{T}}\boldsymbol{y}$ of the normal equations carry the cross energies of the modelled signals and the observations.

Let us now modify (3.2) to

$$\Omega_w = \boldsymbol{v}^{\boldsymbol{T}}\boldsymbol{W}\boldsymbol{v} = min \tag{3.4}$$

with the diagonal matrix **W** = **diag**$\{\boldsymbol{w}_{t_1}, \boldsymbol{w}_{t_2}, \ldots\ldots\ldots \boldsymbol{w}_{t_N}.\}$ containing the discrete values of the window function of (1.4).

Then we will arrive at the normal equations to be

$$\boldsymbol{A}^{\boldsymbol{T}}\boldsymbol{W}\boldsymbol{A}\ \boldsymbol{x} = \boldsymbol{N}\ \boldsymbol{x} = \boldsymbol{A}^{\boldsymbol{T}}\boldsymbol{W}\boldsymbol{y}$$

or

$$\begin{bmatrix} \sum e_1(t)\, e_1(t)w(t) & \cdots & \sum e_1(t) f_u(t)w(t) \\ \vdots & \ddots & \vdots \\ \dots & \cdots & \sum f_u(t)\, f_u(t)w(t) \end{bmatrix} \mathbf{x} = \begin{bmatrix} e_1(t)w(t) & \cdots & e_1(t)w(t) \\ \vdots & \ddots & \vdots \\ f_u(t)w(t) & \cdots & f_u(t)w(t) \end{bmatrix} \mathbf{y} =$$

$$\begin{bmatrix} \sum e_1(t)\, y(t)w(t) \\ \dots \\ \sum f_u(t)\, y(t)w(t \end{bmatrix} \tag{3.5}$$

leading to the window dependent least squares estimator for the parameters

$$\mathbf{x} = (\boldsymbol{A^T W A})^{-1} \boldsymbol{A^T W y} \tag{3.6}$$

It is obvious that when choosing $w_{t_m}$ to be the rectangular window, then (3.6) transforms to the already derived estimator (3.3).
(3.5) shows in detail how the window function $w_{t_m}$ is automatically introduced to the least squares parameter estimation (a detailed presentation is given in (SCHÜLLER, K. 1976)).

The residuals **v** will be obtained by inserting (3.6) into (3.1).

## 3.2 The impact of window functions on least squares parameter estimation

The importance of window functions in least squares tidal analysis is often underestimated because they are only implicitly involved and the impacts are not quite obvious if not presented as in (3.5).

We see 3 major items where the influence of the window functions are of real importance:

- Least squares estimation and interpretation of tidal, non-tidal and meteorological parameters
- Estimation of frequency dependent root mean square errors.
- Estimation and interpretation of the spectral properties of the residuals

Basically, windowing in a least squares adjustment comprises both the modelled and unmodeled parts of the observation record. For the modelled part resolution problem is of utmost interest. For the unmodeled part , it is leakage.
The preceding discussions in sections 1.3 and 3.1 indicate that we are dealing with the rectangular window as representative of providing maximum resolution and the Hanning window as the one of minimum leakage. Hence, it follows quite naturally that we define 2 classes of least squares estimators:

### 3.2.1 Maximum resolution least squares estimator

The **maximum resolution** least squares estimator will be the one using the rectangular window matrix $\boldsymbol{W_R}$

$$\begin{aligned} \boldsymbol{x_{WR}} &= (\boldsymbol{A^T W_R A})^{-1} \boldsymbol{A^T W_R y} \\ &= (\boldsymbol{A^T A})^{-1} \boldsymbol{A^T y} = \boldsymbol{N^{-1} y} \end{aligned} \tag{3.7}$$

### 3.2.2 Minimum leakage least squares estimator

The **minimum leakage** least squares estimator will be the one using the Hanning or similar window matrices $\boldsymbol{W_L}$ exhibiting rapidly converging side lobes:

$$\boldsymbol{x_{WL} = (A^T W_L A)^{-1} A^T W_L y = N_L^{-1} y} \tag{3.8}$$

In the following a set of rules will be derived to decide which one of the estimators to apply appropriately.

### 3.2.3 The condition number $\boldsymbol{\kappa}\ (\boldsymbol{N})$ as criterion for frequency resolution

From (3.5) it is obvious how the window function properties are involved in the normal equations. Assume that 2 tidal frequency bands shall be resolved, which are close in frequency. The spectral window will exhibit that their frequency distance is close to the centre of the main lobe. Hence, the associated parameters become nearly linear dependent . A consequence of linear dependency of any 2 parameters in the normal equations of (3,7), (3,8) results in the normal coefficient matrix **N** being singular or close to singularity : it can either be not inverted or only with considerable loss of numerical accuracy. From linear algebra, it is known that the quality criterion which gives information to what degree a system of normal equations can be solved is the so-called **condition number** $\boldsymbol{\kappa}\ (\boldsymbol{N})$ . It is defined as the quotient of

$$\kappa\ (\boldsymbol{N}) = \frac{\lambda_{max}}{\lambda_{min}} \tag{3.9}$$

where the largest $\lambda_{max}$ and smallest $\lambda_{min}$ eigenvalues of **N.** Note that in case of $\lambda_{min} = 0$ the condition number $\kappa\ (\boldsymbol{N})$ becomes infinite. For this reason STANDARD ETERNA as well as and the new version compute the condition number of $\kappa\ (\boldsymbol{N})$ as criterion for numerical stability with respect to resolution.

As $\kappa\ (\boldsymbol{N})$ is only dependent on the window function, the modelled signal and not on the observations, it follows that statistical criteria (AKAIKE, F-Test etc.) may not be applied as quality criterion, because they are not involved in the resolution problem at all. Using these criteria though, means to confuse cause and effect.

### 3.2.4 The impact of gaps in observation records

Gaps in tidal records are important to consider because they make the interpretation of the estimated parameters more complicated due to the comparably unfavourable properties of the associated window function.

Let us assume a tidal observation record be recorded over the interval –T/2 and T/2 with centre at the overall reference epoch $T_0$ and containing $n_l$ gaps. Consequently, the observation record will consist of $n_l + 1$ blocks of $N_i$ observations. Hence, we find the associated time window function

$w_{tot}(t_m)$ (for simplicity let us assume the rectangular window with sampling interval $\Delta = 1$) as a sequence of values 1 in the block areas and 0 in the gap areas.

Then, the overall time window function $w_{tot}(t)$ covering the whole record can be thought to be composed of $n_l + 1$individual time window functions $w_{i,t0}\ (t_m)$ with individual centre reference points $t_{0i}$ .

The associated spectral windows for each block i can then be written as

$$W_{i,t0}(\omega) = \frac{1}{N_i}\sum_{t=\frac{-N_i+1}{2}}^{\frac{N_i-1}{2}} w_{i,t0}\ (t)\, e^{-i\omega t} \tag{3.10}$$

Before composing the individual spectral block windows to the overall window, they have to be referenced to the central epoch $T_0$ :

$$W_i(\omega) = e^{i\omega(t_{oi}-T_0)} W_{i,t0}(\omega) \tag{3.11}$$

Since Fourier transformation is linear, the individual spectral block windows $W_i(\omega)$ could be summed up to form the overall spectral window and after normalization by the total number of samples, we end up with

$$W_{tot}(\omega) = \frac{1}{N}\sum_{i=1}^{l} N_i W_i(\omega) \tag{3.12}$$

or

$$W_{tot}(\omega) = \sum_{i=1}^{l} \frac{N_i}{N} e^{i\omega(t_{oi}-T_0)} W_{i,t0}(\omega) \tag{3.13}$$

Formulas (3.10- 3.13) show that

- the individual block windows $W_{i,t0}(\omega)$ exhibit different resolutions depending on the amount of samples $N_i$ in each block i,
- the individual block windows $W_{i,t0}(\omega)$ are influencing the total window proportional to the amount of samples $N_i$,
- the analytical expression for the overall spectral window is a sum of sinc-functions (1.7) with in- and out-of-phase components depending on each block. Different from the case of no gaps( where we only have to deal with a single sinc- function of kind (1.7), the behaviour of this composed function is rather difficult to predict. Generally, its properties can only be evaluated numerically. Our experience shows that the resolution and side lobe properties are worse compared to a window without gaps.

**Recommendation:**

**Gaps should be filled, whenever it is possible.** The effects of inserting predicted data cannot be worse than the properties of gappy records.

When using polynomials caution has to be taken with the respect to the choice of the window function. Polynomials in a least squares procedure tend to suck up any energy they can get hold of over the whole frequency domain. The Hanning window, however, is a tool for sheltering frequency domains against leakage from more distant ones. As a consequence, the two concepts are in

competition with each other. Therefore, if **polynomials are applied** in a least squares model the **rectangular window** should be preferred as window function.

### 3.2.5 Wave grouping

Basically, with respect to what was derived in section 2.1, wave **grouping should always occur at maximum possible resolution** (see examples in (SCHÜLLER ,K. 2014)) to avoid model insufficiencies. That means that as much wave groups as possible should be introduced to the functional model (2.1) in order to reduce the assumptions on the parameters to be estimated and so reducing model errors. Having stated this principle, it is recommended to pursue the following procedure for tidal wave grouping:

Given an observation record, one has to calculate the associated spectral window first, find the first zero pass or minimum position in frequency and then do the wave grouping according to the rules derived. Usually, a separation of half or even ¼ of that distance will lead to satisfactory results. The condition number will definitely decide whether the normal equation can cope with the resolution assumptions.

In this respect the Rayleigh-criterion, especially when dealing with least squares adjustment ,is by far too pessimistic, since it postulates a frequency difference of at least the fundamental frequency between two neighbouring harmonics to be resolved (also see Munk, W. ,Hasselmann, K. 1964). Since STANDARD ETERNA automatically eliminates tidal wave groups if the Rayleigh-criterion is not met, this elimination is dropped in **the new version**. If the resolution is supposed to be too optimistically chosen, the normal equations (3.6) can either not or only poorly be solved (see **condition number** as criterion). The user will then be notified to repeat the analysis with less resolution once again.

Modelling the higher potential degrees (see section 2.1) for m < l we face a special situation. The $V_l$ - and $V_{lm}$ - groups will contain harmonics of several standard tidal bands and hence the resolution between single tidal bands and multi-band groups is usually sufficiently guaranteed. However, when dealing with subgroups of a tidal band, the observation record has to be sufficiently long to keep the mutual mathematical correlations low. **The new version** provides an enhanced table of wave groups where the group amplitudes and frequencies are listed. Thus, in a first step of analysis the user can easily obtain an overview about the situation with respect to resolution. For details see (SCHÜLLER,K. 2014).

The similar principle holds for signals of non-tidal origin according to (2.3). Meteorological signals play a different role since they are multi-frequency signals. Provided , the spectrum of these signals do not contain dominant energy concentrations at the tidal frequencies, but are rather smooth over frequency, the resolution problem does not appear, since we are estimating one regression parameter ,i.e. a constant transfer function for all frequencies.

In the **new version** both the spectral rectangular and Hanning window as well as their difference is calculated and print plotted similar to Fig. 5 so that the user will obtain the required information for decision making.

For the rectangular window the required record lengths to resolve tidal bands and constituents respectively are (from the most pessimistic point of view of the Rayleigh resolution):

- 27 days -> 1 month separation distance 0.549017 °/h
- 180 days-> 6 months 0.082000
- 365 days -> 12 month 0.041069
- 435 days 0.034480
- 8.8 years 0.004642
- 18.6 years 0.002206
- 20942 years 0.000002

For the Hanning window the length have to be doubled (see (1.11).

At the Geo-Observatorium Odendorf of Prof. Dr.-Ing. Manfred Bonatz, more than 10 years of observations are available which can resolve the frequency distance = 0.004642°/h equal to the Moon's perigee.

Presently, one of the longest if not the longest superconducting gravimeter record available will be of about 25) years (Calvo, M. et al. 2014) which should easily resolve a frequency distance equal to 0.002206°/h.

Efforts have been made to resolve the K1 triplet being separated by the Moon's ascending node frequency (DUCARME,B. 2011). Resolving these wave groups is nothing special because it only needs a sufficient record length to acquire the necessary resolution. As it is shown in this presentation (see (3.5)), the spectral window functions are most suited for anticipating the resolution and leakage properties of a specific observation record. Therefore, it is highly recommended for future publications to present information about the underlying window properties too. Particularly, when using analysis methods with larger sampling intervals than 1 h, its sampling properties have to be fully understood: it was shown in (SCHUELLER, K. 1978 ) that generally such methods are extremely sensitive to aliasing and leakage effects.

# 4. The stochastical model of least squares

## 4.1 Least squares parameter errors

The errors of the parameters are determined from (3.7),(3,8) by applying the error propagation law as:

$$\begin{aligned} \boldsymbol{m_x} &= m_0 \boldsymbol{N^{-1}} \boldsymbol{A^T Q_W A N^{-1}} \\ &= m_0 \boldsymbol{N^{-1}} \end{aligned} \tag{4.1}$$

Note that according to (2.2) $\boldsymbol{m_x}$ for the tidal model will contain the RMS of the auxiliary unknowns $x_{c_i}, x_{s_i}$. To derive the RMS for the tidal parameters themselves, the error propagation law has to be applied leading to

$$m_{\delta_i^*} = \frac{m_0}{\delta_i^*} \sqrt{x_{c_i}^2 Q_{x_{c_i},x_{c_i}} + x_{s_i}^2 Q_{x_{s_i},x_{s_i}} + 2 x_{c_i} x_{s_i} Q_{x_{cs_i},x_{s_i}}} \tag{4.2a}$$

where $Q_{ij}$ are the elements of $\boldsymbol{N^{-1}}$ .

With $\delta_i = \delta_i^* \, \delta_{ij}^{EM}$

it follows for any constituent j of the i-th tidal frequency band :

$$m_{\delta_i} = \delta_{ij}^{EM} m_{\delta_i^*}$$

and

$$m_{\kappa_i} = \frac{m_0}{\delta_i^{*2}} \sqrt{x_{s_i}^2 Q_{x_{c_i},x_{c_i}} + x_{c_i}^2 Q_{x_{s_i},x_{s_i}} - 2x_{c_i} x_{s_i} Q_{x_{cs_i},x_{s_i}}} \qquad (4.2b)$$

Because the $Q_{ij}$ are determined by the functional model, special attention has to be dedicated to the appropriate estimation of the RMS $m_0$.

## 4.2 Parseval's theorem and root mean square error $m_0$

To reveal the structure of $m_0$, let us consider its representation in the time and frequency domain. The relation is provided by Parseval's theorem **:**

$$\Omega = E_v = \sum_{t=0}^{N-1} v(t)v(t) = \frac{N}{2} \sum_{i=1}^{\frac{N}{2}} A^2(\omega_i) \qquad (4.3)$$

where $A^2(\omega_i)$ are the quadratic amplitudes of the spectrum of the residuals v(t) at integral multiples of the fundamental frequencies. The frequencies $\omega_i$ turn out to be the Fourier frequencies

$$\omega_i = \frac{2\pi}{N} i \qquad (4.4)$$

and are consequently identical with the zero positions of the associated rectangular window; therefore, the $A^2(\omega_i)$ are mutually uncorrelated.

For v(t) as **white noise**, its amplitudes $A^2 = A_{wn}^2$ are by definition constant over frequency; so we can write with u frequencies of the model signals

$$E_v = \sum_{t=1}^{N} v(t)v(t) = \frac{N}{2} \frac{(\mathrm{N}-2\mathrm{u})}{2} A_{wn}^2 \qquad (4.5)$$

Because the parameters are already estimated at u frequencies in a least squares adjustment, there will be (N-2u)/2 frequencies left to contribute to the overall energy.

Dividing both sides by (N-2u) leads to an unbiased estimate of the mean energy which is equal to the estimated variance $m_0^2$ of (4.2a):

$$m_0^2 = \frac{E_v}{N-2u} = \frac{1}{N-2u} \sum_{t=1}^{N} v(t)v(t) = \frac{N}{4} A_{wn}^2 \qquad (4.6a)$$

and

$$A_{wn}^2 = 4\,\frac{m_0^2}{N}$$

or

$$A_{wn} = 2\,\frac{m_0}{\sqrt{N}} \tag{4.6b}$$

The expression (4.3) is the fundamental formula for generalizing the least squares error propagation to non-white noise processes. In this case, the spectrum of the residuals is generally not constant over frequency. However, if we assume that it is fairly constant or at least smooth within certain frequency domains $d_i = \omega_{i_e} - \omega_{i_a}$ covering the whole Nyquist interval, we can rewrite (4.3) with (4.6a) to

$$m_0^2 = \frac{1}{N-u}\sum_{t=1}^{N} v(t)v(t) = \sum_{i=1}^{n_d} m_{0,i}^2 = \frac{N}{4}\sum_{i=1}^{n_d}\frac{1}{n_i-2u_i}\sum_{j=1}^{\frac{N_i}{2}} A^2(\omega_j) =$$

$$\frac{N}{4}\sum_{i=1}^{n_d}\frac{1}{N_i-2u_i}\sum_{j=1}^{\frac{N_i}{2}} A^2(\omega_j) \tag{4.7}$$

with

- $n_d$ = number of frequency domains $d_i$ , i =1… $n_d$ , usually the long periodic, diurnal, semi-, ter-, quad, 12- diurnal bands, where the frequency dependent variances are estimated
- $m_{0,i}^2$ = frequency dependent variances of domain $d_i$ ,
- $\frac{N_i}{2}$ = number of multiples of the fundamental frequency in the ith domain
- $u_i$ = number of tidal groups in domain $d_i$ introduced to least squares analysis
- A($\omega_j$) = amplitudes of the spectrum at multiples of the fundamental frequencies in domain i
- $\omega_{i_a}$ = lowest Fourier frequency of the i-th frequency domain
- $\omega_{i_e}$ = highest Fourier frequency of the i-th frequency domain
- $\nu_i$ = ($N_i$ - $2u_i$ ) = degrees of freedom associated with $m_{0,i}^2$

The individual variances $m_{0,i}^2$ associated with each frequency domain will then be

$$m_{0,i}^2 = \frac{N}{4}\,\frac{1}{N_i-2u_i}\sum_{j=1}^{\frac{N_i}{2}} A^2(\omega_j) = \frac{N}{4}\,A_{M_i}^2 \tag{4.8}$$

where $A_{M_i}$ is the RMS-amplitude of the i-th domain (compare with (4.6b).

A good choice for these domains is a width of $\pm\,3.75°/h$ around 15, 30, 45, 60, 75, 90,..,176.25, 180°/h or 1 to 12 cpd respectively.

Energy averages are then taken other as in the case of white noise not over the whole Nyquist interval, but only within the bounds of these domains.

The RMS errors for the auxiliary tidal parameters $\delta_i^* \cos(\kappa_k)$ and $\delta_i^* \sin(\kappa_k)$ in the i-th domain associated are calculated according to (4.1) as

$$m_{x_k} = m_{0,i}\sqrt{Q_{x_k x_k}} \tag{4.9}$$

(4.9) holds in principle for all parameters of the functional model which can be related to one of the defined frequency domains. However, there are cases where the parameters cannot be related to a specific domain (e.g. regression signals). In this case a good approximation is to choose that $m_{0,i}$ which represents the frequency domain of the most significant model signal energies.

# 5. Frequency dependent least squares error propagation

The previous section emphasized the need for estimating the residual spectral amplitudes for the least squares error propagation. However, we have not yet shown by what method this could be achieved.

In STANDARD ETERNA the Fourier spectrum of the residuals is calculated for determining the residual amplitudes based upon the Fourier decomposition

$$v(t) = \frac{a_0}{2} + \sum_{i=1}^{\frac{N}{2}} \left( a_i \cos\frac{2\pi i}{N} + b_i \sin\frac{2\pi i}{N} \right)$$

with the coefficients

$$a_i = \frac{2}{N}\sum_{i=0}^{N-1} v(t_i)\cos\frac{2\pi i}{N}$$

$$b_i = \frac{2}{N}\sum_{i=1}^{N-1} v(t_i)\sin\frac{2\pi i}{N} \qquad (5.1)$$

and the Fourier amplitude spectrum

$$A_i = A(\omega_i) = \sqrt{a_i^2 + b_i^2} \qquad (5.2)$$

at the Fourier frequencies $\omega_i = \frac{2\pi}{N} i$.

Since v (t) is assumed to be normally distributed with $E[v(t)] = 0$ (section 2.5), it follows that the expectation values of the Fourier series coefficients $a_i$ and $b_i$ , i.e.

$$E[a_i] = 0, \;\; E[b_i] = 0 \qquad \text{and with} \qquad A_i = A(\omega_i) \to 0 \qquad (5.3)$$

the residual amplitudes are tending to zero and so do their squares. This result was also confirmed by means of generated stochastical test series and numerical experiments. Therefore, this approach will not lead to appropriate solutions in case of random time series. Instead, the approach of spectral estimation via the autocovariance function of the residuals will lead to the proper solution as it will be shown in the next sections.

## 5.1 The autocovariance function

### 5.1.1 Definition and properties of the autocovariance function

The autocovariance function $c_{\varepsilon\varepsilon}^*(\tau)$of the stochastic process $\varepsilon(t)$ is defined as

$$c^*_{\varepsilon\varepsilon}(\tau) = E[(v(t) - \mu)(v(t+\tau) - \mu)] \quad (5.4)$$

where $\mu = E[(\varepsilon(t)]$ is the mean and E $[*]$ the expectation operator.

(5.4) can also be written as

$$c^*_{\varepsilon\varepsilon}(\tau) = \lim_{T\to\infty} \frac{1}{T} \int_{-T/2}^{+T/2} \varepsilon(t)\varepsilon(t+\tau)dt \quad (5.4a)$$

From (5.4a) an unbiased estimator of the autocovariance function of a discrete time series (in our case the residuals v(t) from a least squares tidal adjustment with $u^*$ unknown parameters) of finite length T= NΔ , ( Δ= 1 for simplicity) is derived as

$$c_{vv}(\tau) = \frac{1}{N-|\tau|-u^*} \sum_{t=1}^{N-|\tau|} v(t)v(t+\tau) \quad (5.4.b)$$

As v(t) is the estimate of the "true" of the stochastic process $\varepsilon$(t) of (2.8), then with (4.6a) it follows that $c_{vv}$ (0) = $m_0^2$ is the estimated variance from the residuals v(t) of the (Earth tides) observations y(t).

The properties of the autocovariance function can be summarized as follows

- $c_{vv}(\tau)$ also indicates how much any two observations of distance $\tau$ are correlated.
- $c_{vv}(\tau)$ is only dependent on relative time positions $\tau$ (section 2.5)
- Gaps in the observation records are no essential problem for its estimation, since there are a lot of products $v(t)v(t+\tau)$ to average so that the autocovariance function can be estimated without being considerably biased by the gappy parts of the observations.
- $c_{vv}(\tau)$ is symmetrical, i.e. $c_{vv}(\tau) = c_{vv}(-\tau)$.

Further properties of the estimated autocovariance function are as follow:

- For white noise
  - $c_{vv}(\tau) = \begin{cases} c_{vv}(0) = m_0^2, & \tau = 0 \\ 0, & \tau > 0 \end{cases}$
- Coloured noise is indicated by an autocovariance function converging to 0 as $\tau$ is increasing to a finite value $\tau_{conv}$
  - $c_{vv}(\tau) = \begin{cases} c_{vv}(\tau) \neq 0 & \tau < \tau_{conv} \\ 0, & \tau > \tau_{conv} \end{cases}$
- For periodic signals of amplitude A, frequency ( $\omega$) and phase , the auto - covariance function preserves its periodic nature for any lag $\tau$ . However, the phase information is lost, because :
  - $c_{vv}(\tau) = \sum_{i=1}^{M} \frac{A_i^2}{2} \cos(\omega_i \tau)$

The autocovariance function $c_{vv}(\tau)$ is better suited than the residual process v(t) itself for classifying the nature of the residuals either to be random, deterministic or mixed-up of the two different kinds of processes. Moreover, hidden periodicities can easily be observed.

### 5.1.2 Length of the autocovariance function

The length $n_c$ of the autocovariance function consists of an always **odd** number of samples, i.e.

$n_c = 2M + 1$ = N with M= $\frac{N-1}{2}$.

When calculating $c_{vv)}(\tau)$, its maximum lag could theoretically be close to T= N. However, as it should be chosen as

$$\tau_{max} = M\ ,\ M \leq \frac{N-1}{2}\ .$$

in order to be consistent with the record length of the observations. Because the autocovariance function is symmetric, it is then of the same length N as the observation record in case N is odd ; otherwise it will one sample shorter in case N is even.

## 5.2 The spectrum based of the autocovariance function

### 5.2.1 Definition and properties

It follows from the famous Wiener-Khintchine-Theorem that autocovariance function c($\tau$) and spectrum $S\ (\omega)$ are related by Fourier transformation:

$$c_{vv}\ (\tau) = \frac{1}{2\pi} \int_{-\infty}^{+\infty} S(\omega) e^{i\omega t}\ d\omega$$

and

$$S\ (\omega) = \int_{-\infty}^{+\infty} c_{vv}\ (\tau)\ \ e^{-i\omega t}\ d\tau \qquad (5.5)$$

As c($\tau$) is symmetric, its Fourier transform will be symmetric as well , so $S\ (-\omega) = S\ (\omega)$ .
Moreover, the autocovariance function is discrete , so (5.5) will become

$$\mathrm{S}(\omega_i) = \sum_{-M}^{+M} c_{vv}\ (\tau) e^{-i\omega_i \tau} = \sum_{-M}^{+M} c_{vv}\ (\tau) \cos(\omega_i \tau) \qquad (5.6)$$

or with A($\omega_i$) being the amplitude at frequency $\omega_i$ and N=2M+1

$$\mathrm{S}(\omega_i) = \frac{N}{4} A^2(\omega_i) \qquad (5.7)$$

which is equivalent to (4.6a). (5.7) is a fundamental results because it states that the spectral decomposition of the residual variance can be derived from the Fourier transform of the autocovariance function of the residuals.
In case of white noise , the autocovariance function will consist of one value ≠ 0, i.e. $c_{vv}$ (0). Hence, the associated spectrum values will be constant with (5.7) (see also 4.6a,b)

$$\mathrm{S}(\omega_i) = \frac{N}{4} A^2(\omega_i) = \text{const.} = c_{vv}\ (0) = m_0^2 \qquad (5.8)$$

what is completely different as derived (5.3) as Fourier spectrum of the residuals v(t)).

Since we are dealing with Fourier transforms the fundamental frequency $\omega_0$ is likewise defined as $\omega_0 = \frac{2\pi}{n_c} = \frac{2\pi}{2M+1}$ and the harmonic frequencies are $\omega_i = \omega_0 \cdot i, \quad \{ \mathrm{i} = 1, 2 \ldots \mathrm{M}.$

In **the new version** all spectral estimates either for frequency dependant error propagation or detection of additional signals are estimated by the spectrum based on the autocovariance function.

### 5.2.2 Spectral sampling

In STANDARD ETERNA, the frequency interval of the Fourier spectrum of the residuals is fixed to 0.25°/h. To provide a higher resolution, this interval is divided by five, resulting in an increment interval of 0.05°/h, also fixed for all length of observation records. Also, the number of spectral estimates is fixed (1300) so that the spectrum will only be calculated up to 65°/h.

**In the new version** the spectrum itself will be calculated at multiples of the fundamental frequency $\frac{360}{N}$ °/h divided by 5. Consequently, the resolution is dependent on the record length and there is no restriction in frequency but the Nyquist one.

## 5.3 Confidence intervals for frequency dependent RMS $m_{0_i}$

### 5.3.1 Degrees of Freedom

In (4.5) we have shown that the total number of degrees of freedom associated with $m_0^2$ is N-2u, comprising the whole Nyquist interval. It is assumed that the model parameters can be linked to a certain frequency in domain $d_i$. If the parameters are not of harmonic origin, only half of their numbers are to be counted in u.
The total number of degrees of freedom associated with each domain $d_i$ can be derived with (4.7):

$$d_i = \omega_{i_e} - \omega_{i_a} \tag{5.9}$$

and $\omega_{0_i} = \frac{2\pi}{N_i}$ as

$$\nu_{d_i} = 2\frac{d_i}{\omega_{0_i}} - 2u_i \tag{5.10}$$

To obtain reliable error estimates based on a sufficient number of degrees of freedom, each of the frequency domains (5.9) must be large compared the fundamental frequency $\omega_{0_i}$of the domain so that the square residual amplitudes are averaged over a large number of samples. On the other hand, this implies that the residual spectrum has to be fairly smooth within these domains. If this is not the case the functional model must be enhanced for instance by additional model signal defined in section 2.2. This procedure can be considered as a “domain whitening process”.

Applying these rules to the residuals process v(t) of an Earth tide analysis, one has to take into account the unknown tidal parameters by subtracting 2 degrees of freedom for each tidal band from the total degrees of freedom for this domain. This principle also holds for other additional harmonics defined in the adjustment.

### 5.3.2 Deriving confidence intervals

It can be shown (Jenkins ,G.M. et al 1968) that the quantity $\frac{(n-u)\,m_0^2}{\sigma_{\varepsilon\varepsilon}^2}$ is distributed as $\chi_{n-u}^2$ . Likewise, the quantity $\frac{\nu S(\omega)}{\Pi(\omega)}$ is distributed as $\chi_\nu^2$ , where $\Pi(\omega)$ is the "true" spectrum and $\nu$ the number of degrees of freedom associated with $S(\omega)$ .

Then, the confidence interval parameters as lower and upper limits are derived with $\chi_\nu^2\,(\alpha) = x_\nu\,(\alpha)$ as follows (Jenkins ,G.M. et al 1968):

$$\Pr\left\{x_\nu(\tfrac{\alpha}{2}) < \frac{\nu S(\omega)}{\Pi(\omega)} < x_\nu(1-\tfrac{\alpha}{2})\right\} = 1-\alpha$$

or

$$\Pr\left\{\frac{\nu}{x_\nu(1-\frac{\alpha}{2})} < \frac{\Pi(\omega)}{S(\omega)} < \frac{\nu}{x_\nu(\frac{\alpha}{2})}\right\} = 1-\propto \qquad (5.11)$$

which leads to the confidence interval for the true spectrum with probability 1-$\alpha$ :

$$\Pr\left\{\frac{\nu}{x_\nu(1-\frac{\alpha}{2})}S(\omega) < \Pi(\omega) < \frac{\nu}{x_\nu(\frac{\alpha}{2})}S(\omega)\right\} = 1-\propto$$

or

$$\Pr\{f_l \cdot S(\omega) < \Pi(\omega) < f_u \cdot S(\omega)\} = 1-\propto \qquad (5.12)$$

The quantities f are the factors to be applied to the estimated spectrum values to determine the lower and upper bounds for the true spectral values $\Pi(\omega)$ with (1-$\alpha$) –probability. Taking into account the different degrees of freedom of each frequency domain $d_i$ , it follows:

$$f_l\,(d_i) = \frac{\nu_{d_i}}{x_{\nu_{d_i}}(1-\frac{\alpha}{2})} \quad \text{and} \quad f_u(d_i) = \frac{\nu_{d_i}}{x_{\nu_{d_i}}(\frac{\alpha}{2})} \qquad (5.13)$$

Since $m_{0,i}^2$ and $S(\omega_i)$ and therefore $A^2(\omega_i)$ are related by multiplication, these factors $f_l\,(d_i)$ and $f_u(d_i)$ are valid for both the time and frequency domain (4.3). Taking the square roots of f, one obtains with (4.9) for the $m_{0_i}$ the associated confidence intervals

$$\sqrt{f_l(d_i)}\cdot m_{0_i} \le c_{m_{0_i}} \le \sqrt{f_u(d_i)}\cdot m_{0_i} \qquad (5.14)$$

These confidence intervals of $m_{0_i}$ are calculated for each domain **in the new version**. Note that in case of filtering the gain correction is applied for presentation purposes in order to deal with the actual errors and confidence intervals.

## 5.4 Confidence intervals for the estimated parameters

The quantity

$$t = \frac{x_i}{m_{x_i}} \tag{5.15}$$

is distributed according to the Student's t- probability distribution function. For a given probability P and $\nu$ degrees of freedom, factors t of $m_{x_i}$ from (4.9) can be derived so that $x_i$ lie in the confidence interval

$$\Pr\{x_i - t_{P,\nu} m_{x_i} < x_i < x_i + t_{P,\nu} m_{x_i}\} = 1 - \propto \tag{5.16}$$

Applying (5.16) to the estimated parameters, t-values are calculated for a given probability (usually 95%) and the associated degrees of freedom for each tidal domain so that the confidence intervals for the parameters can be calculated.
Note that for a large number of degrees of freedom ( e.g. $\nu$=3000 and P= 95% ) the values for t will be

$$t_{95\%,3000} = 1.96 \approx 2$$

For $\nu$=3000 and P= 68,3%, we obtain

$$t_{68.3\%,3000} = 1$$

This result means that the least squares error are special confidence intervals with t=1.

The confidence intervals for the estimated parameters of a least squares analysis are also provided **in the new version**. This t-statistic can be directly used for testing the significance of modelled parameters from 0 as zero hypothesis and hence leading to a model which is confirmed on a given probability.

## 5.5 Comparisons to STANDARD ETERNA error propagation

In comparison to STANDARD ETERNA we found that the tidal parameter error estimates were too high by a factor of about 1.13. A short examination of this problem leads to the cause for this deviation:

Let $A_{wn}$ be the overall RMS amplitude of the Nyquist interval, in STANDARD ETERNA referred to as white noise amplitude , we can rewrite (4.8) as

$$m_{0,i}^2 = \frac{N}{4} \sum_{i=1}^{d_i} \frac{1}{N_i - 2u_i} \sum_{j=1}^{N_i} A^2(\omega_j) = \frac{N}{4} A_{M_i}^2 = m_0^2 \frac{A_{M_i}^2}{A_{wn}^2} \tag{5.17}$$

(5.17) is the expression used by STANDARD ETERNA and is in total accordance with the least squares principle. (Unfortunately, Ducarme,B. et al. 2006 were not aware of this context, otherwise their criticisms would have been obsolete.)

The overall white noise amplitude was calculated in STANDARD ETERNA as

$$A_{wn} = \sqrt{\pi}\,\frac{m_0}{\sqrt{N}} \qquad (5.18)$$

instead of

$$A_{wn} = 2\,\frac{m_0}{\sqrt{N}} \qquad \text{(see (5.8))}$$

which leads to smaller values by a factor of 0.886. Since it is used as a corrective quantity with respect to white noise parameter errors , it appears in the denominator of (5.17) and thereby enlarging the parameter errors by $\frac{1}{0.886}$ = 1.13. The appearance of $\pi$ in (5.18) is not obvious as already pointed out by (Ducarme,B. et al. 2006).

From Parseval's theorem it follows that **the averaging process of the noise amplitudes has to be quadratic,** whereas STANDARD ETERNA uses the arithmetic mean**.** Moreover, the estimates in STANDARD ETERNA are not taken at integral multiples of the fundamental frequency but at fixed frequencies, so Parseval's equation is only approximately satisfied. The amplitudes are directly estimated from the Fourier spectrum of the residual process v(t) and not by the spectrum of autocovariance function. From a numerical point of view, the results for the error estimates of the tidal parameters of STANDARD ETERNA do not differ too much, if the amplitude distributions are smooth over the frequency domains. This is not surprising because the quadratic and arithmetical means of the amplitudes are then very close.

If, however, the spectrum is considerably varying within the domains, the arithmetic mean of the amplitudes is generally smaller than the RMS one. Hence, the error estimates, being 13% too high, will be compensated by simply averaging the amplitudes. This might be one reason why the numerical results of errors from STANDARD ETERNA are surprisingly close to those derived from the exact theoretical basis.

Furthermore, STANDARD ETERNA provides a specific method of error propagation for the long periodic domain. We are of opinion that there is no reason to treat frequency bands differently.

**Conclusion:**

Ducarme, B. et al. 2006 concluded from all these facts that STANDARD ETERNA error estimates are not based on least squares. It was criticised that (citation) *"ETERNA RMS are, unfortunately, not least squares estimates and they depend on some intuitive assumptions"*. We do not support that statement at all. Instead we would call STANDARD ETERNA error propagation a good approximation to the least squares principle. **The new version**, however, will provide error estimation procedures which are in total agreement with the least squares principle and the rules of statistics.

# 6. Analysis of the residual process for additional signals

## 6.1 The impact of least squares adjustment on the residual process

One consequence of the least squares principle (3.2), (3.4) is that

$$\boldsymbol{A^T v = 0}$$

or

$$\boldsymbol{A^T W v = 0} \tag{6.1}$$

The meaning of these two equations is that least squares estimates parameters in such a way that the residual process is orthogonal with respect to the model signals. It follows that it is free of any information about the modelled signals.

For better understanding the impact of (6.1), let us assume the Fourier decomposition (5.1) as a simple functional model for the least squares analysis. Then, the model signals will be cosine and sine functions of time, each being the representative signal of a multiple of the fundamental frequency. In this case, the meaning of (6.1) is that the residual Fourier spectrum at these frequencies is zero, i.e. the residuals do not contain any energies at the model signals frequencies.

As the model signals for the tidal and non-tidal signals are composed of cos- and sin-functions too, the effect is similar. Therefore, no additional or at least distorted information will be gained from residual spectra at the tidal frequencies with respect to harmonics.

It follows also from (6.1) that feeding back the residuals to the least squares adjustment in place of the observations, a vector $\boldsymbol{\Delta x = 0}$ would be the result.

Therefore, let us regard the $\varepsilon(t)$ of (2.8) to be composed of 2 parts:

$$\boldsymbol{\varepsilon = \varepsilon_1 + \varepsilon_2} \tag{6.2}$$

or

$$\boldsymbol{v = -\varepsilon_1 - \varepsilon_2} \tag{6.3}$$

where $\boldsymbol{\varepsilon_1}$ will influence = disturb the tidal parameters by

$$\boldsymbol{\Delta x = -(A^T W A)^{-1}(A^T W \varepsilon_1)} \tag{6.4}$$

Consequently, $\boldsymbol{\varepsilon_2}$ does not deliver any contribution to $\boldsymbol{\Delta x}$ . This means that the residuals of a least squares adjustment only contain information about $\boldsymbol{\varepsilon_2}$ which, at the tidal frequencies, is of no great interest, because it does not do any harm to the tidal parameters.

Moreover, it follows from (6.2)-(6.4) that the estimated residual process v (t) is predominately suited **to investigate signals at non- modelled** frequencies.

## 6.2 High resolution spectral analysis

An important aspect is the analysis of the residual spectrum, based on the autocovariance function, for signals of non-tidal origin. In order to facilitate this purpose, **the new version** provides a new analysis tool called the "**H**igh **R**esolution **S**pectral **A**nalyser (**HRSA**)".

There, the spectrum is generated at 1/5 of the fundamental frequency all over the defined domains covering the whole Nyquist interval. In the course of these calculations, the averaging of the square amplitudes for the error calculation as well as a search for spectral peaks is performed. For each domain $d_i$, we obtain a mean RMS amplitude which is compared to the spectral peaks within the domain by calculating the signal to noise ratio. A signal to noise ratio > 3 is proposed to be examined in more detail for an underlying cause. Also a print plot of the domain spectrum is presented, from which one can easily observe, whether it exhibits narrow peaks or is scattering in a broadband pattern around the mean. Note that in case of filtering, the gain correction is applied.

Having isolated significant frequency locations, the functional model can be improved by feeding these frequency locations into a further least squares analysis according to (2.3), and observing ,if any improvement in model adaption is gained.

One example of an analysis might illustrate the procedure :

After having analysed a 2 years superconducting record, there were significant peaks in the N2 and L2 frequency bands left. Since the analysis was performed with the DWZ-Earth model, it could be suspected that the V3 –constituents were modelled inappropriately by the Earth model. Hence we modelled these V3 –constituents as separate groups according to step 4, section2.1.

The residual spectrum of this improved V3-model did no longer exhibit any significant peaks. Moreover, the V3-amplitude quotients from the least squares tidal analysis in the N2- and L2 band were significantly different from those of the DWZ- Earth model (such a V3 model problem was indicated by (MERRIAM, J.B 1995)).

By proceeding this way all information can be exploited from the record unless the residuals mostly contain stochastic processes. To come to that conclusion, the convergence of the autocovariance function to a $\delta$ −Funktion or at least to fade out at a certain time lag has to be observed. Equivalently, this means a convergence of the residual spectrum to a constant or at least a smooth characteristic.

## 6.3 Detection of tidal temporal variations in the least squares residuals

An important question which had been dealt with by several scientists is the temporal variation of the tidal parameters (e.g. Calvo, M. et al. 2014).

Since time variant tidal analysis means a considerable amount of effort, the question is, whether or not it is possible to derive this information from the spectrum of the residuals. The following theoretical consideration might contribute to the problem. Let

$$y(t) = A_{ET} cos(\omega_{ET} t + \varphi_{ET}) \tag{6.5}$$

be an Earth tide constituent, the amplitude $A_{ET}$ of which varies with time according to

$$l(t) = A_L cos(\omega_L t + \varphi_L) \tag{6.6}$$

(6.6) is then the signal which modulates $A_{ET}$ . The modulated Earth tide signal can then be written as

$$\begin{aligned} y(t) &= (A_{ET} + l(t))cos(\omega_{ET} t + \varphi_{ET}) \\ &= (A_{ET} + A_L cos(\omega_L t + \varphi_L))cos(\omega_{ET} t + \varphi_{ET}) \\ &= A_{ET} cos(\omega_{ET} t + \varphi_{ET}) + A_L cos(\omega_L t + \varphi_L)cos(\omega_{ET} t + \varphi_{ET}) \end{aligned}$$

or

$$\begin{aligned} y(t) &= A_{ET} cos(\omega_{ET} t + \varphi_{ET}) \\ &+ \frac{A_L}{2}\cos\big((\omega_{ET} - \omega_L)t + (\varphi_{ET} - \varphi_L)\big) + \frac{A_L}{2}\cos\big((\omega_{ET} + \omega_L)t + (\varphi_{ET} + \varphi_L)\big) \end{aligned} \tag{6.7}$$

This is an important formula, since it exhibits the occurrence of (tidal) amplitude modulation as the presence of a main lobe peak and 2 symmetrical side lobe peaks of frequency distance $\omega_L$.

An example might illustrate, how an interpretation of additional observed phenomena could be done. Assume that the amplitude of the **ocean tide** M2 is changing slightly for instance with yearly frequency and amplitude $A_L$ . (6.7) shows that in this case, peaks of $\frac{A_L}{2}$ are folded around M2 at $\omega_{M2} \mp 0.04°/h$ . With a record length of 1 year, the side lobe peaks of equal height $\frac{A_L}{2}$ should be detected in the residual spectrum . To assure the significance of these side peaks, they should be introduced into a least squares adjustment.
With shorter record length, the side lobe peaks will lead to abnormal M2 parameters and could partly be observed in the residual amplitude spectrum. As it was shown in (SCHÜLLER, K. 1976), the subsequent time-variant tidal (auxiliary) parameters of M2 (called parameter functions in SCHUELLER, K. 1986), derived from analyses with a shifted basic interval, will oscillate with $\Delta\omega = 0.04°/h$.

If (6.6) does not only contain a single harmonic, but a series with a broad spectrum, (6.7) would exhibit not only 2 symmetric peaks but a fanned out pattern of peaks around the modulated signal. This pattern would be reflected in the residual spectrum as well. All frequencies with significant peaks would then lead to a set of additional harmonics (2.3) to model this rather complicated process appropriately.

# 7. Conclusions and outlook

The basic principles of least squares tidal analysis and spectral analysis of the residuals have been presented as the theoretical background for the enhancements of new ETERNA34-ANA-V4.0 program. Implementation aspects and the program description have been kept to a minimum and are published in a different presentation, the user's guide (SCHÜLLER,K. 2014).

The program itself is ready for distribution to interested parties by beginning of the year 2015. It is available upon request as executable on Windows 7, 32- and 64 bit, and Windows 8.1 platforms totally free of charge.

## Acknowledgements

Such a project cannot be set up without helping hands from a great variety of supporters. I am sure that I will miss somebody, and therefore I am asking for apologizes in advance.

Special thanks owed to Mrs. Marion Wenzel, who kindly supports this initiative by authorizing me to further maintain and enhance the programs of her late husband.

The FORTRAN source code of the ETERNA programs together with a comprehensive amount of sample data was provided by the ICET, Tahiti. Moreover, the ICET was a great help to get this presentation published in the BIM very rapidly. Special thanks are owed to Prof. Dr. Jean-Pierre Barriot for his kind support.

Also I would like to express my thanks to Dr. Walter Zürn, BFO Schiltach, who dedicated a lot of his precious time for providing overall encouragement and help as well as scientific consultancy and a data set for testing purposes.

My special thanks are dedicated to Prof. Bernard Ducarme for thoroughly reviewing the manuscript of this paper. His valuable remarks contributed to improve the quality of this presentation considerably.

It was a real pleasure to get in contact again with my teammate from Bonn University, Dr. Herbert Wilmes, BKG Frankfurt, who confirmed me to proceed on this project. Dr. Wziontek, BKG, was a challenging partner in scientific discussions and provided data sets for testing, thank you for that.

My sincere thanks are owed to my highly respected teacher, PhD -supervisor and friend Prof. Dr.-Ing. Manfred Bonatz, GeoOberservatorium Odendorf, who gave so many encouragements and valuable advises for getting started with this project. He also provided all of his data for testing. I am really grateful and proud that after more than a generation of pursuing different fields of activity we are working together again as a team that apparently has never been separated. Since he was the first who installed and tested the new software he chose the hard way of our cooperation.

Last but not least I would like to express my deepest thanks to my wife Arunee for her loving patience and endless support while her husband was caught in chasing some thought or code problems.

Thanks a lot to you all again.

## References:


Box,G.E.P. et al. : Time series analysis. Forecasting and Control. Prince Hall Inc., New Jersey 1994. ISBN 0-13-060774-6.

Chojnicki, T. : Ein Verfahren zur Erdgezeitenanalyse in Anlehnung an das Prinzip der kleinsten Quadrate. Mitteilungen aus dem Institut fuer Theoretische Geodaesie der Universitaet Bonn Nr. 15, Bonn 1973.

Calvo, M. et al. : Time stability of spring and superconducting gravimeters through the analysis of very long gravity records. J. Geodyn .2014

Ducarme, B.,Vandercoilden,L., Venedikov,A.P. : Estimation of the precision by the tidal analysis programs ETERNA and VAV. Bulletin d'Informations Marees Terrestres, vol. 147, Bruxelles 2011.

Ducarme, B. : The K1 triplet: Can Lunar nodal waves contribute to th study of the Free Core Nutation (FCN)? Bulletin d'Informations Marees Terrestres, vol. 141, Bruxelles 2006.

Hartmann, T., Wenzel, H.-G. : Catalogue of the earth tide generating potential due to the planets. Bulletin d'Informations Marees Terrestres, vol. 119, Bruxelles 1994.

Jenkins, G.M., Watts, D.G. : Spectral analysis and its applications. Emerson-Adam Press,Inc., Boca Raton , Florida,USA.1968. ISBN 1-892803-03-8.

Kudryavtsev, S.M. : Improved harmonic development of the Earth tide-generating potential. Journal of Geodesy (2004) 77.

Merriam, J.B. : Non-linear tides observed with the superconducting gravimeter. Geophy. J .Int. (1995) 123.

Munk, W., Hasselmann, K. :Super-resolution of tides. Studies on Oceanography 1964.

Schüller, K. : Ein Beitrag zur Auswertung von Erdgezeitenregistrierungen. Deutsche Geodätische Kommission, Reihe C Heft Nr. 227, München 1976.

Schüller, K. : About the sensitivity of the Venedikov tidal parameter estimates to leakage effects. Bulletin d'Informations Marees Terrestres , vol. 81, Bruxelles 1978.

Schüller, K., Wenzel, H.-G., Zürn, W.: Analysis of simulated nonlinear systems driven by tides. Deutsche Geodätische Kommission, Reihe B Heft Nr. 231, München 1979.

Schueller, K.: Simultaneous tidal and multi-channel input analysis as implemented in the HYCON-method. Proceedings 10th International Symposium on Earth Tides, Madrid 1986.

Schüller, K.: USER'S GUIDE ETERNA34-ANA-V4.0, Installation Kit ETERNA34-ANA-V4.0, Surin 2014

Wenzel, H.-G. : The nanogal software: Earth tide data processing package ETERNA 3.30. Bulletin d'Informations Marees Terrestres, vol. 124, Bruxelles 1996.

Wolf, H. : Ausgleichungsrechnung nach der Methode der kleinsten Quadrate. Ferdinand Dümmlers Verlag Bonn. 1968.

Zschau, J., R. Wang (1981): Imperfect elasticity in the Earth's mantle. Implications for Earth tides and long period deformations. Proceedings of the 9th International Symposium on Earth Tides, New York 1981,editor J.T. Kuo, Schweizerbartsche Verlagsbuchhandlung, Stuttgart 1981.

# ATLANTIDA3.1_2014 FOR WINDOWS: A SOFTWARE FOR TIDAL PREDICTION

**E. Spiridonov, O. Vinogradova, E. Boyarskiy, and L. Afanasyeva**

Schmidt Institute of Physics of the Earth, Russian Academy of Sciences, ul. B. Gruzinskaya 10, Moscow, 123995 Russia, e-mail: *sp287@mail.ru*

In this paper, we describe the possibilities of the ATLANTIDA3.1_2014 software, which was recently developed for predicting tidal parameters on the Earth. These possibilities include the calculation of the gravimetric oceanic effect, the amplitude delta-factors for oceanless Earth, as well as the modeled amplitude factors and phase shifts for the Earth with ocean. The program also calculates the tidal series. We present the highlights of the program and discuss the underlying theoretical and methodical ideas. The detailed installation guidelines and user manual are presented. The results of the calculations are compared with the observations.

## INTRODUCTION

At present, there are about ten programs for calculating the prognostic delta-factors and phase shifts of the tides as well as oceanic gravimetric effect. Among the first group of the software, the most popular are the *PREDICT* program of the *ETERNA* package developed by Wenzel [Wenzel G., 1996], *T-soft* [Van Camp & Vanterin, 2005], and *MT80w* programs [*ICET*]. The calculations of the oceanic effect are conducted by the *LOAD97 (ETERNA 3.3)* [Francis O. and Mazzega P., 1990], **GOTIC2** [Matsumoto et al., 2001], **OLFG** [Scherneck, 1991], and **SPOTL** programs [Agnew, 1996, 1997].

The detailed intercomparison of these programs and the analysis of their performance against the ATLANTIDA3.1._2014 program fall beyond the scope of the present work. However, we briefly outline the main features of our program, which distinguish it from the previous programs.

First, for calculating the Love numbers and delta-factors of the body tides, we applied the latitudinal dependences of these parameters obtained in [Spiridonov E.A., 2014]. These dependences differ from those calculated by Dehant V. et al. [1999] for the DDW/NH model. Our curves have a somewhat steeper latitudinal gradient, which is particularly important in the prediction of tidal data at high latitudes (see Fig. 6). The latitudinal dependence used in our work does not depend on the form of the tidal or loading potential. Besides, we also calculated the

latitudinal variations of the loading Love numbers and delta-factors. This is the first distinction of our program from the other programs.

The calculations of the loading Love numbers take into account dissipation of tidal energy in the mantle according to the logarithmic creep function. Dissipation is allowed for by some but not all programs. For instance, LOAD97 does not consider this dependence despite the fact that nothing prevents this program from specifying the loading Green's functions calculated with the allowance for the dissipation.

In *ATLANTIDA3.1_2014*, calculations can be conducted in two models of the Earth's structure: *PREM* [Dzeiwonski, A.M.&Anderson, D.L., 1981] and a later IASP91 model [Kennett B.L.N., Engdahl E.R., 1991]. Although some authors in their calculations use, in fact, several Earth's models (e.g., besides PREM, the 1066A model, which is obsolete) or modified versions of PREM, this approach has not yet become common, and still less is it popular when designing the programs for tidal computations.

In each and every program calculating the oceanic loading effect, this effect is determined by the convolution of the tidal height with the Green's functions. In these calculations, it is common to separate the near zone (2–5 degrees), within which the data are subjected to the procedure of interpolation. Thus, the high spatial frequencies of tidal height are taken from the near zone, whereas the data falling beyond this area are coarsely described by the values at the grid nodes of the oceanic model. In our opinion, this approach is not quite reasonable because, first, the high-frequency components affect the entire Earth and, therefore, they should be calculated over the entire surface. Second, instead of the near zone, it is the far zone that provides the largest contribution to the modeled oceanic gravimetric effect, and the calculations for the far zone are less accurate. Therefore, when designing our program, we implemented a different approach, which is based on the spherical harmonic decomposition of tidal height after the preliminary interpolation of all the data of the oceanic models with the degree of detail that is not worse than in the near zone in the calculations of the other authors. Thus, the near zone covers the entire Earth. Strictly speaking, the approaches that are based on the application of the Green's functions and spherical harmonic decomposition of the tidal height are fully identical from the mathematical standpoint. At the same time, the attempt to specify the near zone (e.g. in the LOAD97 model) with a size of a few tens of degrees infinitely increases the time of the computations and the obtained result tends to our estimates obtained without the allowance for the dissipation.

In addition, our program also provides the possibility of calculating the oceanic effect at the grid nodes. However, in the case of the calculations at a point, the program separately yields the

loading and Newtonian (direct attraction) components of the oceanic effect as well as their sum. By no means all programs provide this option.

In contrast to almost all the other programs of this kind, ATLANTIDA3.1_2014 has a intuitively transparent user-friendly interface, which enables the user to run the program straightforwardly, without referencing to the manual.

In the first section of this work, we discuss the general principles of the program and the physical sense of the corresponding computational procedures. The second section, in fact, presents the user's manual. Finally, in the third part, we show some results of our calculations and compare the output of our program to the observations.

## 1. MAIN COMPUTATIONAL PROCEDURES

The general flow-chart of the calculations that are carried out when preparing the initial data for the ATLANTIDA3.1_2014 program and the calculations that are carried out directly by our program are illustrated by Fig. 1.

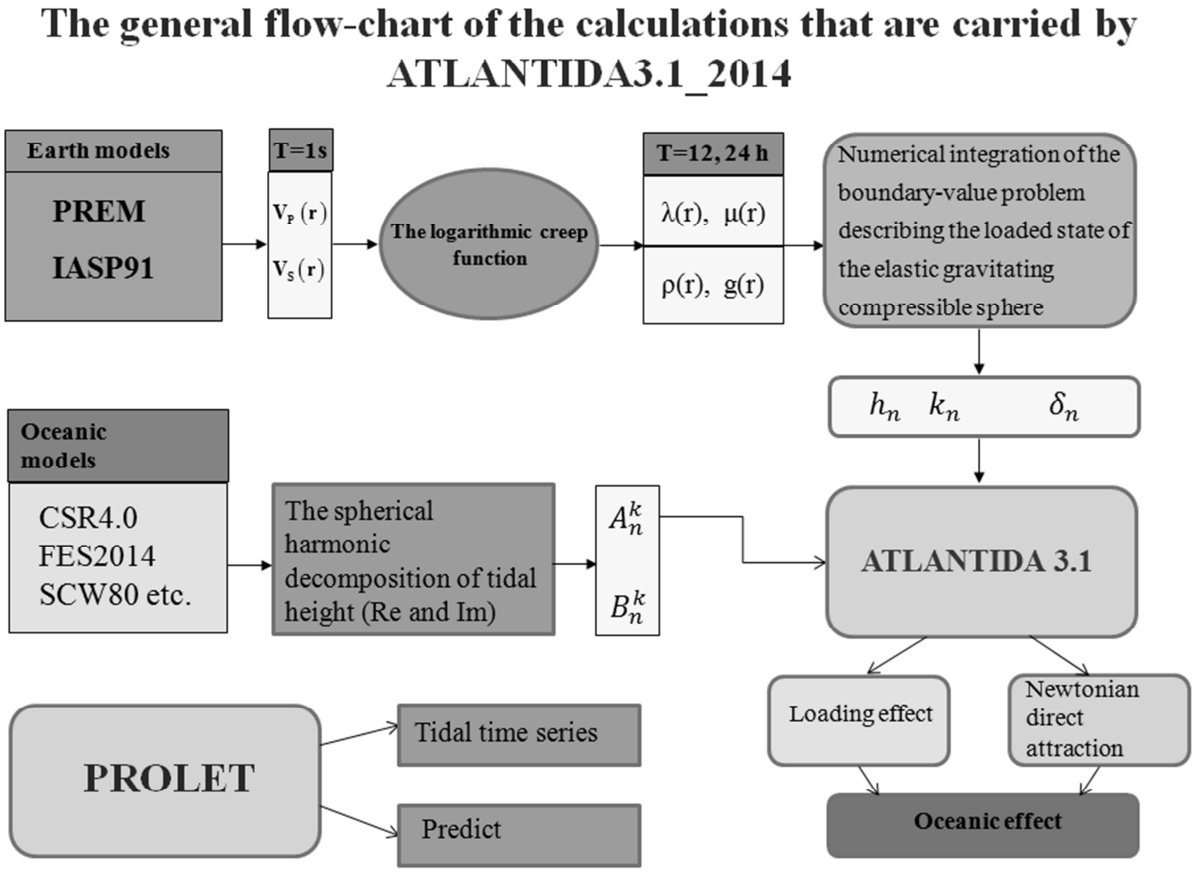


**Fig 1. The general flow-chart of the calculations**

In the calculations of the oceanic loading effect, Love numbers, and delta-factors of the body tide, we applied, as was mentioned above, two models of the interior structure of the Earth,

namely, PREM and IASP91 [Vinogradova, Spiridonov, 2012; Spiridonov, 2014]. The second model, for example, more adequately describes the structure of the crust and upper mantle of Europe and is more advanced. For the both models, the velocity curves of the seismic compressional and shear waves were recalculated from the reference period of 1 s to the periods of the tidal waves using the logarithmic creep function. Then, with the use of the obtained values, the Love parameters, density curves, and the curves of gravitational acceleration were calculated. These four dependences as well as the curves of compression and its derivative, served as the main input data required for numerical integration of the boundary-value problem describing the loaded state of the elastic gravitating compressible sphere with the allowance for the latitudinal variations in the elastic parameters and potential.

The problem is described by the set of the six ordinary first-order differential equations with three boundary conditions on the Earth's surface and three conditions on the mantle-core boundary [Spiridonov, 2014]. The method of numerical integration of the boundary problem is most thoroughly expanded in [Spiridonov E. and Vinogradova O., 2013; Vinogradova, Spiridonov, 2013b]. Integration was carried out with a 0.1-km step along the depth.

When determining the delta-factors of the M2 wave, the corresponding corrections for the effects of inertia forces presented in [Molodenskiy S.M., 1984] were added to the Love numbers $k_2$ and $h_2$.

For the diurnal waves, we applied the resonance curve (24) from [Dehant V. et al., 1999]. We constructed this curve for the amplitude delta-factors of the waves in the near-diurnal period range for the DDW/H and DDW/NH models. After this, for the same models we calculated the ratios of the obtained delta-factors of diurnal waves to the delta-factor of the M2 wave and the average values of these ratios over two models. The need for calculating the average over two models was motivated by the fact that the latitudinal average delta-factor for the M2 wave obtained for the PREM model fell, within 0.004% accuracy, between the delta-factors of this wave in the DDW/H and DDW/NH models. At the same time, the averages for IASP91 have practically coincided with the averages for DDW/NH (see section 3).

Based on the values of the ordinary and loading Love numbers, the corresponding amplitude delta-factors are calculated. In contrast to the loading delta factors up to order 10000 and their latitudinal dependence (with a step of 0.1 degree), which were calculated a priori and, in fact, served as the input data for the program, the second-order delta-factors of the body tide are calculated every time the program is run.

The load was specified by the tidal masses of the six tidal models: CSR3.0, FES95.2, the Schwiderski model (SCW80), NAO99b, CSR4.1, and FES2012. The tidal heights were

expanded into the spherical harmonic series up to order 720 (up to order 1120 for FES2012). For doing this, we used the system of recurrent formulas for the integrals of the Legendre polynomials and associated polynomials [Spiridonov, Afanasyeva, 2014; Spiridonov 2013].

The obtained coefficients of the expansion together with the loading delta-factors composed the input data for the ATLANTIDA3.1_2014 program. Based on the obtained expansions and loading delta-factors, the program calculates the value of the loading effect, direct Newtonian attraction by the mass of water, and their sum.

The amplitudes and phases of the oceanic gravimetric effect as well as the delta factors of the body tide calculated by the program for 63 groups of the waves are inputted to the PROLET program developed by E.A. Boyarsky and L.V. Afanasyeva. Being the part of the ATLANTIDA3.1_2014 package, PROLET calculates the prognostic values of delta-factors and phase shifts for the Earth with ocean as well as the tidal series for the time interval of interest. The prognostic amplitude delta factors are only calculated for those waves for which the oceanic effect is known. The time series are separately calculated for the oceanic and body tide as well as for their sum. The computational scheme of PROLET largely follows the PREDICT program from the Wenzel's ETERNA 3.3 package. The expansion of tidal potential into 1200 Tamura's waves (1987) is applied. The corrections for the conversion from UTC to TDT time are taken from the USNO website http://maia.usno.navy.mil/ser7/deltat.data and decimated in such a way that for the time after 1973, the error of the correction does not exceed 1 s (the error of the tidal effect is less than 1 nm /$s^2$).

## 2. HOW TO WORK WITH THE PROGRAM

### 2.1 Downloading and installation

To download the program, please follow the link:

https://yadi.sk/d/hszRKInqcrDSC

or

https://drive.google.com/open?id=0B_PQJhBLmMBrWnpfanpYT01qeEE&authuser=0

and download the ATLANTIDA.EXE file to your computer. This a self-extracting archive, which should be installed to the root directory on any desired disc.

Attention! Unless installed to a root directory, the program won't run.

To run the program, hit **/ATLANTIDA31/ATLANTIDA31.EXE.** Select the desired options (see Fig.2 below) in the dropdown menu.

Warning! In the work with this menu, the separator between the integer part and fractional part of the entered numbers is a dot. However, by default, the WINDOWS settings prescribe this separator to be a comma. In order to correctly run the program, one should either replace the

separator in the form of a comma in the WINDOWS settings by the separator in the form of a dot, or to fill the menu prompts using the separator in the form of a comma. In the next versions of the program, we intend to make it independent on this OS setting.

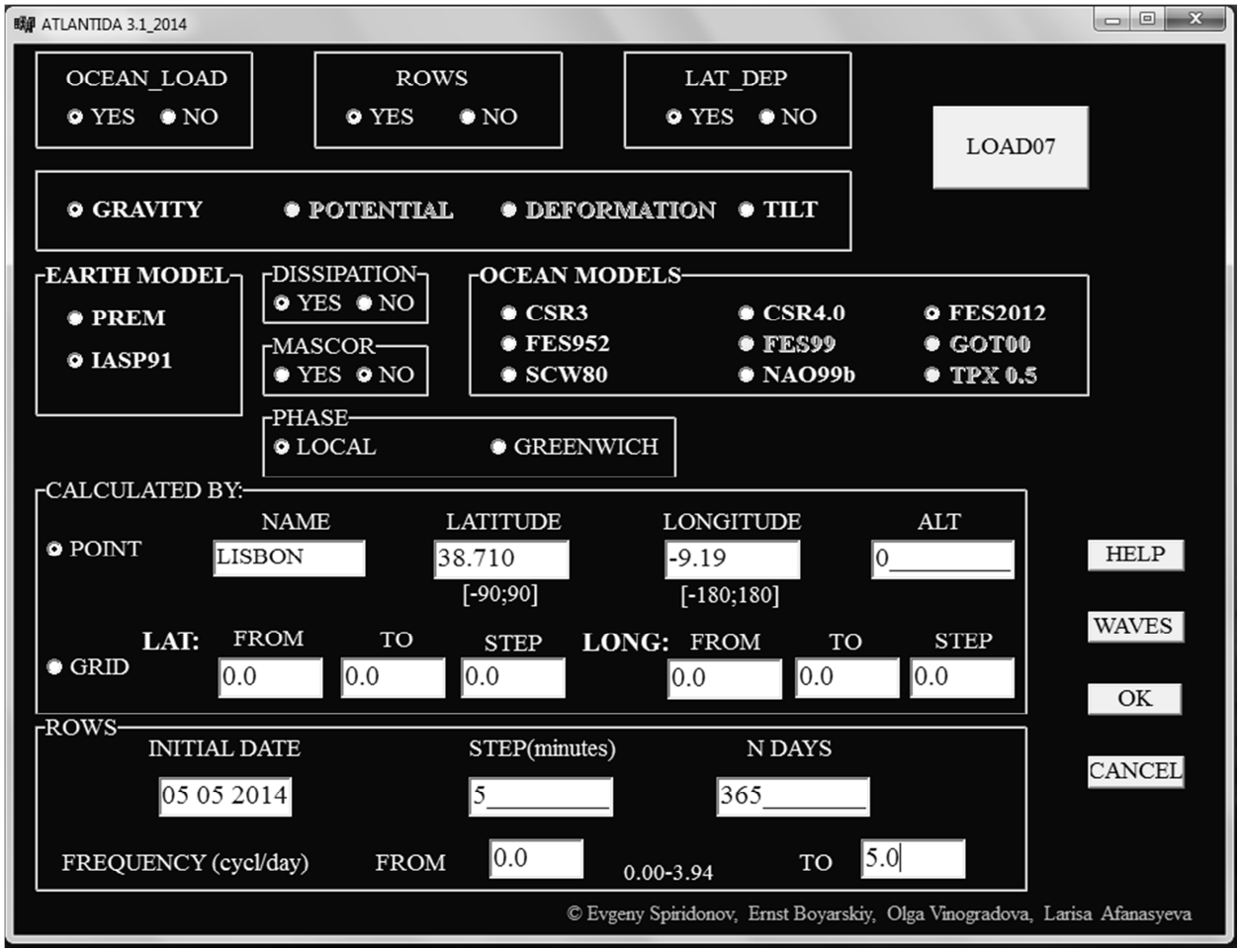


Fig 2. The ***ATLANTIDA 3.1_2014*** interface

## 2.2 Selecting the options

2.2.1. General options

***OCEAN_LOAD YES*** or ***NO***: Calculate or not calculate the oceanic effect;
***ROWS YES*** or ***NO***: Calculate or not calculate the tidal time series;
***LAT_DEP***: To take or not to take into account the latitudinal dependence of the ordinary and loading delta-factors.

After the desired options are selected, this version of the program can be used in either of the two possible modes: ***GRAVITY*** or ***TILT***. For tilt it is only possible now to compute ocean tide loading in the NS and EW directions.

***EARTH_MODEL*** – Selecting the Earth model (PREM or IASP91);

2.2.2. Selecting the parameters of calculations of the oceanic gravimetric effect

***OCEAN_MODELS*** - Selecting the tidal ocean model (***YES*** if ***OCEAN_LOAD*** is selected).

The calculations for the selected oceanic model can be conducted with the allowance for dissipation (***DISSIPATION***) and mass correction (***MASCOR***). The ***DISSIPATION*** option only applies to the loading delta factors. By default, the delta factors of the body tides are calculated with dissipation.

You can select the phase: ***LOCAL*** or ***GRENWICH***. (If the ***ROWS*** option is enabled, the ***GRENWICH*** option is unavailable.)

When calculating the oceanic effect (***OCEAN_LOAD: YES***), you should also specify the set of the waves for the selected oceanic model. For doing this, click on the ***WAVES*** bottom, select the desired waves in the popup window and be sure to hit the ***SAVE*** button (Fig. 3).

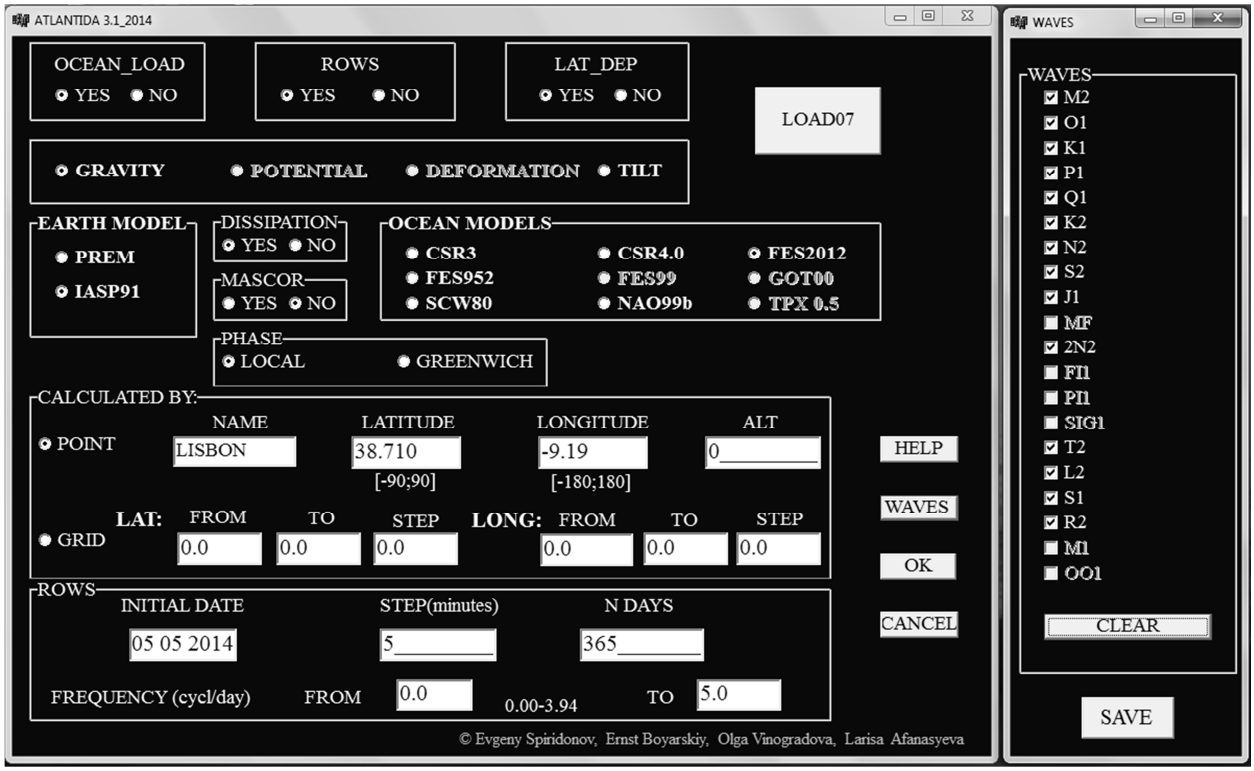


Fig.3. The ATLANTIDA 3.1_2014 program interface with the pop-up window to select the waves.

2.2.3. The name and location of the site

By default, all the options listed above (except for the selection of the waves and tidal time series parameters) are set optimal by the program. To get started, you should only specify the name of the station (***NAME***), the site latitude (***LATITUDE***) in degrees, longitude (***LONGITUDE***) in degrees, and altitude (***ALT***) in meters and tidal time series parameters.

2.2.4. The parameters of calculation of the time series

Then, in order to construct the time series in the ***ROWS*** mode, you should specify the start date (***INITIAL DATE***), the time step in minutes (***STEP (min)***), the number of the days (***N DAYS***), and the frequency band (***FREQUENCY***) in cycles per day. The entire tidal frequency band is subdivided into 63 groups of waves (Table 1). If the user specifies a limited frequency band, the group of the waves that contains the boundaries of this band is selected as a whole for the further calculations. If some of the waves that were previously selected for calculating the oceanic effect do not fall in the last frequency band, the program automatically removes them and issues the warning message.

**NOTE:** The additional ***GRID*** mode (creation of the gridded ocean loading data) only works in the ***GRAVITY*** mode with ***ROWS NO***. Here, you may only select a single wave from ***WAVES***. The additional ***TILT*** mode only works for ***POINT*** and ignores ***ROWS*** mode by default.

**WARNING!** In this version of the program, the ***ALT***, ***N DAYS*** and ***STEP*** fields are integers.

In case of a wrong choice of the parameters, the program displays the error message (see section 2.4).

The interface has also a button that runs the ***LOAD07*** program. This program is completely identical to the ***LOAD89 (97***) program of the Wenzel's ***ETERNA3.3*** package. At the same time, ***LOAD07*** has a convenient user-friendly interface, which makes it possible to conduct calculations both at a single point and on a grid and to select the waves of interest for the user. This interface was designed by Ernst Aronovich Boyarskiy in 2011. Later, two updates were introduced into the program. They provided the possibility to account for the effect of the **M2** wave of ***FES95.2*** model, which was previously impossible, and fixed the bugs associated with introducing the station height corrections and mass correction in the ***FES95*** and ***SCW80*** models. The ***LOAD07*** program has its own ***HELP*** (only available in Russian in this version of the program).

## 2.3. Running and operation of the program

After specifying all the required settings, click **OK**. The names of the results files are generated automatically.

If the OCEAN_LOAD YES option (calculation of the oceanic gravimetric effect) is selected, immediately after the start of the program, a popup window will appear (Fig. 4). This window displays the number of the wave for which the calculations are being conducted and the total number of the waves specified for calculating the oceanic effect.


Fig. 4. The popup window of calculations of the oceanic effect

Immediately upon the completion of the calculations of the oceanic effect, ATLANTIDA3.1 passes the control to the PROLET program. This only occurs if the ROWS YES option is selected. The PROLET program calculates the tidal series as well as the prognostic values of delta-factors and phase shifts for those waves for which the oceanic effect has been calculated previously. After the termination, the program displays the popup window shown in Fig. 5:

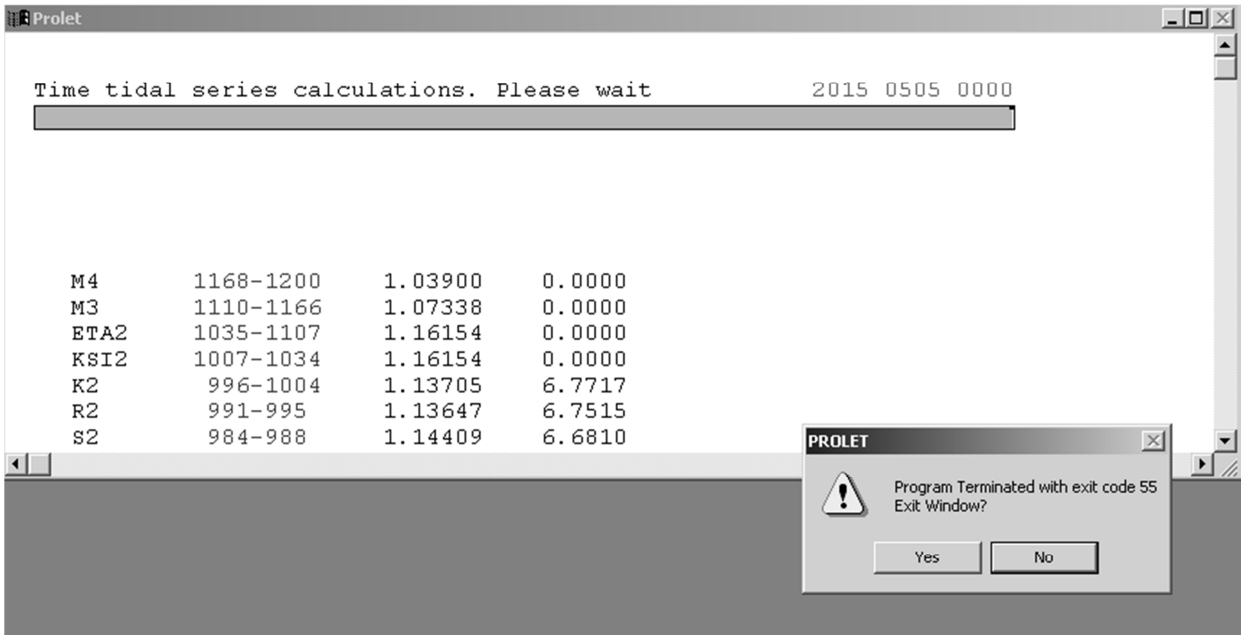


Fig. 5. The popup window of program termination

If the program was successfully terminated with exit code 55, press YES. Otherwise (exit code 0) press NO and reinstall the whole program package or contact the author of the program. Program termination with exit code 55 informs the user that failures were absent at all the steps of the calculations.

## 2.4. Program messages

The program issues more than thirty different messages overall. Below, we present short comments on each message. The messages are listed in the alphabetical order. By checking the messages, the user can also obtain the information on some limitations assumed in a given version of the program.

**0<N_DAYS<=9800!** The number of the days used for constructing the tidal series should be at most 9800 (26.8 years)

**Access violation in CC3260MT.DLL.** This system message appears if the program is installed in other than a root directory.

**ALTITUDE is not valid!** The height of the observation site specified for the program should range within -9000 to +9000 m.

**DAY is not valid!** The day of the month starting from which the user would like to calculate the tidal time series should be specified in the range from 1 to 31.

**FILE [FILE_NAME ] already exist! Replace it? (Y or N)** This message may only appear in the case of repeated computations for the same site if the calculation is fully identical to the previous one or if a different set of the waves is selected for this oceanic model. By pressing Y and Enter, you can rewrite the new file over the old one (replace the old file by the new one). If you press No and Enter, the program terminates. The file can be copied from the RESULTS directory to any other directory.

The following three messages are concerned with specifying the frequency band in the calculations of the tidal time series. They appear if the lower specified frequency is higher than the higher frequency or if the specified frequencies are negative.

**Frequency2 must be greater then frequency1.**

**Frequency1 is not valid!**

**Frequency2 is not valid!**

**GREENWICH PHASE does not work with ROWS option.** The option of selecting the Greenwich phase in our program is only available for calculating the amplitudes and phases of the oceanic effect. This option does not work with the mode of constructing the tidal series (ROWS).

**Latitude for this model must be >= -78 deg.** This message only concerns the CSR3.0 and Schwiderski tidal oceanic models.

**Latitude for this model must be >= -85 deg.** This message only concerns the FES95 tidal oceanic model.

**Latitude for this model must be from -89.75 to 89.75 deg.** This message only concerns the NAO99b tidal oceanic model.

One of the following seven messages appears if the latitude specified for a site or for a grid node falls beyond the interval from -90 to +90 degrees, or if the longitude is lower than --180 degrees or higher than +180 degrees, or if the value of the lower latitude (longitude) in the grid calculations is greater than or equal to the larger latitude.

**LatFin is not valid! (-90 90)**

**LATITUDE is not valid! (-90 90)**

**LATITUDE: LatStart>=LatFin!**

**LONGITUDE is not valid! (-180 180)**

**LONGITUDE: LongStart>=LongFin!**

**LongFin is not valid! (-180 180 for GRID)**

**LongStart is not valid! (-180 180 for GRID)**

**MONTH is not valid! (1 12)** The number of the month specified in the initial date in the calculations of the time series should range from 1 to 12.

**NO sp.exe!** The program warns that the installation package lacks the sp.exe program, which checks the completeness of the whole package. This check is executed every time the ATLANTIDA3.1 program is run.

**NO subject computing. OCEAN_LOAD or ROWS must be YES.** The both **OCEAN_LOAD** and **ROWS** options are set to **NO.**

**NO WAVES!** This is the most frequent message warning that the waves for calculating the oceanic effect in the selected tidal model are not specified. To specify the waves, click on the ***WAVES*** button, select the desired waves in the popup menu and press ***SAVE***. This message often appears if the user had selected the waves but changed some other settings afterwards.

**Option ROWS for TILT does not work in this version.** The tidal series of the tilts are not calculated in this version.

**ROWS option: latitude must be from -89 to 89 degrees.** In the calculations of the tidal time series, the latitudes should range within -89 and 89 degrees.

**STEP>NDAYS*24*60!** The time step in minutes indicated for the calculations of the time series cannot be longer than the length of the series.

The following three messages appear if in the calculations of the oceanic effect on the numerical grid, the selected step of calculations along the latitude (longitude) is larger than the entire range of calculations or if it is negative.

**Step by latitude is too large!** (the step along the latitude exceeds the entire latitudinal range of the calculations).

**Step by longitude is too large!**

**Step by latitude or longitude is not valid! (**the specified step is negative ).

**TILT GRID is not possible in this version.** The grid calculations of the amplitude and phase of the oceanic effect for the tilts are not possible in this version of the program.

**The ocean model wave [WAVE_NAME] is outside the rows frequency band. These waves will exclude from the list of the ocean model!** This is a purely informational message. The waves of the oceanic effect that were not included in the frequency band selected for calculating the tidal series are excluded from the further calculations.

**YEAR is not valid!** The first year of calculations of the tidal series should fall in the interval from 1000 to 9999.

**You can calculate only one wave for GRID!** The calculations of the amplitudes and phases of the oceanic effect at the grid nodes are only possible for a single wave of the selected tidal oceanic model. This message appears if the user specifies many waves.

### 2.5. The Results Files

The files of the results are located in **\ ATLANTIDA31 \ RESULTS**.

For the example shown in the Fig. 2, the program displays the following three files in the ***RESULTS*** directory:

**LISBON_FES12_IASP_L_DY_MN_LAT_DEP_YES_GRAV.dat**
**LISBON_FES12_IASP_L_DY_MN_LAT_DEP_YES_GRAV.prn**
**LISBON_FES12_IASP_L_DY_MN_LAT_DEP_YES_GRAV.grw**

The first file (**.DAT**) contains the tidal time series, the second file **(. PRN**) contains the constants used in the calculations, the amplitude delta-factors, and phase shifts for the Earth without and with the ocean for the groups of the waves. The amplitude factors and phase shifts for the Earth with ocean are only calculated for the waves for which the oceanic effect is calculated. These waves can easily be distinguished in the list of the waves by the non-zero phase shifts (Table 1).

The third file (**.GRW**) contains the amplitudes and phases of the gravity oceanic effect (the Newtonian attraction of water masses, the loading effect, and their sum). In the ***TILT*** mode, the **NS** and **EW** components are provided.

Table 1.

MAIN WAVE theoretical parameters
Delta-factors and phase lags for the Earth with ocean

| N | Wave Group | <------- From...To -------> Cycle/Day | | Numbers | AMPL. nm/s**2 | FREQUENCY Cycle/Day | Amplitude Factor | Phase Lag. Deg. |
|---|---|---|---|---|---|---|---|---|
| 1 | M4 | 2.935321 | 3.937897 | 1168-1200 | 0.91451 | 2.97161 | 1.03900 | 0.00000 |
| 2 | M3 | 2.753244 | 2.935174 | 1110-1166 | 7.01912 | 2.89841 | 1.07338 | 0.00000 |
| 3 | ETA2 | 2.039339 | 2.182843 | 1035-1107 | 3.23297 | 2.04177 | 1.16154 | 0.00000 |
| 4 | KSI2 | 2.005623 | 2.039177 | 1007-1034 | 1.87187 | 2.00577 | 1.16154 | 0.00000 |
| 5 | K2 | 2.003032 | 2.005622 | 996-1004 | 57.82324 | 2.00548 | 1.13705 | 6.77168 |
| 6 | R2 | 2.000619 | 2.003031 | 991-995 | 1.77965 | 2.00274 | 1.13647 | 6.75150 |
| 7 | S2 | 1.998287 | 2.000456 | 984-988 | 212.74914 | 2.00000 | 1.14409 | 6.68103 |
| 8 | T2 | 1.997115 | 1.997493 | 980-982 | 12.43269 | 1.99726 | 1.11181 | 6.44535 |
| 9 | TL2 | 1.968876 | 1.997114 | 956-979 | 3.23189 | 1.96918 | 1.16154 | 0.00000 |
| 10 | L2 | 1.968271 | 1.968875 | 950-955 | 12.92498 | 1.96857 | 1.10354 | 6.82502 |
| 11 | LM2 | 1.932421 | 1.968270 | 904-949 | 3.37194 | 1.96371 | 1.16154 | 0.00000 |
| 12 | M2 | 1.931817 | 1.932420 | 895-901 | 457.27659 | 1.93227 | 1.06495 | 7.96007 |
| 13 | MNI | 1.901459 | 1.931816 | 871-894 | 1.57185 | 1.92954 | 1.16154 | 0.00000 |
| 14 | NI2 | 1.900545 | 1.901458 | 865-870 | 16.62923 | 1.90084 | 1.16154 | 0.00000 |
| 15 | NIN | 1.896602 | 1.900544 | 855-863 | 0.81804 | 1.89872 | 1.16154 | 0.00000 |
| 16 | N2 | 1.895363 | 1.896601 | 843-854 | 87.55012 | 1.89598 | 1.00349 | 7.12819 |
| 17 | NMI | 1.865167 | 1.895362 | 818-842 | 0.94334 | 1.86729 | 1.16154 | 0.00000 |
| 18 | MI2 | 1.864253 | 1.865166 | 813-816 | 13.98132 | 1.86455 | 1.16154 | 0.00000 |
| 19 | MIN | 1.861663 | 1.864252 | 804-812 | 0.35759 | 1.86424 | 1.16154 | 0.00000 |
| 20 | 2N2 | 1.859071 | 1.861662 | 795-802 | 11.58524 | 1.85969 | 0.94940 | 4.57114 |
| 21 | NEP | 1.830685 | 1.859070 | 779-794 | 0.65254 | 1.83311 | 1.16154 | 0.00000 |
| 22 | EPS2 | 1.827342 | 1.830684 | 771-777 | 3.37798 | 1.82826 | 1.16154 | 0.00000 |
| 23 | 3N2 | 1.822633 | 1.826136 | 763-769 | 1.30356 | 1.82340 | 1.16154 | 0.00000 |
| 24 | 222 | 1.719381 | 1.822486 | 733-761 | 0.55939 | 1.79196 | 1.16000 | 0.00000 |
| 25 | V1 | 1.111613 | 1.216397 | 686-731 | 2.49611 | 1.11223 | 1.15605 | 0.00000 |
| 26 | OV | 1.080797 | 1.109950 | 663-683 | 0.62659 | 1.10676 | 1.15605 | 0.00000 |
| 27 | OO1 | 1.073202 | 1.078825 | 644-662 | 13.03706 | 1.07594 | 1.15610 | 0.00000 |
| 28 | OJ | 1.039193 | 1.073201 | 613-643 | 3.95301 | 1.07046 | 1.15631 | 0.00000 |
| 29 | J1 | 1.036910 | 1.039192 | 606-612 | 23.83138 | 1.03903 | 1.15894 | 0.75464 |
| 30 | THE1 | 1.010333 | 1.036748 | 584-604 | 4.55719 | 1.03417 | 1.15685 | 0.00000 |
| 31 | FI1 | 1.007904 | 1.008655 | 576-581 | 6.06752 | 1.00821 | 1.17011 | 0.00000 |
| 32 | PSI1 | 1.003651 | 1.007903 | 569-575 | 3.33251 | 1.00548 | 1.26954 | 0.00000 |
| 33 | K1 | 1.002575 | 1.003650 | 557-568 | 426.17775 | 1.00274 | 1.12803 | 0.74981 |
| 34 | KS | 1.001826 | 1.002574 | 553-556 | 0.23882 | 1.00243 | 1.13841 | 0.00000 |
| 35 | S1 | 0.997734 | 1.001825 | 546-552 | 3.33228 | 1.00000 | 1.08476 | -4.46744 |
| 36 | P1 | 0.995143 | 0.997733 | 537-544 | 140.99789 | 0.99726 | 1.14204 | 0.69984 |
| 37 | PI1 | 0.989049 | 0.995142 | 532-536 | 8.24189 | 0.99452 | 1.15054 | 0.00000 |
| 38 | PIC | 0.971598 | 0.989048 | 525-530 | 0.19465 | 0.97404 | 1.15272 | 0.00000 |
| 39 | CH1 | 0.970994 | 0.971597 | 521-523 | 4.55788 | 0.97130 | 1.15351 | 0.00000 |
| 40 | CHM | 0.968566 | 0.970993 | 515-519 | 0.14720 | 0.96918 | 1.15360 | 0.00000 |
| 41 | M1 | 0.963399 | 0.968565 | 494-512 | 23.83207 | 0.96645 | 1.15366 | 0.00000 |
| 42 | MTU | 0.940017 | 0.963398 | 482-492 | 2.23608 | 0.96097 | 1.15376 | 0.00000 |

| | | | | | | | | |
|---|---|---|---|---|---|---|---|---|
| 43 | TAU1 | 0.932583 | 0.940016 | 463-481 | 3.95233 | 0.93501 | 1.15405 | 0.00000 |
| 44 | TO | 0.929684 | 0.932582 | 450-461 | 1.95353 | 0.93015 | 1.15406 | 0.00000 |
| 45 | O1 | 0.928932 | 0.929683 | 439-449 | 303.02724 | 0.92954 | 1.14443 | -0.62527 |
| 46 | OR | 0.898264 | 0.928931 | 412-438 | 1.04220 | 0.92680 | 1.15408 | 0.00000 |
| 47 | RO1 | 0.896129 | 0.898263 | 406-410 | 11.02046 | 0.89810 | 1.15408 | 0.00000 |
| 48 | RQ | 0.893407 | 0.896128 | 394-405 | 0.54121 | 0.89598 | 1.15408 | 0.00000 |
| 49 | Q1 | 0.892934 | 0.893406 | 387-392 | 58.01826 | 0.89324 | 1.16337 | -1.39957 |
| 50 | QSIG | 0.866977 | 0.892933 | 369-386 | 0.55459 | 0.89279 | 1.15404 | 0.00000 |
| 51 | SIG1 | 0.859381 | 0.866976 | 352-368 | 9.26549 | 0.86181 | 1.15399 | 0.00000 |
| 52 | 2Q1 | 0.721500 | 0.859380 | 283-349 | 7.67667 | 0.85695 | 1.15397 | 0.00000 |
| 53 | MSQM | 0.132715 | 0.249951 | 206-281 | 0.33202 | 0.14093 | 1.34442 | 0.00000 |
| 54 | MTM | 0.106756 | 0.130596 | 174-204 | 2.07906 | 0.10949 | 1.15753 | 0.00000 |
| 55 | MSTM | 0.075321 | 0.106446 | 140-171 | 0.39489 | 0.10464 | 1.15754 | 0.00000 |
| 56 | MF | 0.070317 | 0.073806 | 118-139 | 10.85895 | 0.07320 | 1.15767 | 0.00000 |
| 57 | MSF | 0.062103 | 0.070155 | 92-117 | 0.95163 | 0.06773 | 1.15770 | 0.00000 |
| 58 | MM | 0.033716 | 0.060132 | 53-91 | 5.73751 | 0.03629 | 1.15794 | 0.00000 |
| 59 | MSM | 0.028844 | 0.033701 | 40-52 | 1.09728 | 0.03143 | 1.15800 | 0.00000 |
| 60 | SSA | 0.004710 | 0.028697 | 21-39 | 5.05292 | 0.00548 | 1.15884 | 0.00000 |
| 61 | SA | 0.002428 | 0.003425 | 11-18 | 0.80223 | 0.00274 | 1.15924 | 0.00000 |
| 62 | 186 | 0.000141 | 0.000913 | 3-9 | 4.55421 | 0.00015 | 1.16144 | 0.00000 |
| 63 | M0S0 | 0.000000 | 0.000140 | 1-2 | 51.30260 | 0.00000 | 1.00000 | 0.00000 |

The names of these files only differ by their extensions. The filename consists of the following parts:

- ***LISBON*** – site name (In the ***GRID*** mode, instead of the site name, this part of the filename is composed of the wave name and a flag that is indicative of the ***GRID*** mode, for example: ***M2_GR_*** .....);
- ***FES12*** – oceanic model ***FES2012***;
- ***L*** – local phase (***G*** – Greenwich);
- ***DY*** – dissipation ***YES*** (or ***DN*** - dissipation ***NO***);
- ***MN*** – mass correction ***NO*** (or ***MY*** - mass correction ***YES***);
- ***LAT_DEP_YES*** – dependence from latitude ***YES*** (or ***LAT_DEP__NO***);
- ***GRAV*** – gravimetric effect (or ***TILT***).

If only the oceanic effect is calculated (***ROWS NO***), a single file with **.GRW** extension is yielded.

The content of the Results file for the parameters shown in Figure 1 can be found in the **ATLANTIDA31 \ EXAMPLE** directory.

The theoretical and practical results that were used when designing the program are described in some ours papers. All these publications are available in the \ **ATLANTIDA31 \ PAPERS** directory.

## 3. SOME NUMERICAL ESTIMATES OBTAINED DURING THE DEVELOPMENT OF THE ATLANTIDA3.1_2014 PROGRAM

In this section, we briefly discuss some numerical results that we obtained when developing and testing our program. These results are provided by the different variants of calculations of the oceanic gravimetric effect and amplitude delta-factors for the oceanless Earth.

### 3.1. Oceanic Effect in Europe

3.1.1. Earth models PREM and IASP

The differences in the amplitudes of ocean loading effect calculated for the PREM and IASP91 models in Europe reach 0.1 μgal (M2 wave) near the Moroccan coast and increase to 0.3 μgal at the western coasts of Portugal and France [Vinogradova, Spiridonov, 2012]. Here, the maximum discrepancies in phases do not exceed 0.1°. However, near the tip of Cape Cornwall and close to the Irish seaboard, in the region of Le Havre and Calais, the differences in the amplitudes and phases reach 0.35–0.4 μgal and 3–5°, respectively. The maximum differences in amplitude for sums of semidiurnal and all (semidiurnal and diurnal) waves were observed near Cape Lands-End (Cornwall) and reach to 0.5–0.55 μgal. In Britany these values reach to 0.35 μgal and up to 0.2 μgal near southern coasts of Europe and Morocco. The difference for the sum of diurnal waves is negligible and it do not exceeds as rule 0.01 μgal.

3.1.2. Dissipation

Dissipation induces variations in the amplitude of M2 wave, which do not typically exceed 0.1 μgal in the immediate proximity of the coastline [Vinogradova, 2012; Vinogradova, Spiridonov, 2013a]. Somewhat higher values (up to 0.2–0.3 μgal) are only observed near the mentioned St. Matthew and Land’s End Capes, which sharply project into the ocean. Again, the specific structure of the isolines in the Irish Sea and English Channel is remarkable. The phase differences do not normally exceed a few hundredths of a degree and can reach several degrees only in the specific knotty zones mentioned above. At more than 100 km distance from coastline the influence of dissipation is smaller than 0.01 μgal. The geographical distribution of considered differences derived for sums semidiurnal and all waves practically repeat the scheme of M2. In fact, in the transition from M2 to the sum of all semidiurnal waves the amplitude of differences increases upon the average to 0.05 μgal and considering the sum of eight waves it reaches 0.15–0.2 μgal. Almost half the discussed difference is obtained already even upon the transition from a reference period of 1 s to 200 s. The transition from 12 h to 24 h yields the corrections below 0.005 μgal to the amplitude and 0.1 degree to the phase.

So, the dissipation contributes 0.1-0.2 μgal to the amplitude and, typically, with a few hundredths of a degree to the phase of the total oceanic gravimetric effect near the coast of Europe

3.1.3. Spherical harmonic expansion of the oceanic tidal heights.

The comparison between the methods of calculating the oceanic load effect through Green's functions and by spherical harmonic expansion of the oceanic tidal heights up to $n$ = 720 have revealed minimal discrepancies in the results at distances exceeding 50–100 km off the coast [Vinogradova, Spiridonov, 2013a]. The differences in the amplitudes of the effect are on the order of a few tenths of microgal, and the phase differences are hundredths and thousandths of a degree. In the immediate neighborhood of the coast in the zones of moderate gradients, these discrepancies do not typically exceed 0.2–0.3 μgal and a few tenths of a degree, respectively. In the very narrow zones, the amplitude differences may reach 0.5–0.8 μgal, and this situation certainly requires further analysis. In any case, the discrepancies make up at most 2–2.5% of the studied values.

The expansion of the tidal heights in the higher order spherical harmonics does not change this pattern significantly.

3.1.4. The latitudinal dependence of the oceanic gravimetric effect

The calculations by the ATLANTIDA3.1_2014 program have shown that the latitudinal dependence of the loading Love numbers only slightly affects the calculated oceanic loading effect. Significant contribution was only revealed for the islands in the open ocean and for the zones with high gradient of the amplitudes of the oceanic effect. For example, in the Canary Islands, the difference between the amplitudes of the oceanic effect for the M2 wave calculated with and without the allowance for the latitudinal variations reaches 0.15 μgal, which makes up 0.2–0.25% of the amplitude of the body tide for this wave.

3.1.5. Comparison of oceanic effect with observations

The comparative analysis of the oceanic gravitational effect calculated in this study with the observations is based on the results obtained by different authors at 21 stations using 22 instruments. Two stations are located on the Canary Islands; two, on Svalbard; five stations carried out measurements with SLR instruments in Europe; 12 stations with superconducting gravimeters are part of the GGP network. The instruments included 12 superconducting gravimeters, eight LaCoste_Romberg gravimeters, and two Askania gravimeters. Besides comparing our calculations with the observations, we also compared them with the model predictions by other authors using the programs based, inter alia, on the regional oceanic models.

The number of cases (in%), in which the results of ATLANTIDA 3.1 are closer to those observed than calculations performed by other programs are: Canary Islands - 62%; Spitsbergen - 69%; European LCR stations - 64%; GGP network - 59%. In 77% of the cases obtained in this study the results are closer to the observations than those computed using the package Load97 from ETERNA3.30. More results of this analysis refers to the article [Spiridonov E.A. Vinogradova O.Yu, 2014].

Low-frequency sea level T/P non-tidal perturbations give the magnitude of the gravimetric load effect of order 1 mgal. [Vinogradova, Spiridonov, 2013b].

### 3.2. The delta-factors for the oceanless Earth

We compared the amplitude factors for oceanless Earth obtained in [Spiridonov, 2014] and applied in ATLANTIDA3.1_2014 with the observations using the results presented in [Ducarme B. et al., 2009]. In the quoted study, the authors analyzed the measurements by seven modern instruments of the GGP network in Europe (the CT and CD series). The effect of the ocean was considered as the average over nine oceanic models. The results are presented for the M2, O1, and K1 waves.

In more than half cases, the empirical values differed from the model predictions by about 0.01% for PREM and by about 0.1% in the other cases. In this respect, it is worth noting that the standard deviation of the amplitudes for nine oceanic models used in [Ducarme B. et al., 2009] mainly corresponded to the error of 0.1%. Nevertheless, the slightly closer agreement between the observations and model predictions in our calculations was obtained for the *IASP91* model. The discrepancies between the theory and observations in most cases do not exceed a few hundredths percent [Spiridonov, 2014, Tables 3 and 4].

It was also found that the standard deviation of the differences between the delta-factors estimated with the use of the model of [Spiridonov, 2014] and the observations at all the seven stations and for the three waves is almost 8.4% lower than the estimation based on the DDW/NH model ($8.794 \cdot 10^{-4}$ against $9.600 \cdot 10^{-4}$). However, this discrepancy is small since all the seven analyzed stations are located in the middle latitudes, where the values predicted by our model for IASP and DDW/NH barely differ (Fig. 6).

In order to compare the results derived for these two models, we carried out detailed additional processing of the gravimetric data obtained at the Syowa Antarctic station operated by Japan [Kim et al., 2011]. These data are mainly interesting by the fact that they are acquired at very high latitude (69.007 S). At the same time, this station is marked with rather wide scatter of the amplitudes and phases of the oceanic tidal models. Nevertheless, it was shown that, irrespective of the oceanic tidal model used, almost in 70% cases (for 14 oceanic models and

eight waves), the application of the theoretical delta-factors of DDW/NH model for calculating the oceanic effect observed at the Syowa station leads to poorer results in comparison with the application of the modeled amplitude factors used in the ATLANTIDA3.1_2014 program.

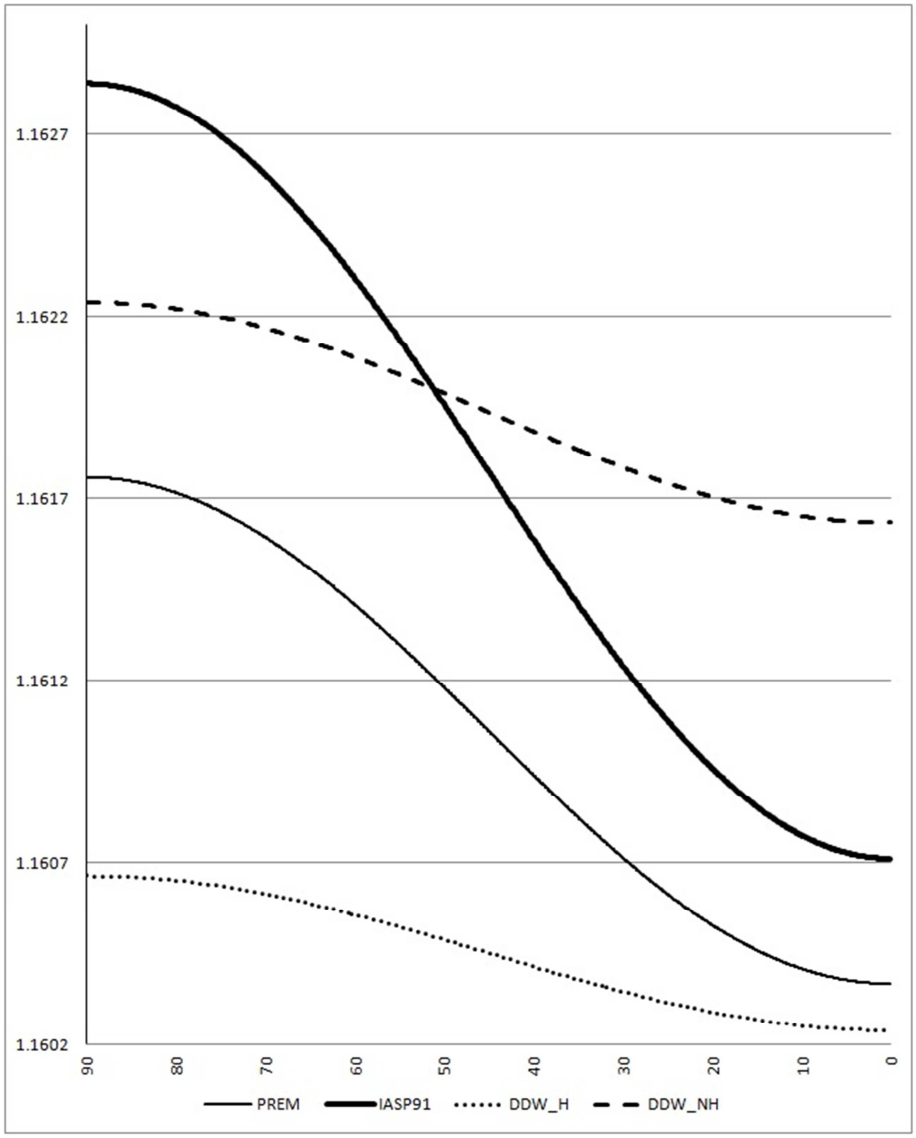


Fig. 6. Latitude dependence of M2 amplitude delta-factor calculated Spiridonov [2014] for Earth's structure models PREM and IASP91 in comparison with DDW/H and DDW/NH models of Dehant et. al. [1999].

## CONCLUSIONS

We have considered the main characteristics and possibilities of ATLANTIDA_3.1_2014 --- the new program for tidal prediction, and described the internal structure of the methods that were applied for its design. We briefly described the comparison of the output of ATLANTIDA_3.1_2014 program with the observations. Of course, the further testing will significantly expand the comparative analysis

Even in the next version (ATLANTIDA_3.1_2015) whose release is expected in the fall 2015, it is planned to increase the number of the oceanic models and to include the program for calculating the observed delta-factors and phase shifts.

After this, we will take into account the latitudinal variations of delta-factors for the waves of the zero, third, and fourth order and expand the program package by the calculations of the potential, deformations, and displacements; we will also update the computations of the tilts (the present version of our program only calculates the tilts for the oceanic effect).

The comments on the operation of the program and the suggestions for the further improvements are greatly appreciated.

**REFERENCES**

*Agnew, D. C.*, SPOTL: Some programs for ocean-tide loading. //SIO Ref. Ser. 98-8, 35 pp., Scripps Inst. of Oceanogr., La Jolla, Calif., 1996.

*Agnew, D. C.*, NLOADF: A program for computing ocean-tide loading. //J. Geophys. Res., 102, 5109– 5110, 1997.

*Dehant, V., Defraigne, P., Wahr, J.M.,* Tides for a convective Earth. //J. Geophys. Res.,1999, 104, 1035-1058.

Ducarme B., Rosat S., Vandercoilden L., Xu J.Q., Sun H.P., European Tidal Gravity Observations: Comparison with Earth Tide Models and Estimation of the Free Core Nutation (FCN) Parameters. M.G. Sideris (ed.). Observing our Changing Earth, International Association of Geodesy Symposia 133, Springer-Verlag Berlin Heidelberg 2009, pp.523-531.

*Dzeiwonski, A.M., Anderson, D.L.,* 1981. Preliminary Reference Earth Model. // Phys. Earth planet Inter., 25, 297-356.

*Francis, O., Mazzega, P.,* Global charts of ocean tide loading effects, J.geophys. Res.,1990, 95, 11411-11424.

*Kennett B.L.N., Engdahl E.R.,* 1991. Traveltimes for global earthquake location and phase identification. //Geophys. J. Int. (1991) 105, 429-465.

*Kim, Tae-Hee, et al.,* Validation of global ocean tide models using the superconducting gravimeter data at Syowa Station, Antarctica, and in situ tide gauge and bottom-pressure observations. //Elsevier, Polar Science 5 (2011), 21-39.

*Matsumoto, K., T. Sato, T. Taanezawa, and M. Ooe*, GOTIC2: A program for computation of oceanic tidal loading effect. //J. Geod. Soc. Jpn., 2001, 47, 243–248, 2001.

*Molodenskiy, S.M.*, Tides, nutation and Earth's structure. AN SSSR. IPE. Moscow 1984, 215 p.

*Scherneck, H. G.,* A parameterized Earth tide observation model and ocean tide loading effects for precise geodetic measurements. // Geophys. J. Int., 106, 677–695, 1991.

*Spiridonov E., Vinogradova O.*, ***2013***, Gravimetric oceanic loading effect. Lambert Acad. Publishing. 2013 (*in Russian*).

*Spiridonov Evgeny*, ***2013***, Oceanic Loading Effect for Gravity Prospecting, SPE Arctic and Extreme Environments Technical Conference and Exhibition, 15-17 October, Moscow, Russia, 2013, Society of Petroleum Engineers**, DOI** http://dx.doi.org/10.2118/166838-RU**, ISBN** 978-1-61399-284-5, V.1, pp. 380-412.

*Spiridonov E. A. and Vinogradova O. Yu.*, ***2014***, Comparison of the Model Oceanic Gravimetrical Effect with the Observations. *Izvestiya, Physics of the Solid Earth, 2014, Vol. 50, No. 1, pp. 118–126.*

*Spiridonov E.A.*, ***2014***, Tidal-Amplitude Delta-Factors and Their Dependence on Latitude. //Geophysical Research Abstracts, Vol. 16, EGU2014-1296, 2014.

*Spiridonov, E.A., Afanasyeva, L.V.*, ***2014***, The Program for the Oceanic Gravimetric Effect Computation (ATLANTIDA 3.0). Proceedings, IAG Symposium on Terrestrial Gravimetry: Static and Mobile Measurements (Saint Petersburg, Russia 2013).

*Van Camp, M. and Vanterin P.*, 2005: T-soft: graphical and interactive software for the analysis of the time series and Earth tides. //Computers and Geosciences, 31, 631-640.

*Vinogradova, O.Yu., Spiridonov, E.A.*, ***2012***, Comparative Analysis of Oceanic Corrections to Gravity Calculated from the PREM and IASP91 Models. *Izvestiya, Physics of the Solid Earth, 2012, Vol. 48, No. 2, pp. 162–170.*

*Vinogradova, O.Yu*, ***2012***, Oceanic tidal loads near the European coast calculated from Green's functions., *Izvestiya, Physics of the Solid Earth, 2012, Vol. 48, No.* 7-8, *pp. 572-586.*

*Vinogradova, O.Yu., Spiridonov, E.A.*, ***2013a***, Comparison of Two Methods for Calculating Tidal Loads Comparison of Two Methods for Calculating Tidal Loads. *Izvestiya, Physics of the Solid Earth, 2013, Vol. 49, No. 1, pp. 83–92.*

*Vinogradova O. Yu., Spiridonov E.A.*, ***2013b***, Some Features of TOPEX/POSEIDON Data. In 2 Application in Gravimetry Z. Altamimi and X. Collilieux (eds.), Reference Frames for Applications in Geosciences, International Association of Geodesy Symposia 138, DOI 10.1007/978-3-642-32998-2_35, Springer-Verlag Berlin Heidelberg 2013, pp.229-235.

*Wenzel, H.G.*, The Nanogal Software: Earth Tide Data Processing Package Eterna3.30. //Bull. D'Inf. Maree Terr., 1996, 124, 9425-9439.

# 60 years of Earth Tide observations in Strasbourg (1954-2014)

Marta Calvo[1,2], Severine Rosat[1], Jacques Hinderer[1], Hilaire Legros[1], Jean-Paul Boy[1], Martine Amalvict[1], Yves Rogister[1], Bernard Luck[1], Frederic Littel[1], Jean-Daniel Bernard[1]

[1] Institut de Physique du Globe de Strasbourg, IPGS - UMR 7516, CNRS/Université de Strasbourg (EOST), 5 rue René Descartes, 67084 Strasbourg Cedex, France

[2] Observatorio Geofísico Central, Instituto Geográfico Nacional (IGN), c/ Alfonso XII 3, 28014 Madrid, Spain

## Abstract

There is a tradition in gravity recording of Earth tides at Strasbourg which was initiated by Prof. Robert Lecolazet in the 50s. Since then, the surface time gravity changes have been measured locally using different kinds of gravimeters (spring, absolute and superconducting) at two different stations; first in the Seismological Observatory of Strasbourg for almost 13 years (1954-1967) and later on since the 70s at the J9 Observatory, 10 km far away from Strasbourg city. Over these years many kinds of improvements have been achieved in terms of instrumentation, of tidal potential developments and more specifically in terms of data analysis techniques, which have allowed obtaining some fundamental results.

**Keywords:** earth tides, spring gravimeter, superconducting gravimeter, absolute gravimeter

## 1. Introduction

The first observations of the Earth tides in Strasbourg were carried out in 1954 using a North American spring gravimeter, which is the first permanent gravimeter installed by R.Lecolazet in the Seismological Observatory of Strasbourg. It was the first time that such a 'long series' (almost 6 months) was recorded. Since then, first in the Seismological Observatory of Strasbourg and later on in the 70s in the J9 Observatory, the surface time gravity changes have been measured locally at different consecutive periods; at the beginning using spring gravimeters, and since 1987 using superconducting gravimeters (SG) and also absolute gravimeters (AG) since 1997. The different improvements (instrumental, processing) over these years allowed obtaining some fundamental results that we recall hereafter.

We will first review all the instrumentation (Fig. 1) that has been used in both observatories to observe Earth tides during those 60 years, and we will highlight some of the major results obtained directly from these data series as for example the observation of long period waves (Mm, Mf, Mtm) in 1966, the observation of the Free Core Nutation resonance in diurnal waves in 1974 or the first observations of the quarter-diurnal tidal waves of a few pico-g amplitude in 1995.

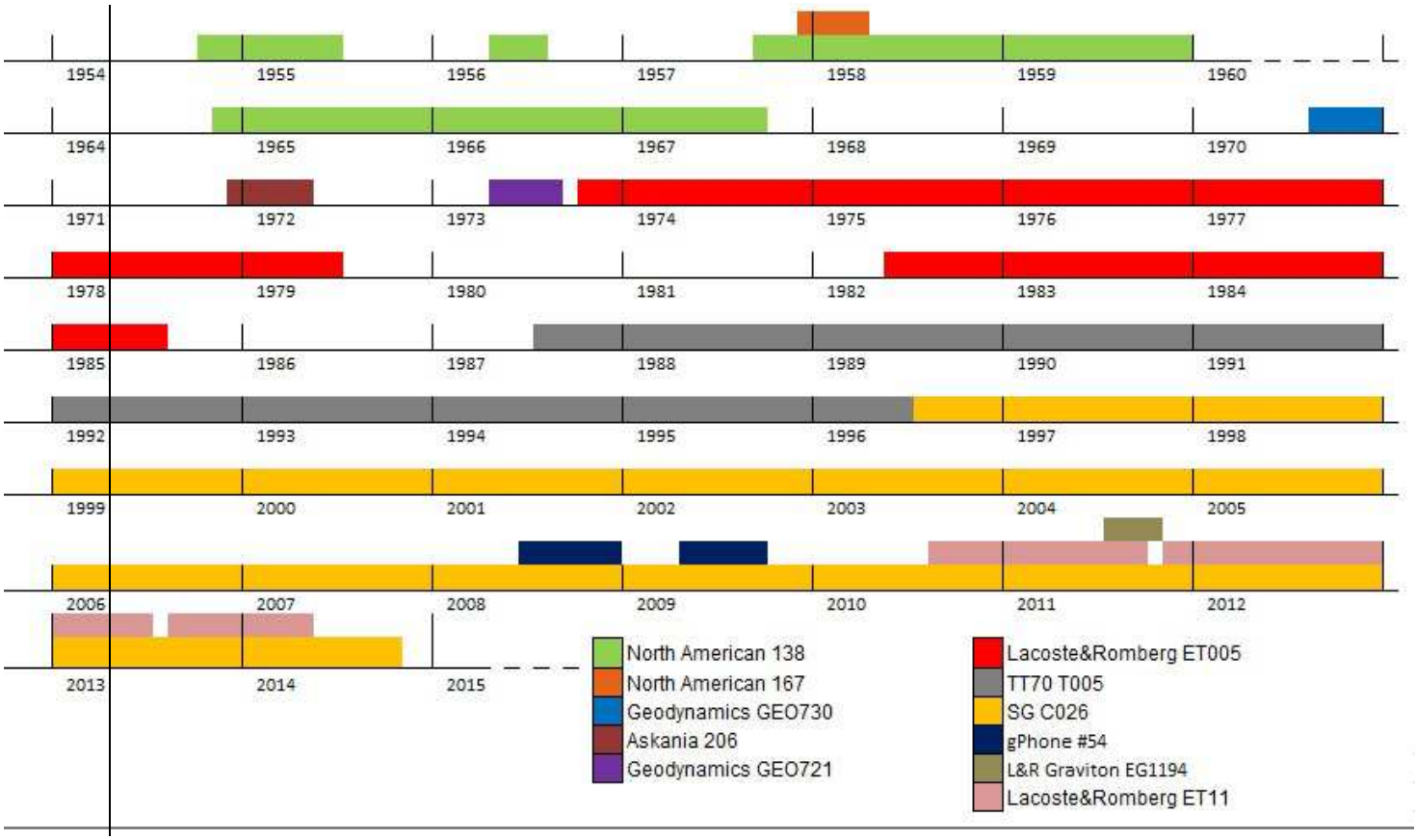


*Fig 1: Summary of the time periods when the various gravimeters have been recording at the Seismological Observatory (1954-1967) in Strasbourg, and then at J9 Observatory (1970-today), close to Strasbourg.*

## 2. Seismological Observatory of Strasbourg (1950-1970)

The first location that R. Lecolazet chose to install permanent gravimeters was inside the Seismological Observatory of Strasbourg, a building belonging to the University in the city center (48.583 ° N, 7.767 ° E, 138 m). The first observations there were carried out in 1954 using a spring gravimeter, the North American 138, which was equipped with a photographic recording device. Pr. Lecolazet and co-workers obtained more than 5 months of consecutive record, precisely 163 days from October 1954 to March 1955. This series was published as the longest series recorded at that time (Lecolazet, 1956, Melchior 1957). Since then, they continued to gradually improve their equipment obtaining longer and better data series. In November 1964 they installed the sensor in an isolated box thermostatically controlled. The gravimeter was equipped, among other improvements, with a permanent electrostatic calibration device. Moreover the photographic recording system was highly improved. As expected, the drift became much more regular and gradually decreased, making it possible to study long-period waves.

### 2.1 Observations of Long Period tidal waves

Since November 1964 this gravimeter was continuously recording for almost 3 years. Using the first 13 months of this series, they were able to observe for the first time the monthly, fortnightly and ter-monthly waves Mm, Mf and Mtm (Fig. 2 - Lecolazet and Steinmetz, 1966). These first results were still not very precise but were very encouraging. Such observations were possible not only because of the data quality, but also because of the use of new techniques of signal processing.

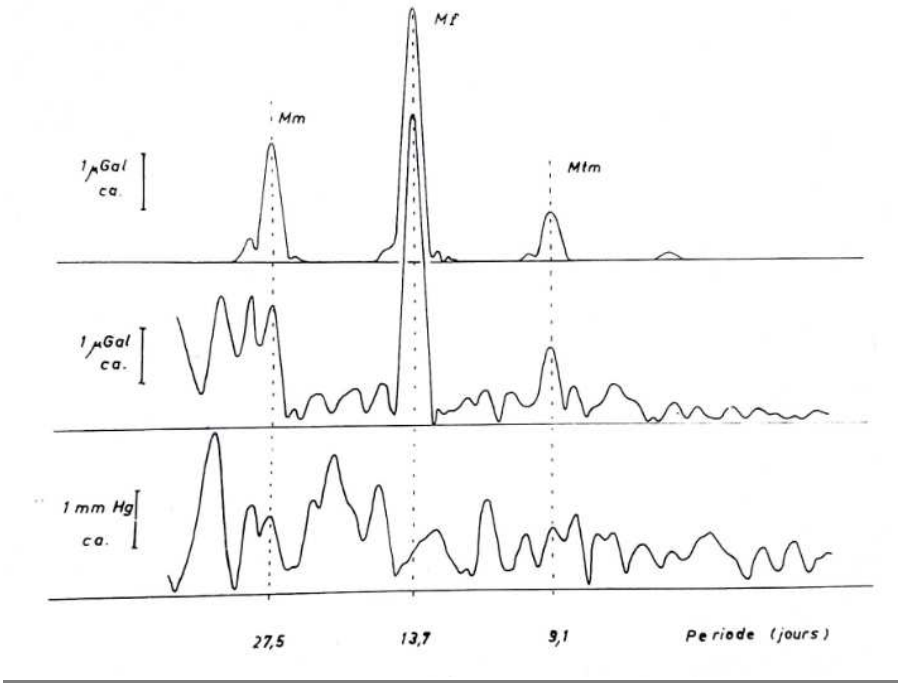


*Fig.2: First observation of the monthly, fortnightly and ter-monthly waves Mm, Mf and Mtm, using the 3 year series recorded by the North American 138 gravimeter installed in Strasbourg from 1964 until 1967 (extracted from Lecolazet and Steinmetz, 1966). Upper plot; theoretical waves. Medium plot; observed waves. Lower plot; observed air pressure variation.*

The North American AG 138 recorded at the same site until 1967. Another North American gravimeter (AG 167) was also recording in parallel during 82 days at the end of 1957 beginning of 1958. The aim was to study and compare the sensitivity and accuracy of both instruments (Lecolazet 1958). Using the last period of data recorded by the North American 138 (1012 days between November 1964 and August 1967) they were able to observe the Free Core Nutation resonance.

### 2.2 First observation of Free Core Nutation resonance with gravimetric data

The fluid core resonance phenomenon affects the amplitude of the tidal waves close to the Free Core Nutation (FCN) period in the diurnal frequency band. Although this has been studied for a long time, the accuracy in the determination of most relevant resonance parameters (resonance frequency and quality factor) has improved rather slowly.

As the rest of the gravity community, Lecolazet became interested in searching for the FCN in gravity records after the theoretical works of Jeffreys (1949, 1950, 1957), Vicente (1964, 1971) and Molodensky (1961, 1971) in the middle of last century, concentrating much effort to try to detect it in the data series recorded in Strasbourg.

In a first step, the study of the existence of the Earth's FCN focused on the computation of gravimetric delta factors $\delta$ of the main diurnal tides. Lecolazet initiated the search for a clear evidence of the FCN by its associated resonance effects on the diurnal tides using the 5-month data recorded with the North American AG 138 from October 1954 until March 1955. Unfortunately, the first results he published were in disagreement with the theoretical models (Lecolazet 1957, Melchior 1957). Two years later, using the series from 1957 to 1958, he published the first clear observation of $\delta(O1) > \delta(K1)$ in agreement with Jeffreys' theory

(Lecolazet, 1959). Then Lecolazet (1960) obtained even better results using the complete series of 860 days of the NA 138 registered between August 1957 and December 1960.

After these first results, correct values were found at other stations all around the world, a few years later. We can cite Pariiskii (1963) who confirmed Lecolazet's results using an Askania GS 11, and also Popov's results (Popov, 1963). Later Melchior (1966) compiled the results obtained at different worldwide stations even though some of them did not achieve the expected results.

In a second step, once the existence of this resonance was confirmed, efforts were focused on the search for its frequency. After some failed attempts (Lecolazet and Steinmetz, 1973) where they were not able to locate correctly the frequency, Lecolazet and Steinmetz published in 1974 the first results of the discovery of the resonance of the core (Lecolazet and Steinmetz, 1974) determining that the eigenfrequency should be located either between K1 and PSI1, or between K1 and PHI1 frequencies.

These results were then much improved by using a longer series recorded between 1973 and 1975 with a LaCoste-Romberg Earth-Tide (LR-ET005) gravimeter equipped with a feedback system installed at the J9 Gravimetric Observatory of Strasbourg, definitively confirming that the FCN frequency lies between K1 and PSI1 frequencies (Abours and Lecolazet, 1978, Lecolazet and Melchior, 1977).

Since then, developments in both theory and observations have allowed substantial improvements in the estimation of the FCN resonance parameters, especially with the development of the superconducting gravimeters (SGs) during the 80s.

Finally, we have to mention that a Geodynamics model, the GEO730 owned by J.T. Kuo, recorded during 79 days in Strasbourg between September and December 1970. Within the international context of the station, these data were included in different international profiles and networks (Melchior et al., 1976, Melchior et al., 1981).

**3. Gravimetric Observatory of Strasbourg J9 (1970s – today)**

At the beginning of the 70s, R.Lecolazet and co-workers decided to move the gravimetric observatory to a quieter place situated outside the city. The chosen place is located about 10 km from Strasbourg in a bunker named J9 built by the Germans after the 1870 war on the top of a sedimentary hill (48.622 ° N, 7.684 ° E, 180 m).

The new gravimetric observatory is settled at J9 since 1970. Thereafter gravity variations have been observed and recorded at J9 with various spring and superconducting gravimeters (Figure 3). Besides, since 1997, absolute gravity measurements are also performed regularly. During this long period, the relative gravimeters (sensors and electronics) and the acquisition systems were drastically improved. These improvements allowed increasing the measurement accuracy by more than 10 times (Calvo et al. 2014a).

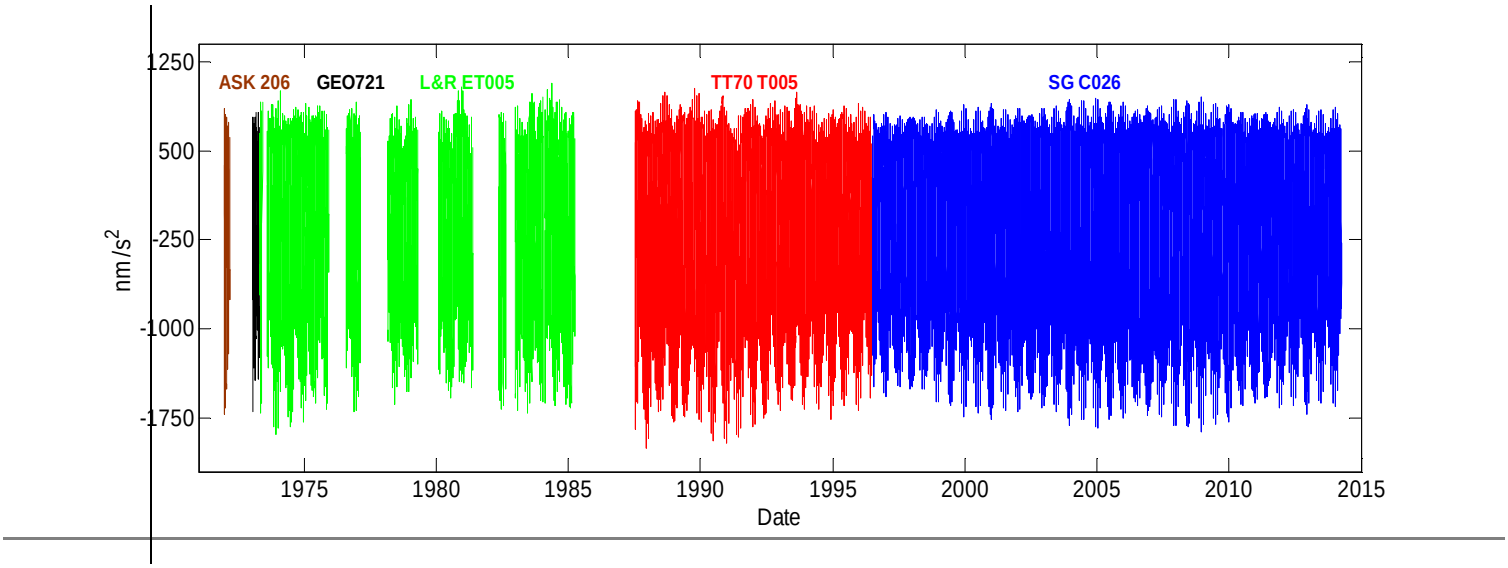


*Fig 3: Time-varying gravity measured at the Gravimetric Observatory J9, located near Strasbourg, from 1970 to 2014. The first 3 series were recorded by spring gravimeters; Askania model in brown, Geodynamic model in black and Lacoste and Romberg model in green. The last 2 series were obtained by superconducting gravimeters; TT70-T005 model in red and SG-C026 model in blue.*

### 3.1 Spring gravimeters

The first 10 years of observations were carried out by different models of spring meters: the first one was an Askania gravimeter belonging to M. Bonatz, ASK206, which was recording for 77 days at the end of 1971 beginning of 1972. After that, a Geodynamic gravimeter GEO721, was installed by B. Ducarme during 82 days in 1973. Later a Lacoste&Romberg ET005 modified in order to record earth tides by R. Lecolazet and J. Gostoli in 1970 with an electrostatic feedback system and a digital recording, was recording with a sampling rate of 1 hour (J. Gostoli, 1970). This later gravimeter was operational during two periods of 2100 and 1120 days respectively from August 1973 until middle 1981. This series was used in several studies, including the observation of the FCN resonance as seen before in section 2.2.

The spring meters are too sensitive to the changes of temperature, so to avoid such perturbations the L&R ET005 was installed in an isolated box thermostatically controlled. The box was located in a room itself thermally stable of the underground fort; the sealed box protected also the sensor against the direct influence of barometric pressure variations. This gravimeter was calibrated by a direct comparison with an Askania gravimeter GS15 in 1972 (Abours, 1977).

More recently, there have been also different spring gravimeters temporarily installed in J9, such as the Microg-LaCoste gPhone 054 owned by IGN-Spain and which was recording for almost 1 year between 2008 and 2009 (Riccardi et al., 2011). A LaCoste & Romberg Graviton-EG1194 from Instituto de Geociencias of Spain was operating there for 3 months during 2011, aiming to check its instrumental response, both in amplitude and phase as well as its time stability (Arnoso et al., 2014). Currently a Lacoste-Romberg ET11, belonging to BFO was installed by W. Zürn and is recording since 2012 (Rosat et al. 2015).

### 3.2 Superconducting gravimeters

Since 1987 two different superconducting gravimeters have been recording in two consecutive periods at J9. The first superconducting gravimeter was a TT70 model from GWR Instruments installed in 1987. This meter was recording for almost 10 years. Using the first 8 years of this series, Florsch et al. (1995) were able to

observe for the first time 3 of the quarter-diurnal tides waves M4, N4, K4 (degree and order 4) with extremely small amplitude. Later on, Boy et al. (2004) definitively confirmed these observations by comparing observed gravity changes with loading estimates using different models of non-linear tides over the North-Western European shelf.

The loading contribution of non-linear oceanic tides has already been clearly observed using measurements from spring gravimeters (Baker, 1980). In 1990, Wenzel and Zürn identified tidal terms of 4$^{th}$ order in the 1 to 3 cycle/day frequency bands using the data from the Lacoste-Romberg ET19 installed in the Black Forest Observatory (Wenzel and Zürn, 1990) but thanks to the high precision of SG data, Florsch et al. (1995) could also identified the degree-four lunar tidal waves in the quarter-diurnal frequency band (fig. 4).

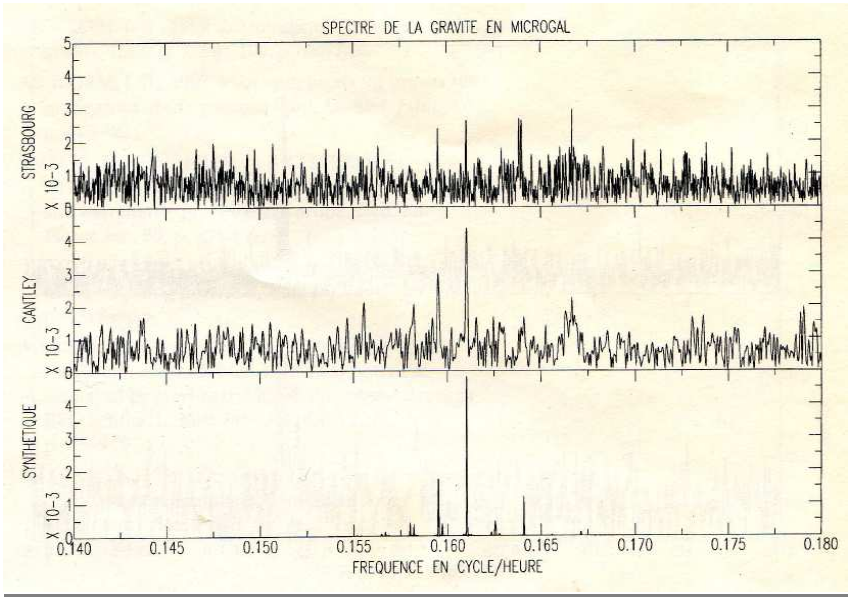


*Fig 4: Gravity spectra recorded by the T005 SG at Strasbourg (France) and T012 at Cantley (Quebec) and comparison with spectra of the theoretically predicted tide calculated at Strasbourg, highlighting 3 of the quart-diurnal tides waves M4, N4, K4. Extracted from Florsch et al., 1995.*

In 1996 this gravimeter was replaced by a more compact model, the C026, which is still recording (Fig 5.). These data are collected within the global GGP (Global Geodynamics Project) network (Crossley et al., 1999). This project began in 1997, as a long term initiative in order to establish a worldwide network of SG stations. The high accuracy and time stability of these gravimeters are useful to study of a wide range of geophysical applications (Hinderer et al., 2007).

*Fig. 5: Superconducting gravimeters installed at the J9 Observatory. Left: TT70 model (T005). Right: OSG model (C026).*

The SGs are using magnetic levitation against gravity on the contrary to the mechanical meters which use a spring. The SG long term stability is hence much better than in the case of spring meters mainly because of the unavoidable creep of any spring whatever its constitutive material (Torge 1989). The high sensitivity of the SGs is achieved by an efficient adjustment of a vertical magnetic gradient, so compared to the spring instruments, the superconducting gravimeters are characterized both by a higher accuracy and a significantly lower instrumental drift.

The model C026 was also improved with respect to the previous T005 version in terms of noise levels (Rosat et al., 2002) and drift rates (Amalvict et al., 2001) because of upgrades of the instrument itself and also of the data acquisition system. The high quality of this gravimeter records has allowed to carry out extensive researches on different topics of global geodynamics such as the study of global Earth deformation (tides, surface loading, etc.), non-linear ocean tides (Boy et al. 2004), hydrology (Longuevergne et al., 2009, Rosat et al., 2009) and metrological aspects such as calibration (Amalvict et al.,2002), long-term drift (Amalvict et al.,2001; Boy et al., 2000), noise levels estimates (Rosat et al., 2004) and comparison with other temporary instrumentation like the gPhone previously mentioned (Riccardi et al. 2011) or a broad-band seismometer (Rosat et al. 2015).

Considering only the J9 Observatory, we have almost 40 years of time-varying gravity record, more than 27 years of which have been registered with superconducting gravimeters, leading to the longest available series ever recorded by SGs at the same site. The SG C026, will be replaced in a near future by a more compact observatory model (iOSG), ensuring continuity of this long series.

We can benefit from this unprecedented length in different ways; both in achieving high spectral resolution in the tidal bands and also in obtaining higher precision in the tidal determination, allowing to separate small amplitude waves in the major tidal groups and also to attempt the detection of very long period tides that have

never been observed in gravity data of shorter duration. Several examples (e.g. tides generated by the third-degree potential) are shown elsewhere (Calvo et al., 2014b).

### 3.3 Absolute gravimeters

Since 1997, there is also a portable absolute gravimeter FG5 # 206 manufactured by Micro-g Solutions which is regularly measuring at the J9 Observatory in parallel with the SG, but also at different sites in France and abroad. The main purposes of these AG measurements performed at J9 are the drift control and the calibration of the superconducting gravimeters.

For the T005, the absolute measurements were carried out by J. Makinen with the absolute gravimeter JILAg-5 belonging to FGI (Finnish Geodetic Institute). We only dispose of 6 measurements for all the period. For the C026, there have been numerous absolute measurements since its installation with instruments of the new generation of ballistic gravimeters, mainly the FG5#206. There was also one measurement realized in parallel with both instruments (JILAg-5 and FG5#206) in 1996 for comparison.

We have also used the AG measurements to determine the SG amplitude scale factor. Several scale factor experiments of different durations (from several hours up to 9 days) were regularly performed since 1996. These results allow us to discuss the time stability of the calibration of the SG. (Hinderer et al., 1991; Amalvict et al., 1999, 2001, 2002; Calvo et al., 2014a).

Furthermore, these absolute measurements have been combined with GPS data or hydrological data in different studies to investigate the long term evolution of gravity that was observed at J9 (Amalvict et al., 2004; Rosat et al., 2009).

In addition to all the gravimetric instrumentation, many other auxiliary sensors are installed at the observatory, such as a weather station, GPS permanent antenna, and different hydrological sensors (piezometers, soil moisture sensors).

## 4. Conclusion

The beginning of the Strasbourg tradition to record gravity Earth tides is due to Robert Lecolazet who decided to investigate this field in Strasbourg in the 50s. The first permanent gravimeter was installed in 1954 (a North American 138 spring meter) in the Seismological Observatory of Strasbourg. Since then, different models of gravimeters (spring, superconducting and absolute gravimeters) have been recording at different consecutive periods. In the 70s, the observatory was moved to a bunker, 10km from Strasbourg, the J9 Observatory. We have reviewed all the instrumentation that has been used in both observatories and we have pointed out some of the major results obtained using the recorded data.

Several major scientific achievements have been derived from the use of these data series, such as the observation of long period waves (Mm, Mf, Mtm) in 1966, the observation of the Free Core Nutation resonance in diurnal waves in 1974 or the first observations of the quarter-diurnal tidal waves of a few pico-g amplitude in 1995. Today, considering the J9 Observatory only, we have almost 40 years of record, more than 27 continuous years of which have been registered with superconducting gravimeters, leading to the longest SG record available. This exceptional duration helped us to separate tidal contributions of near frequencies, to detect some very weak amplitude signals and to exhibit signals of very low frequency. In a near future, the SG C026 will be replaced by a more compact SG observatory model (iOSG). This new gravimeter will ensure the continuity of this long series in Strasbourg, for further improvement in the study of time-varying gravity.

## References


Abours S., 1977. Exploitation des enregistrements de marée gravimétrique à Strasbourg - aout 1973/février 1977. Diplôme d'Ingénieur Géophysicien. Univ. De Strasbourg, Strasbourg

Abours S., Lecolazet, R., 1978. New results about the dynamical effects of the liquid outer core as observed at Strasbourg, in Proc. 8th Int. Symp. Earth Tides, pp. 689–697, eds Bonatz M., Melchior P., Bonn.

Amalvict, M., Hinderer, J., & Boy, J.P., 1999. A comparative analysis between an absolute gravimeter (FG5-206) and a superconducting gravimeter (GWR C026) in Strasbourg: new results on calibration and long term gravity changes, Boll. Geofisica Geodetica, 40, n°2-3, 519-525.

Amalvict M., Hinderer J., Boy J-P., Gegout P., 2001. A 3 year comparison between a superconducting gravimeter (GWRC026) and an absolute gravimeter (FG5#206) in Strasbourg (France). J. Geod. Soc. Jpn. 47, 334 – 340.

Amalvict M., Hinderer J., Gegout P., Rosat S., Crossley D., 2002. On the use of AG data to calibrate SG instruments in the GGP network: example of Strasbourg - J9. Bull. Inform. Marees Terr. 135, 10621– 10626.

Amalvict, M., Hinderer, J., Mäkinen, J., Rosat, S., Rogister, Y., 2004. Long-term and seasonal gravity changes at the Strasbourg station and their relation to crustal deformation and hydrology. J. Geodyn. 38 (3-5), 343–353.

Arnoso, J., Riccardi, U., Hinderer, J., Córdoba, B. Montesinos, FG., 2014. Analysis of co-located measurements made with a LaCoste&Romberg Graviton-EG gravimeter and two superconducting gravimeters at Strasbourg (France) and Yebes (Spain). Acta Geodaetica et Geophysica, doi: 10.1007/s40328-014-0043-y

Boy J-P., Hinderer J., Amalvict M., Calais E., 2000. On the use of long records of superconducting and absolute gravity observations with special application to the Strasbourg station, France. Cahiers Centre Eur. Géodyn. Séismol. 17, 67–83

Boy, J.-P., M. Llubes, R. Ray, J. Hinderer, N. Florsch, S. Rosat, F. Lyard and T. Letellier, 2004. Non-linear oceanic tides observed by superconducting gravimeters in Europe, J. Geodyn., 38, 391-405.

Baker, T.F., 1980. Tidal gravity in Britain: tidal loading and the spatial distribution of the marine tide. Geophys. J.R. Astron. Soc. 62, 249–267.

Calvo, M., S. Rosat, J. Hinderer, Legros, H., Boy, J.-P., Riccardi, U., 2014a. Study of the time stability of tides using a long term (1973-2011) gravity record at Strasbourg, France. Earth on the Edge: Science for a Sustainable Planet, vol. 139, Rizos C. and Willis P. (Ed.), Springer-Verlag, Berlin Heidelberg, pp 377-381, doi: 10.1007/978-3-642-37222-3_50

Calvo M., Hinderer, J., Rosat, S., Legros H., Boy J-P., Ducarme, B., Zürn, W., 2014b. Time stability of spring and superconducting gravimeters through the analysis of very long gravity records. J. Geodyn., 80, 20-33.

Crossley, D., Hinderer, J., Casula, G., Francis, O., Hsu, H.-T., Imanishi, Y., Meurers, B., Neumeyer, J., Richter, B., Shibuya, K., Sato, T., van Dam, T., 1999. Network of superconducting gravimeters benefits a number of disciplines, Eos Trans. AGU, 80(11), 121–126.

Florsch N., Hinderer, J., Legros, H., 1995. Mise en évidence d'ondes de marée quart-diurnes de quelques pico-g d'amplitude à l'aide de gravimètres supraconducteurs. C. R. Acad. Sci. Paris, t. 321, 279-285.

Gostoli J., 1970. Etude et construction d'un dispositif d'asservissement pour un gravimètre LaCoste–Romberg. Enregistrement numérique de la marée gravimétrique. Thèse de Dr. Ing, Univ de Strasbourg, Strasbourg.

Greff-Lefftz, M., Legros, H., & Dehant, V., 2000. Influence of the inner core viscosity on the rotational eigenmodes of the Earth. Physics of the Earth and Planetary Interiors, 122(3), 187-204.

Greff-Lefftz, M., Dehant, V., & Legros, H., 2002. Effects of inner core viscosity on gravity changes and spatial nutations induced by luni-solar tides. Physics of the Earth and Planetary Interiors, 129(1), 31-41.

Hinderer, J., Legros, H., & Amalvict, M. (1982). A search for Chandler and nearly diurnal free wobbles using Liouville equations. Geophysical Journal International, 71(2), 303-332.

Hinderer, J., Legros, H., Jault, D., & Le Mouël, J. L., 1990. Core-mantle topographic torque: a spherical harmonic approach and implications for the excitation of the Earth's rotation by core motions. Physics of the earth and planetary interiors, 59(4), 329-341.

Hinderer, J., Florsch, N., Mäkinen, J. , Legros, H. & Faller, J.E., 1991. On the calibration of a superconducting gravimeter using absolute gravity measurements, Geophys. J. Int., 106, 491-497.

Hinderer, J., Crossley, D., Warburton, R., 2007. Superconducting gravimetry. Treatise on Gheophysics. Amsterdam: Elsevier, Vol. 3, pp. 65-122.

Jeffreys H., 1949, Dynamic effects of a liquid core. Monthly Notices of the Royal Astronomical Society, Vol. 109, No. 6, p.670

Jeffreys H., 1950. Dynamic effect of a liquid core (II). Monthly Notices of the Royal Astronomical Society, 110, 5, 460-466.

Jeffreys H., 1957. Theoretical values of the bodily tides numbers. Bull. Inf. Marées Terrestres, 3, 29.

Lecolazet, R., 1956. Application, a l'analyse des observations de la marée gravimétrique, de la méthode de H. et Y. Labrouste, dite par combinaisons linéaires d'ordonnées. Extrait des ANNALES DE GÉOPHYSIQUE. Tome 12, p. 59-71.

Lecolazet, R., 1957. Enregistrement et analyse harmonique de la marée gravimétrique à Strasbourg

Extrait des ANNALES DE GÉOPHYSIQUE. Tome 13, p. 186-202.

Lecolazet, R., 1958. Résultats provisoires des enregistrements de la marée gravimétrique, effectués à Strasbourg d'aut 1957 à février 1958. Deuxième Colloque international de la commission du CSAGI pour l'étude des marées terrestres.

Lecolazet, R., 1959. Résultats des observations de marée gravimétrique effectuées à Strasbourg jusqu'en 1958. Third International Symposium on Earth Tides. Trieste 1959.

Lecolazet, R., 1960. Rapport sur les observations de marée gravimétrique faites à Strasbourg en 1957, 1958 et 1959. B.I.M Nº21, p. 387-395.

Lecolazet, R., Steinmetz L., 1966. Premiers résultats expérimentaux concernant la variation semi-mensuelle lunaire de la pesanteur à Strasbourg. C. R. Acad. Sci. Paris, t. 263, p. 716-719.

Lecolazet, R., Steinmetz L., 1973. Nouveaux résultats expérimentaux concernant les ondes diurnes de la marée gravimétrique. Journal of the international association of geodesy. Nº 109, p. 301-307.

Lecolazet, R., Steinmetz L., 1974. Sur les ondes diurnes de la marée gravimétrique observée à Strasbourg. C. R. Acad. Sci. Paris, t. 278, p. 295-297.

Lecolazet, R., Melchior, P., 1977. Experimental determination of the dynamical effects of the liquid core of the Earth. Ann. Geophys., t.33, fasc. 1 / 2, p. 11-22.

Legros, H., Hinderer, J., Lefftz, M., & Dehant, V., 1993. The influence of the solid inner core on gravity changes and spatial nutations induced by luni-solar tides and surface loading. Physics of the earth and planetary interiors, 76(3), 283-315.

Longuevergne L., Boy J-P., Florsch N., Viville D., Ferhat G., Ulrich P., Luck B., Hinderer J., 2009. Local and global hydrological contributions to gravity variations observed in Strasbourg. J. Geodyn 48 p. 189 - 194

Melchior, P., 1957. Rapport sur les marées terrestres. B.I.M Nº8, p. 1-30.

Melchior, P., 1966. The earth tides. Pergamon Press. Ltd., New York.

Melchior, P., Kuo, J.T., Ducarme, B., 1976. Earth tide gravity maps for Western Europe. Physics of the Earth and Planetary Interiors. Volume 13, Issue 3, p. 184–196.

Melchior, P., Moens, M., Ducarme, B., Van Ruymbeke, M.,1981. Tidal loading along a profile Europe-East Africa-South Asia-Australia and the Pacific Ocean. Physics of the Earth and Planetary Interiors. Volume 25, Issue 1, p. 71–106.

Molodenskii, M.S., 1961. The theory of nutations and diurnal Earth Tides. IVème Symp. Int. Marées Terrestres, Obs. Royal de Belgique, comm. 188, s. geoph. 58, 25-56.

Molodenskii, M.S., 1971. Les marées de la Terre élastique en rotation avec un noyau liquide. Bull. Inf. Marées Terrestres, 60, 2979-2987.

Pariiskii, N.N., 1963. The discovery of the Earth's Diurnal Nutation. Soviet Astronomy, Vol. 7, No.3, p.424.

Popov, N. A., 1963, Nutational motion of the Earth's axis. Nature, 193, 1153.

Riccardi, U., Rosat, S., Hinderer, J., 2011. Comparison of the Micro-g LaCoste gPhone-054 spring gravimeter and the GWR-C026 superconducting gravimeter in Strasbourg (France) using a 300-day time series. Metrologia, 48, 28-39.

Rosat, S., Hinderer, J., Crossley, D., 2002. A comparison of the seismic noise levels at various GGP stations. Bull. Inf. Marées Terr. 135, 10689–10700.

Rosat, S., Hinderer, J., Crossley, D. and Boy, J.P., 2004. Performance of superconducting gravimeters from long-period seismology to tides, J. of Geodyn., 38, (3-5), 461-476.

Rosat, S., Boy, J.-P., Ferhat, G., Hinderer, J., Amalvict, M., Gegout, P. and B. Luck, 2009. Analysis of a ten-year (1997-2007) record of time-varying gravity in Strasbourg using absolute and superconducting gravimeters: new results on the calibration and comparison with GPS height changes and hydrology, J. of Geodyn., 48, 360-365.

Rosat, S., Calvo, M., Hinderer, J., Riccardi, U., Arnoso, J. and W. Zürn, 2015. Comparison of the performances of different Spring and Superconducting Gravimeters and a STS-2 Seismometer at the Gravimetric Observatory of Strasbourg, France, Stud. Geophys. Geod., 59, doi:10.1007/s11200-014-0830-5

Torge W., 1989. Gravimetry. Walter de Gruyter. Berlin 465 pp.

Vicente, R.O., 1964. The influence on the core on Earth tides. 5ème Symp. Int. Marées Terrestres, Observatoire Royal Belgique, comm. 236, s. Geoph. 69, 40-60.

Vicente, R.O., 1971. Influence of the core on the nutations. Mantello e nucleo nella fisica planetaria, Scuola Int. di Fisica E. Fermi, Academic Press, 17-26.

Wenzel, H.G.and Zürn, W., 1990. Errors of the Cartwright-Tayler-Edden 1973 tidal potential displayed by gravimetric Earth tide observation at BFO Schiltach. Bull. Inf. Marées. Terr., 107, 7555-7574.

BLANK PAGE